Electromagnetic corrections to pseudoscalar decay constants

Dissertation

zur Erlangung des Doktorgrades
der Naturwissenschaften (Dr. rer. nat.)
der Fakultät für Physik
der Universität Regensburg

vorgelegt von

Benjamin Simon Gläßle

aus Reutlingen

im Jahr 2017

Promotionsgesuch eingereicht am: 10. Mai 2016
Die Arbeit wurde angeleitet von: Prof. Dr. G. Bali
Termins des Promotionskolloquiums: 6. März 2017

Prüfungsausschuss:	Vorsitzender:	Prof. Dr. K. Rincke
	1. Gutachter:	Prof. Dr. G. Bali
	2. Gutachter:	Prof. Dr. V. Braun
	weiterer Prüfer:	Prof. Dr. J. Schliemann

Contents

List of Figures

1. Introduction

Particle physics is well described by the so-called *Standard model* (SM) [1] which contains the electroweak and the strong interactions, and predicted the recently detected Higgs boson [2]. The SM is based upon the development of the electroweak theory [3–5], the proof of renormalizability [6] and the postulation and confirmation of *quantum chromodynamics* (QCD) as the theory of the strong interaction [7].

It was able to predict many of its constituent particles ($W^{\pm}$, Z^0, top, Higgs) and certain observables such as the anomalous magnetic moment of the electron with unprecedented accuracy.

In spite of its enormous success it is unquestionable that it is just an effective low energy description of a more fundamental theory: No SM effect can explain the abundance of baryonic matter over antimatter in the visible universe [8], or that the majority of the universe's matter is not directly observable [9]. Other issues like the surprisingly light Higgs boson mass, and the large number of parameters[1] also indicate the effective nature of the SM. Furthermore a more unified theory should (and might be required to) include gravity.

The search for physics beyond the SM aims at directly detecting new particles and interactions or finding deviations of observables from SM predictions. The energy range accessible by human build terrestrial experiments is limited by physics and economical considerations. With presently known technology accelerators cannot reach the Planck scale M_p and experiments might forever be limited to energies at which the SM is a good effective description. This possibility increases the importance of indirect searches and therefore the requirement of precise theoretical predictions.

1.1. QFT on the lattice

The most challenging and therefore least well quantitatively understood interaction of the SM is QCD. The main difficulty is that the QCD exchange particles, the so-called *gluons*, self interact. This gives rise to the running of the coupling α_{QCD} towards small values at large momentum transfers which facilitates asymptotic freedom, and a large coupling constant at low energies. Perturbative weak coupling expansions fail when the coupling becomes of order one. More rigorously defined, this associated energy scale is commonly referred to as Λ_{QCD}.

[1] It has more than 20 free parameters. Several of these parameters are required to be finely tuned to allow the stable universe we see today: The mass of the Higgs particle is restricted to certain ranges [10, 11]. Another example is the electromagnetic coupling α_{QED} in relation to the light quark mass difference $m_d - m_u$. If these are outside of a certain parameter space there would either be no nuclear fusion and therefore no stars or a universe with an abundance of small stars.

Nonperturbative methods such as *Lattice QCD* (LQCD) are required to overcome this problem. LQCD discretizes spacetime on a lattice and samples the path integral with *Monte Carlo* (MC) methods. Infrared and ultraviolet cutoffs can be systematically removed to give correct infinite volume and continuum results. Modern computer architectures, development in algorithms and a lot of theoretical progress have allowed LQCD to evolve from its infancies in the 1970s [12, 13] to become a tool that can verify and predict masses and matrix elements from first principle [14]. High precision lattice calculations provide valuable input for SM tests.

Most of the current lattice QCD simulations assume isospin symmetry and neglect the electromagnetic charge of the quarks, and the non-degeneracy of light quark masses. The inclusion of these effects is computationally expensive and might have only negligible effects on most observables within their respective errors. The comparison of QCD and *quantum electrodynamics* (QED) coupling constants shows that QED corrections become relevant for high precision calculations at percent level accuracy. Until recently lattice QCD+QED calculations have only been performed for hadron and quark masses.

The work presented here is one of the first lattice calculations of QED corrections to matrix elements. Specifically, this work is a case study for QCD+QED matrix element calculations on the lattice, showing the feasibility of the method and highlighting the crucial components. As it turns out full pre- or postdiction of QCD+QED matrix elements from first principle requires a lot of computer time, and theoretical input for the understanding of systematic effects - such as the effect of the finite volume, the definition of the continuum limit, and QED quenching effects.

1.2. Outline

The task of this thesis is the development, description and analysis of lattice calculations of QCD+QED matrix elements. We try to highlight systematic uncertainties for future work. The thesis is therefore organized as follows.

The relevant concepts of isospin, its breaking and meson decay in continuum *quantum field theory* (QFT) are introduced in chapter 2. After establishing QED, QCD and continuum methodology we will cover hadronic bound states and associated decay constants. The role of symmetries is discussed, in particular (approximate) isospin and chiral symmetry which motivates *chiral perturbation theory* (χPT). χPT in turn plays a vital role in the extrapolation of lattice results to the physical point in the quark mass plane.

Chapter 3 is a short introduction into Lattice QCD. It explains how a QFT is discretized on a finite lattice and how the path integral is evaluated. We describe the measurement of twopoint correlators which can be used to extract ground state masses and amplitudes. Basic methods used in analysis and a summary of the required physical limits conclude this chapter.

Because this is the first work on QED corrections to hadronic matrix elements, chapter 4 is dedicated to a broad review of present QCD+QED lattice simulations. We detail the different methods used for the simulation of the modified lattice theory, and discuss

the additional challenges, most notably finite size effects, in the analysis. Furthermore we present a method for the determination of non-degenerate light quark masses in the presence of a general dynamic $U(1)$ field.

The specifics of our QCD+QED lattice simulations and their analysis are detailed in chapter 5. We describe the ensembles used in our analysis and explain our choice of parameters including the smearing, charges and mass tuning. The analysis of QED mass-splitting is restricted to pions and kaons which can be used to calculate the up, down and strange quark masses as well as corrections to Dashen's theorem. The analysis of the electromagnetic decay constant splitting will cover all physically relevant light, strange and charmed pseudoscalars. A particular focus will be given to finite volume effects which severely limit our predictive power. We are nevertheless able to show QED splittings that qualitatively conform to phenomenological descriptions. The last section of the chapter covers the shortcomings of and alternatives to our methodology.

The conclusion in chapter 6 summarizes our findings and gives an outlook into the future of QCD+QED effects on matrix elements and their calculations.

2. Continuum QFT

The following chapter intends to introduce mesonic decay constants and their relevance in *Standard model* tests. Related concepts and common approximations are explained.

For these purposes *quantum field theory* (QFT) will be introduced using QED as an example. The first section will cover the Dirac equation for the fermions, the role of gauge invariance, the emerging gauge fields and the action. I will further mention basic theoretical methodology, like the path integral formalism, the perturbative expansion of the theory and the problems and limitations that arise. The following section 2.2 will introduce QCD, its deviant behavior and characteristics. Its non-perturbative nature is highlighted.

The introduction of experimental observables in section 2.3 will cover bound states, decays and scattering. The description of decay in the QFT formalism will introduce the CKM matrix, (hadronic) matrix elements and therefore decay constants. I mention past and future experimental determinations of pseudoscalar decay constants and remark on differences of charged and uncharged pion decay constants.

Exact and approximate symmetries of the theory are discussed in section 2.4. Discrete symmetries are used to distinguish bound states and allowed processes. The spontaneous breaking of approximate chiral symmetry separates the masses of pions from all other hadrons and motivates *chiral perturbation theory* (χPT). Approximate isospin symmetry is discussed.

A good general introduction into the methodology and problematics of QFT can be found in [15] or [16].

2.1. Quantum electrodynamics

The Dirac equation [17]

$$\left(\mathrm{i}\partial\!\!\!/ - m\right)\psi(x) = 0 \tag{2.1}$$

unifies quantum mechanics and the special theory of relativity. The slash notation $\partial\!\!\!/$ is a shorthand for $\gamma_\mu\partial_\mu$ where the Einstein sum convention is used. Equation (2.1) incorporates spin into the equations of motion and requires negative energy solutions. These were eventually interpreted as antiparticles, whose existence were later confirmed by the discovery of the positron. Left-multiplying eq. (2.1) with the adjoint $\overline{\psi} = \psi^\dagger\gamma_0$ yields the Lorentz-invariant Lagrangian (density)

$$\overline{\psi}\left(\mathrm{i}\partial\!\!\!/ - m\right)\psi(x) = 0 \tag{2.2}$$

of the Dirac theory.

Interactions between massive particles were introduced by requiring local gauge invariance, meaning the invariance of the Lagrangian under transformations such as

$$\psi(x) \to \psi'(x) = \Omega(x)\,\psi(x), \quad \overline{\psi}(x) \to \overline{\psi}'(x) = \overline{\psi}(x)\,\Omega^\dagger(x), \tag{2.3}$$

where $\Omega(x) \in U(1)$ for QED, and $\Omega(x) \in SU(2)$ or $SU(3)$ for the weak interaction or QCD. Note that $\Omega(x)$ is unitary ($\Omega^\dagger(x) = \Omega^{-1}(x)$). When eq. (2.3) is inserted into the Lagrangian (eq. (2.2)) the left hand side

$$\overline{\psi}\,\Omega^\dagger(x)\left(\partial\!\!\!/ - m\right)\Omega(x)\psi \neq 0 \tag{2.4}$$

no longer vanishes due to the derivative of a nontrivial $\Omega(x)$. Gauge invariance can be restored by inserting a vector field $B_\mu(x)$ which absorbs the $\Omega^\dagger(x)\partial_\mu\Omega(x)$ term. This new field represents the gauge bosons of QED - the so-called photons - and is required to transform under gauge transformations like

$$B_\mu(x) \to B'_\mu(x) = \Omega(x)B_\mu(x)\Omega^\dagger(x) + \mathrm{i}\big(\partial_\mu\Omega(x)\big)\Omega^\dagger(x). \tag{2.5}$$

QED thus consist of the fields

$$\psi^f(x)_\alpha\,, \quad \overline{\psi}^f(x)_\alpha \quad \text{and} \qquad B_\mu(x), \tag{2.6}$$

where the superscript f indicates the individual lepton (or quark) flavor, subscript α is a spin index and the index μ indicates that the gauge field is a vector field. Their interaction is fully encoded in the modified fermion action

$$S_F[\psi,\overline{\psi},B_\mu] = \sum_{f=1}^{N_f}\int \mathrm{d}^4x\,\overline{\psi}^f(x)\left(\mathrm{i}\gamma_\mu\left(\partial_\mu + \mathrm{i}e^f B_\mu(x)\right) - m^f\right)\psi^f(x) \tag{2.7}$$

where the fermion charge e^f contains the QED coupling e and quantifies the strength of the fermion-photon interaction. The coupling constant at energies below the positronium threshold $2m_{e^\pm}$ is given by the fine structure constant $\alpha \simeq 1/137$:

$$e^2 = 4\pi\alpha. \tag{2.8}$$

The QED gauge action S_G can be derived by using the covariant derivative $D_\mu(x) = \partial_\mu + \mathrm{i}e^f B_\mu(x)$. Its commutator turns out to be the field tensor well known from classical electrodynamics

$$G_{\mu\nu}(x) = \frac{-\mathrm{i}}{e^f}\,[D_\mu(x), D_\nu(x)] = \partial_\mu B_\nu(x) - \partial_\nu B_\mu(x) \tag{2.9}$$

which will transform under gauge transformations in the same way as the covariant

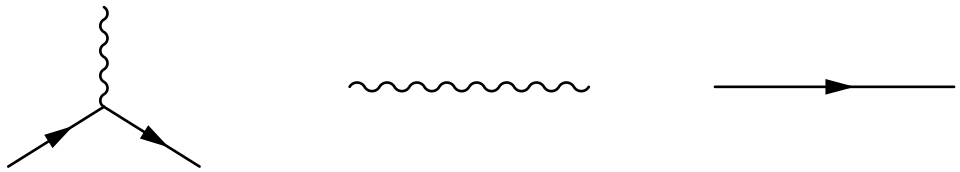

(a) Photon-fermion vertex (b) Photon propagator (c) Fermion propagator

Figure 2.1.: The basic elements for QED Feynman diagrams. The time direction in this work is assumed to be in horizontal direction.

derivate itself. The therefore gauge invariant QED gauge action is then given by

$$S_G[B_\mu] = \frac{1}{2}\int \mathrm{d}^4x \,\mathrm{tr}\,[G_{\mu\nu}(x)G_{\mu\nu}(x)] \tag{2.10}$$

which is a Lorentz scalar due to summation over the spin indices μ, ν.

2.1.1. The path integral and perturbation theory

The partition sum of a QFT (for QED the replacement $[\phi] = [\psi, \overline{\psi}, B_\mu]$ is implied) is given by

$$Z[\phi] = \int \mathcal{D}[\phi]\, \mathrm{e}^{\mathrm{i}S[\phi]} \tag{2.11}$$

and can be used to formally express the expectation value of arbitrary observables $\mathbf{O}$ in equilibrium

$$\langle \mathbf{O} \rangle = \frac{1}{Z[\phi]} \int \mathcal{D}[\phi]\, \mathrm{e}^{\mathrm{i}S[\phi]}\, \mathbf{O}[\phi]. \tag{2.12}$$

This equation is often called path integral because the integral averages over all field configurations $[\phi]$, and the field configurations are paths in simple quantum mechanical settings like the double slit experiment. The exact and explicit evaluation of the path integral for 4 dimensional field theories, like QED, is impossible due to the infinite dimensional integral.

Weak coupling allows the systematic Taylor expansion of the path integral in even powers of the (bare) coupling constant e^2. This so-called perturbative approach is tedious and error prone. Feynman proposed to identify reoccurring elements of the expansion and to derive laws from the Hamiltonian that are valid to all orders [18]. The reoccurring elements (illustrated in fig. 2.1) of QED are photon and lepton propagators which connect photon-fermion vertices. These are then used to construct contributions at a fixed order and weight them according to their degeneracy. Theses contributions have a useful symbolic representation the so-called Feynman diagrams. External lines are amputated,

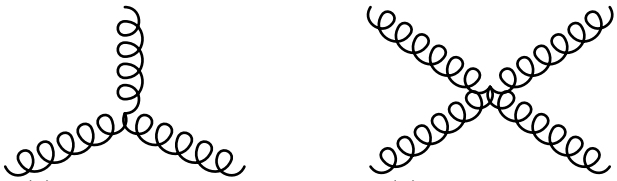

(a) 3 gluon vertex (b) 4 gluon vertex

Figure 2.2.: Gluon self interaction.

meaning they are not integrated over and not written out. Contributions can be divided into diagrams that are fully connected and diagrams that contain disconnected elements. Disconnected elements also appear in the expansion of the vacuum state and therefore cancel after normalization with the partition function. The expectation value eq. (2.12) of an observable can in perturbation theory be approximated by a (correctly weighted) truncated sum of all connected diagrams. Observation of the transition of initial $|\{k\}_i\rangle$ to final $|\{p\}_f\rangle$ states can be described by the unitary scatter matrix $S = \mathbb{1} + \mathrm{i}T$. The (non-forward) interaction

$$\langle\{p\}_f|\mathrm{i}T|\{k\}_i\rangle = (2\pi)^4\delta^{(4)}\left(\sum_i k_{\mu,i} - \sum_f p_{\mu,f}\right)\mathrm{i}\mathcal{M}\big(\{k\}_i \to \{p\}_f\big) \tag{2.13}$$

can be separated into kinematics and the internal dynamics described by the amplitude $\mathcal{M}$, which contains the amputated diagrams.

Regularization and renormalization

The perturbative expansion yields ultraviolet divergent loop integrals. The divergences can be regularized by cutoffs or other means. Prescriptions that can be shown to be equivalent to any valid regulator, and that only redefine the normalization of the bare fields and the coupling constant are called renormalization schemes. This procedures can be performed order by order. Ambiguities are thereby successively pushed into higher orders and until they remain in orders above the order of the truncation. Regardless of the remaining ambiguity the perturbative expansion accurately predict various experimental observables such as the anomalous magnetic moment of the electron with unprecedented accuracy, which is the foundation of the enormous success of QFT. A common continuum renormalization scheme is the so-called *modified minimal subtraction* scheme ($\overline{\mathrm{MS}}$).

2.2. Quantum chromodynamics

Rutherford found [19] that the angular distribution of α particles scattering of a gold foil could be explained if the charge distribution of the heavy atomic nuclei is confined to a sphere with radius $r < 10^{-14}\,\mathrm{m}$. The fact that no known interaction could explain

the binding energy of atomic nuclei caused Yukawa to postulated a strong, short ranged interaction which is mitigated by a massive, spin-zero exchange particle [20]. The approximate range (1 fm) of its force led to the first estimate of what is now understood to be the pion mass.

Early particle accelerator experiments discovered an abundance of new particles, called hadrons. The mass spectrum of spin-$\frac{1}{2}$ hadrons could be described by the so-called *Eightfold way*, which assumed that proton, neutron and the newly discovered bound states were composed of three fermions, the so-called (up, down and strange) quarks. The hadronic wave function of the Ω^- and Σ^{++} baryon required the fermion fields to have an additional hidden quantum number to be total antisymmetric and obey Fermi's exclusion principle. This quantum number is called color. The observed $\pi^0 \to \gamma\gamma$ decay rate (which will be discussed in section 2.3.2) and the cross-section in $e^+e^- \to$ hadron scattering required the number of colors to be $N_c = 3$. The fact that only color singlet states can be observed is called confinement. Scattering experiments revealed further substructure of the nucleon. *Deep inelastic scattering* (DIS) showed that the nucleon contains partons which are asymptotically free at large energies.

Requiring $SU(3)$ gauge invariance and incorporating the color quantum number c into the fermion fields allows the derivation of QCD, which contains the fields

$$\psi^f(x)_{\alpha,c}\,, \quad \overline{\psi}^f(x)_{\alpha,c} \quad \text{and} \qquad A_\mu(x)_{cd}. \tag{2.14}$$

The vector gauge field $A_\mu(x)_{cd}$ is a traceless, unitary matrix. It represents gluons that carry an octet color in contrast to fermions (quarks) which have a normal color charge. The electromagnetic charge e in eq. (2.7) is replaced by the QCD coupling g in the analogous QCD action. The non-abelian nature of QCD is non-abelian is explicit in its field tensor which contains a field commutator

$$F_{\mu\nu}(x) = -\mathrm{i}\,[D_\mu(x), D_\nu(x)] = \partial_\mu A_\nu(x) - \partial_\nu A_\mu(x) + \mathrm{i}\,[A_\mu(x), A_\nu(x)]\,. \tag{2.15}$$

This commutator yields two vertices that couple three and four gauge fields (see fig. 2.2) in Feynman diagrams.

Careful derivation of QCD Feynman rules reveals an additional element, called *Faddeev-Popov ghost* field [21]. The effective Lagrangian density of the ghost fields c is given by

$$\mathcal{L}_{\text{ghost}} = \bar{c}^a \left(-\partial^2 \delta^{ac} - g\partial^\mu f^{abc} A^b_\mu\right) c^c. \tag{2.16}$$

The corresponding ghost propagator and ghost-gauge vertex must be included into the Feynman diagrams of the amplitude $\mathcal{M}$. This removes a remnant gauge ambiguity and ensures that unphysical gluon polarizations in the amplitude cancel. Faddeev-Popov ghosts are required in all gauge theories to ensure unitarity. Abelian gauge theories do not contain a ghost-gauge interaction term and therefore require no additional diagrams.

It can be shown that QCD is renormalizable and that all regulators yield the same physical results [22]. Approximate symmetries of QCD, like isospin and chiral symmetry, are discussed in section 2.4.

2.2.1. Running of the strong coupling

In order to discuss the QCD properties confinement and asymptotic freedom, it is instructive to investigate the momentum dependence of the coupling expressed in the function

$$\beta(g) = -\frac{\partial g}{\partial \ln \mu}. \tag{2.17}$$

This function can be calculated in perturbation theory, which up to *next-to leading order* (NLO) yields

$$\begin{aligned} \beta(g) &= -\beta_0 g^3 - \beta_1 g^5 + \mathcal{O}(g^7) \qquad (2.18)\\ \text{with} \qquad \beta_0 &= \frac{1}{(4\pi)^2}\left(\frac{11}{3}N_c - \frac{2}{3}N_f\right)\\ \text{and} \qquad \beta_1 &= \frac{1}{(4\pi)^2}\left(\frac{34}{3}N_c^2 - \frac{10}{3}N_c N_f - \frac{N_c^2-1}{N_c}N_f\right). \end{aligned}$$

The negative slope of eqs. (2.17) and (2.18) can be attributed to the gauge bosons as long as the number of colors N_c is sufficiently large. Solutions of eq. (2.17) confirm asymptotic freedom: The coupling g^2 converges to zero as the momentum scale μ is sent to infinity. A large number N_f of effectively massless quarks below the momentum scale μ prevents this behavior.

The behavior of the coupling constant g at low momenta proofs to be more troublesome: It increases until our approximation of $\beta(g)$ (eqs. (2.17) and (2.18)) becomes invalid and perturbation theory fails at a scale Λ_{QCD}, which is roughly comparable to the masses of light hadrons. The non-perturbative behavior can be used for a hand waving explanation of confinement: The coupling is strong when color charges are separated by more than ${\Lambda_{\text{QCD}}}^{-1}$. Gluons then (due to their self interaction) create flux tubes, the energy required to separated the charges grows linearly with the distance and will result in pair creation before isolated color charges can be observed.

2.3. Experimental observables

Elementary particle physics experiments observe and measure bound states, their decay and scattering processes. We will in the following focus on hadronic observables which are dominated by the strong interaction. Other interesting observables for SM test are for example measurements of neutrino oscillations which probe the weak interaction and the CKM matrix equivalent in the leptonic sector. Hadronic observables can be split into perturbative and non-perturbative contributions such as high momenta scattering and (hadron) masses.

pseudoscalar	quark content	m[MeV]	f[MeV]	τ[s]
π^+	$u\bar{d}$	139.57	130.4	2.60×10^{-8}
π^0	$\frac{u\bar{u}-d\bar{d}}{\sqrt{2}}$	134.98	"130.0"	8.52×10^{-17}
K^+	$u\bar{s}$	493.68	156.1	1.24×10^{-8}
K^0_L	$d\bar{s}$	497.61		5.099×10^{-8}
K^0_S				8.954×10^{-10}
D^+	$c\bar{d}$	1869.5	209	1040×10^{-15}
D^0	$c\bar{u}$	1864.8		410×10^{-15}
D_s	$c\bar{s}$	1969.0	249	500×10^{-15}

Table 2.1.: Arbitrary listing of pseudoscalar ($J^{PC} = 0^{-(+)}$) particles and their properties. Mass values and life times are from [23], the decay constants are out of [24], which are usually calculated with degenerate light quark masses. The neutral pion decay constant was adjusted according to the approximations in [25].

2.3.1. Bound states

Although hadron masses are non-perturbative, their spectrum provides information on QCD symmetry and dynamics. Particles may be observed directly or as a mass resonance in scattering cross sections. The most prominent and only stable[1] hadron is the proton. Its mass is notably far larger than the mass of its constituents, almost degenerate to the mass of its "isospin" partner the neutron (which does decay) and far lighter than the mass of its negative parity partner N^*. This indicates that most of the nucleons mass is due to QCD dynamics, approximate isospin symmetry and that chiral symmetry is likely spontaneously broken. Furthermore protons and neutrons form bound states which are sometimes stable. Their binding energies can be used to estimate the mass of the pion, and investigate effective theories of nucleon interaction.

The hadronic mass spectrum contains a large number of states which have a long enough lifetime such that their mass can be measured. Mass hierarchy and the lightness of pions strengthens the evidence of the spontaneous breaking of chiral symmetry. The masses of η and η' give further information about $SU(3)$ flavor symmetry and η, η' mixing. Exited states of hadrons give further information about the non-perturbative regime. Large magnetic fields modify the spectrum of charged particles. Predicted suppression of the charmonium vector state J/ψ in heavy ion collisions may indicate the quark gluon plasma and gives information about the QCD high temperature phase. The ultimate goal in searches for new physics is obviously the detection of particles whose properties (mass and quantum numbers) cannot be associated with the predicted spectrum.

[1] Unified theories allow proton decay. The approximate proton lifetime becomes large when the unification scale M_{GUT} is large. Experimental limits on the proton lifetime can therefore put limits on the unification scale of a specific theory.

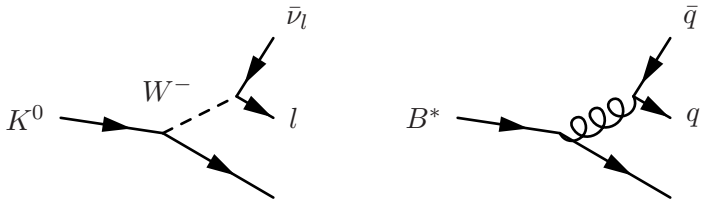

(a) Semileptomic weak decay

(b) Strong decay of an exited state

Figure 2.3.: Mesonic decay channels

2.3.2. Decays

The lifetime τ of unstable particles is the inverse of the total decay rate Γ which is sometimes also called decay width. The total decay rate is made out of the sum of rates of all channels c

$$\Gamma = \sum_c \Gamma_c \tag{2.19}$$

which is often dominated by a few selected channels. The quantity $B_c = \Gamma_c/\Gamma$ is called the branching fraction. Many theoretically possible channels are highly unlikely due to their kinematics and might never have been observed in experiment. Detection of forbidden decays and deviations from predicted decay rates Γ_c may indicate new physics or problems in our theoretical understanding.

Measurement of decay rates and branching ratios generally provide information about kinematics, matrix elements, couplings and masses. Although all interactions of the SM can facilitate decay processes (see fig. 2.3) we will in the following focus on weak decays of mesons and rely heavily on information taken out of [26]. These decays can be described by the coupling term

$$\frac{G_F}{\sqrt{2}} V_{q'Q} \left(\bar{q}' \gamma_\mu (1-\gamma_5) Q\right) \left(\bar{u}_l \gamma_\mu (1-\gamma_5) v_\nu\right) \tag{2.20}$$

in the weak interaction Hamiltonian which contains the CKM matrix element $V_{q'Q}$. This is necessary because strong and weak interaction do not couple to the same flavor states. The individual flavor bases are instead connected by the unitary CKM matrix [27]

$$\begin{pmatrix} d \\ s \\ b \end{pmatrix}_{\text{weak}} = V_{CKM} \begin{pmatrix} d \\ s \\ b \end{pmatrix}_{\text{strong}} = \begin{pmatrix} V_{ud} V_{us} V_{ub} \\ V_{cd} V_{cs} V_{cb} \\ V_{td} V_{ts} V_{tb} \end{pmatrix} \begin{pmatrix} d \\ s \\ b \end{pmatrix}_{\text{strong}} \tag{2.21}$$

which can be parametrized by 3 mixing angles θ_i and a CP violating phase δ_{13}. Further details of the CKM matrix will be discussed in section 2.4.1. If radiative QED corrections are ignored, the dynamics of the decay rate $\Gamma(M_{Q\bar{q}} \to X\, l\, \nu)$ are described by the

amplitude

$$\mathcal{M}\left(M_{Q\bar{q}} \to X\, l\, \nu\right) = -\mathrm{i}\frac{G_F}{\sqrt{2}} V_{q'Q} L^\mu H_\mu \tag{2.22}$$

which can be factorized into the leptonic current

$$L^\mu = \bar{u}_l \gamma^\mu (1-\gamma_5) v_\nu \tag{2.23}$$

and a hadronic current which is given by the non-perturbative QCD matrix element

$$H_\mu = \langle X | \bar{q}' \gamma_\mu (1-\gamma_5) Q | M \rangle. \tag{2.24}$$

Formulae for pure leptonic decay ($M \to l\nu$) can be obtained if $\bar{q}$ is the anti-quark of the decay product q' and $|X\rangle$ is assumed to be the vacuum. In this case decay constants f are used to describe the matrix element in the rest frame of the hadron. *Leading order* (LO) QED corrections to pure leptonic decay contain an infrared divergent photon [28]. The divergence cancels if the channel is combined with the corresponding radiative channel $M \to l\nu\gamma$. The hadronic matrix element in semi-leptonic decay channels

$$\begin{aligned}\langle X(p_f)|V_\mu(q^2)|M(p_i)\rangle = &\left[p_i + p_f - q\frac{m_i^2 - m_f^2}{q^2}\right]_\mu f_+(q^2) \\ &+ \left[q\frac{m_i^2 - m_f^2}{q^2}\right]_\mu f_0(q^2)\end{aligned} \tag{2.25}$$

can be parametrized with vector f_+ and scalar f_0 transition form factors [29] if the final state $|X\rangle$ is also a pseudoscalar. For small lepton mass m_l the q_μ terms are negligible and the differential decay rate can be approximated by

$$\frac{d\Gamma}{dq^2} = \frac{G_F^2 |V_{q'Q}|^2 p_f^3}{24\pi^3} \left|f_+(q^2)\right|^2. \tag{2.26}$$

Charged pion decay

The dominant charged pion decay channel is the pure leptonic process $\pi^\pm \to \mu\, \nu_\mu$. The energetically favored channel $\pi^\pm \to e\, \nu_e$ is suppressed by helicity. The generic $\pi^\pm \to l\, \nu_l$ decay rate is at tree level given by

$$\Gamma_0^{\text{tree}}(\pi^+ \to l^+ \nu_l) = \frac{G_F^2 \left|V_{ud}^2 f_\pi^2\right|}{8\pi} m_\pi m_l^2 \left(1 - \frac{m_l^2}{m_\pi^2}\right)^2 \tag{2.27}$$

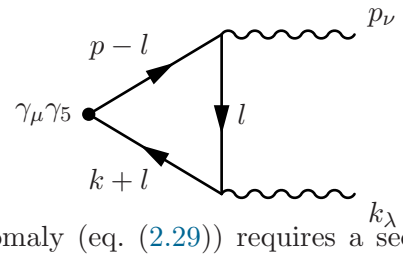

Figure 2.4.: The axial anomaly (eq. (2.29)) requires a second term with interchanged vector vertices.

where V_{ud} is the CKM matrix element that couples up and down type quarks[2], and the decay constant f_π describes the hadronic matrix element

$$\langle 0|A_0|\pi^\pm\rangle = \mathrm{i}m_{\pi^\pm} f_{\pi^\pm}, \tag{2.28}$$

where A_0 is the time component of the axial current $A_\mu = \bar{u}\gamma_\mu\gamma_5 d$. Depending on the definition of the states the value of f_π might differ by a factor of $\sqrt{2}$. Measurement of the $\pi^\pm$ lifetime τ and branching fractions are used to determine the $f_{\pi^\pm}$ value.

Knowledge of $f_{\pi^\pm}$ allows to determine $|V_{ud}|$ from the experimentally measured product $f_{\pi^\pm}|V_{ud}|$. The value of f_π in the chiral limit will turn out to be a fundamental parameter of an effective theory (χPT).

Neutral pion decay

Neutral pions have different decay channels and a slightly modified decay constant. Mass isospin breaking effects of $f_{\pi^0} \leftrightarrow f_{\pi^\pm}$ have been estimated in [25]. The dominating neutral pion decay rate $\Gamma(\pi^0 \to \gamma\gamma)$ (or the corresponding η decay) is formally strongly suppressed. This puzzle was solved in a sigma model description [31] and shortly afterwards in spinor electrodynamics [32]. The decay is allowed due to the non-conservation of the axial current, the so-called axial anomaly

$$\partial_\mu j^{\mu 5} = \partial_\mu \bar{\psi}\gamma_\mu\gamma_5\psi \propto g^2 \varepsilon^{\mu\nu\alpha\beta} F_{\mu\nu} F_{\alpha\beta} \tag{2.29}$$

which is illustrated by the triangle diagram in fig. 2.4. The approximate prediction

$$\Gamma(\pi^0 \to \gamma\gamma) = \frac{\alpha^2 m_\pi^3}{64\pi^3 f_{\pi^0}^2} \tag{2.30}$$

based on eq. (2.29) agrees reasonably well with experimental data. Amonst many phenomena, the axial anomaly is furthermore responsible for the large η' mass, the

[2] The CKM matrix element V_{ud} is well known from measurements of nuclear decay. Lattice calculations of the ratio f_K/f_π and experimental decay rates allow the subsequent determination of V_{us}[23, 30].

Goldberger-Treiman [33] relation[3]

$$g_A = \frac{f_\pi}{m_N} g_{\pi NN} \tag{2.31}$$

and can be used to derive relations for $\pi - \pi$ and $\pi - N$ scattering [15].

Nowadays the rate (eq. (2.30)) is measured indirectly through Primakoff experiments $\gamma A \to \pi^0 A$ experiments [34, 35] by $\gamma\gamma \to \pi^0$ fusion. Results from these experiments are model dependent, due to a large hadronic background. The newly proposed experiment `KLEO-2` utilizes π^0 production from $\gamma\gamma$ fusion in e^+e^- scattering [36, 37] and simulations promise 1% level accuracy.

The decay width $\Gamma(\pi^0 \to \gamma\gamma)$ is used as a constraint for effective models [38], which can be used to calculate the hadronic contribution to the muon anomalous magnetic moment. Alternatively, LQCD calculations [39] provide results from first principle.

2.3.3. Scattering

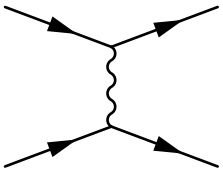

Figure 2.5.: Leading order elastic scattering of two fermions.

Scattering experiments played a vital role in the development of QFT and QCD in particular. As previously mentioned DIS of electrons on a fixed proton target at the *Stanford Linear Accelerator Center* (SLAC) found scaling and therefore point-like partons which were later identified as quarks [40]. Experiment with an e^-e^+ storage ring at SLAC found the heavy τ lepton [41, 42].

Scattering is also important for the investigation of the weak interaction and the CKM matrix. Proton-antiproton collisions at *super proton synchrotron* (SPS) provided sufficient energy for the creation of the weak gauge bosons $W^\pm, Z^0$ and the detection of their signatures [43, 44]. Furthermore collision with asymmetrical beam energies proofed to be highly useful. The B factories BaBar [45] and Belle [46] tune their center of mass energy to the $\Upsilon(4S)$ resonance which decays with to 25% to a $B_d^0 - \overline{B_d^0}$ meson state. The forward rapidity prolongs the lifetime of these mesons and allows testing of CP, T and CPT invariance [47].

Scattering of gold nuclei at the *relativistic heavy ion collider* (RHIC) led to the discovery of the *quark gluon plasma* (QGP) a strongly interacting, high temperature phase of nuclear matter that appears to contain deconfined quarks and to be a liquid with almost minimal viscosity [48]. Lastly inclusive measurements at high energies at the *large hadron collider* (LHC) led to the discovery of the Higgs boson [2].

[3] Experimental results agree within approximately 15%.

2.3.4. Beyond the standard model

In light of the fact that the standard model is merely an effective theory for the observable universe the question arises how to detect violations and discover the nature of a - *or* the - underlying theory. One possibility is to detect small deviations in scattering or decay processes predicted by the standard model. These follow from the fact that hidden couplings at large energies (never or currently not accessible by experiments) may modify the effective interaction. Comparing standard model predictions with experimental results yields bounds on, or in case of actual violations hints at, possible extensions.

2.4. Symmetries

Symmetry means the invariance of an equation or physical law under a transformation ω. Symmetries of the action and the Lagrangian are important in classical physics, special and general relativity, in quantum mechanics, in QFT and in particular in gauge theories which use gauge invariance to introduce interaction. Weak violations of symmetries are often negligible or can be treated as a perturbation. There are discrete symmetries (often used for selection rules and classifying states) and continuous symmetries which have associated conserved currents. Transformations can be further distinguished to be global ω_g or local transformations $\omega_l(x)$. Symmetries of a physical (quantum) system can spontaneously break, meaning the groundstate of such a system does not obey the symmetry of the action. Every spontaneously broken, continuous symmetry yields a massless mode, a so-called Nambu-Goldstone boson. Spontaneous symmetry breaking is responsible for a wide range of physical phenomena such as Bose-Einstein condensation, super conductors, the light pion masses and many more.

2.4.1. Discrete symmetries

Discrete symmetries are often used to distinguish bound states and isolate the contributions to scattering processes. The parity operator P mirrors space $(t, \mathbf{x}) \to (t, -\mathbf{x})$, the time reversal operator T does the same with time $(t, \mathbf{x}) \to (-t, \mathbf{x})$ and charge conjugation C interchanges particles and antiparticles. All of these symmetry operations have eigenvalues $\eta_\pm = \pm 1$. Many of the meson resonances[4] observed in experiments have definite P and C quantum numbers in accordance with quark bilinears. Time reversal symmetry T is violated by the second law of thermodynamics.

Naively QCD and QED are invariant under these transformation, but parity P and charge conjugation C are maximally violated by the weak interaction because of its chiral components. This was initially suggested by Lee and Yang in 1956 [49] and subsequently observed in ^{60}Co β decay [50] as well as in π^+ and μ^+ decay [51]. QCD theory allows parity P to be broken by the so-called θ term. Recent experiments suggest to have found local parity violation of QCD in quark gluon plasma bubbles [52] although the interpretation of the data is under debate [53–55].

[4] Only uncharged mesons are eigenstates of C.

The combined symmetry of charge conjugation and parity CP is violated by a small amount which is described by the phase δ_{13} in the CKM matrix that violates the symmetry explicitly. It can be shown that the combined CPT symmetry is preserved. CP violation, which can be found in B meson and kaon (K^0) physics, can be categorized to be direct, indirect or both. All unitary triangles have equal area proportional to the phase δ_{13}. The CKM matrix can be connected to the Yukawa couplings of Higgs field and quarks, which do not need to be diagonal. Diagonalization yields the quark masses and unitary matrices which can be combined to the therefore naturally unitary CKM matrix [26].

2.4.2. Isospin and chiral symmetry

The similarity of proton and neutron despite their different charges led to their classification as different (isospin) states of the nucleon and therefore isospin ($SU(2)$ flavor) symmetry of the strong interaction. Similary the 3 pions (π^+, π^0, π^-) and other sets of hadrons could be classified as multiplets of isospin states. The extended, approximate $SU(3)$ flavor symmetry is suggested by the mass spectrum of light, spin 1/2 baryons which can be described by an octet, the so-called *Eightfold way* [56].

Current algebra predicted many low energy relations such as the Goldberger - Treiman (eq. (2.31)) and the Gell-Mann - Oakes - Renner relation (GMOR) [57]

$$F_\pi^2 M_\pi^2 = (m_u^{(r)} + m_d^{(r)})\Sigma^{(r)} \tag{2.32}$$

describing light pseudoscalar masses in dependence of renormalized quark masses $m^{(r)}$ and chiral condensate $\Sigma^{(r)} = \langle \bar{q}q \rangle$. The positive and finite constant F_π is the pion decay constant in the chiral limit.

As previously mentioned, light quark masses $m_{u,d}$ are small compared to the scale Λ_{QCD}. Projectors $P_\pm = (1 \pm \gamma_5)/2$ can be used to separate spinors into left- and right-handed components $\psi_{L,R} = P_\mp \psi_{L,R}$ and $\overline{\psi}_{L,R} = \overline{\psi}_{L,R} P_\pm$. The fermion Lagrangian of QCD is then written as

$$\mathcal{L}_{QCD} = \overline{\psi}_L \not{D} \psi_L + \overline{\psi}_R \not{D} \psi_R + \overline{\psi}_L M \psi_R + \overline{\psi}_R M \psi_L \tag{2.33}$$

with the spinors $\psi = (u, d)^T, \overline{\psi} = (\overline{u}, \overline{d})$ and the mass matrix $M = \mathrm{diag}(m_u, m_d)$. Vanishing light quark masses make the (light quark) action invariant under flavor transformations that can be decomposed into

$$SU(2)_L \times SU(2)_R \times U(1)_V \times U(1)_A. \tag{2.34}$$

The $SU(2)$ transformations correspond to independent flavor rotations ω_L and ω_R of left- and righthanded field which are spontaneously broken to $SU(2)_V : \omega_L = \omega_R$ flavor symmetry by the chiral condensate $\langle \bar{q}q \rangle$. The $U(1)$ vector symmetry enforces baryon number conservation and the remaining $U(1)$ axial symmetry is broken on the quantum level due to the axial anomaly discussed in section 2.3.2.

The arguments above can also be extended to $SU(3)_L \times SU(3)_R$ symmetry by treating the strange quark as light. The experimental observed mass gap between pseudo Goldstone bosons and other light hadrons as well as the absence of parity doubling $m(P = +1) \neq m(P = -1)$ suggest that chiral symmetry is spontaneously broken. Following the textbook knowledge on symmetry breaking, Noether's theorem states that every continuous symmetry (of the action) is associated with a conserved current. Furthermore Goldstone's theorem states that for every spontaneously broken continuous symmetry there is a corresponding massless mode, the so-called Goldstone boson. Those turn out to be the light pseudoscalars, which will be - due to non-vanishing physical quark masses - (massive) pseudo Nambu-Goldstone bosons.

χPT

Chiral perturbation theory (χPT) is an effective theory based on chiral symmetry which naturally reproduces the low energy relations from current algebra [58, 59]. Its degrees of freedom are the previously mentioned light pseudoscalar fields. Explicit breaking by quark masses can be included as currents that perturb chiral symmetry. One distinguishes $SU(2)$ and $SU(3)$ χPT which ex- and include the strange as a light quark. Treating the strange quark as light does not converge well. Most of the following information is taken out of [60], other instructive summaries are [61, 62].

Experimental data of hadronic quantities shows a separation of scales

$$p_\pi \propto m_\pi \ll m_\rho, m_N. \tag{2.35}$$

χPT separates those scales by introducing an intermediate scale Λ, integrating out the energies above and replacing them by effective, local interactions (of size Λ^{-1}) as illustrated in fig. 2.6. Instead of explicitly integrating out the degrees of freedom, it is sufficient to identify the symmetries of the microscopic theory, the new degrees of freedom and include all possible interactions that are allowed up to an specific order that one decides to work at. The order of an interaction depends on the power counting. After truncation the remaining task is to determine the values of so-called *low energy constants* (LEC), the unknown couplings of our new vertices, from experimental or lattice data. These values depend on the order of the truncation and are assumed to follow a hierarchy. Some of them can be estimated or are bound by phenomenology. It is inevitable that the truncated series breaks down at scales above Λ.

The effective theory can be extended/adjusted for various applications. Examples include additional coupling to an external electromagnetic field, inclusion of baryon resonances, estimation of finite volume effects, discretization artifacts, partial quenching and heavy baryons. χPT and other effective theories are required for the extrapolation of LQCD results to the physical limit.

χPT predicts chiral logarithms, which describe the dynamics of the new degrees of freedom, e.g. the pion loops. These contributions have no additional free parameters. Although LQCD is often well described by χPT without chiral logarithms [63], is has recently been able to resolve them [24].

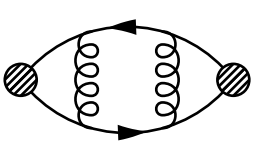

(a) QCD Feynman diagram contributing to a meson correlator.

(b) Tadpole contribution to a meson mass in χPT.

Figure 2.6.: An effective field theory (fig. 2.6b) can approximate the dynamics of the microscopic theory (fig. 2.6a). Note that the diagrams above are not their respective equivalents.

Note that naive chiral Lagrangians have, in contrast to the microscopic theory of QCD, an additional symmetry P_0 leaving them invariant under interchange of $U \leftrightarrow U^\dagger$ [5]. The so-called Wess-Zumino-Witten term reduces this symmetry to the real parity $P = (-1)^{N_B} P_0$ and inserts the axial anomaly into the effective theory [64].

[5] The variable U represents the effective fields and can be written as an exponentiated matrix of pseudoscalar fields.

3. Lattice QCD

In this chapter I want to introduce the basic concepts of Lattice QCD and the methods relevant to the simulation described in chapter 5. The current status of simulations that include QED and some of its subtleties will be discussed in the following chapter 4.

After discussing the discretization of the QCD path integral and the Wilson fermion action, the representation of the gauge fields is addressed. The generation of suitable ensembles and the algorithms required for importance sampling are explained in section 3.2, which is followed by section 3.3 where techniques for the measurement of euclidean correlation functions are described. The chapter is concluded by section 3.4 that examines the physical limit including continuum, chiral and infinite volume extrapolations as well as improvement and renormalization.

Good and more extensive introductions into Lattice QCD, on which I relied heavily in the following summary, are [65–68]. Short available primers are [69, 70]. An extensive and useful review of current results is [14].

3.1. Making the QCD path integral finite

To tackle the non-perturbativeness of low energy QCD it is useful to see how a correlation function of two operators $\mathbf{O}_2(t), \mathbf{O}_1(0)$ is expressed in the path integral formulation of quantum field theories [68]. After a Wick rotation $t \to \tau = -\mathrm{i}t$ the correlation function is written as

$$\begin{aligned}\langle\Omega|\mathbf{O}_2(t)\mathbf{O}_1(0)|\Omega\rangle_T &= \frac{1}{Z_T}\mathrm{tr}\left[\mathrm{e}^{-(T-t)\hat{H}}\hat{\mathbf{O}}_2\mathrm{e}^{-t\hat{H}}\hat{\mathbf{O}}_1\right] \\ &= \frac{1}{Z_T}\int \mathcal{D}[\phi]\,\mathrm{e}^{-S_e[\phi]}\mathbf{O}_2[\phi(\cdot,t)]\mathbf{O}_1[\phi(\cdot,0)], \end{aligned} \tag{3.1}$$

where $|\Omega\rangle$ denotes the vacuum state, $\hat{H}$ is the Hamilton operator, S_e is the euclidean action, and T refers to a time scale, which is significantly larger than the time separation of the operators. In the limit $T \to \infty$, the correlation functions can be related to energies E_n and matrix elements $\langle n|\mathbf{O}|m\rangle$.

$$\lim_{T\to\infty}\frac{1}{Z_T}\mathrm{tr}\left[\mathrm{e}^{-(T-t)\hat{H}}\hat{\mathbf{O}}_2\mathrm{e}^{-t\hat{H}}\hat{\mathbf{O}}_1\right] = \sum_n \langle\Omega|\hat{\mathbf{O}}_2|n\rangle\langle n|\hat{\mathbf{O}}_1|\Omega\rangle\,\mathrm{e}^{-tE_n} \tag{3.2}$$

$$\text{with} \qquad Z_T = \mathrm{tr}\left[\mathrm{e}^{-T\hat{H}}\right] \tag{3.3}$$

To compute correlation functions such as eq. (3.1) and therefore determine masses and matrix elements through eq. (3.2), spacetime is discretized and restricted to a lattice in

the finite volume $V = L_x L_y L_z L_t$, as first worked out in [12]. The remaining spacetime points are

$$x_\mu \to \tilde{x}_\mu = a m_\mu \qquad \text{with} \quad m_\mu \in [0, L_\mu - 1] \tag{3.4}$$

where $\mu = 0 \ldots 3$ represents time and three spatial components. This yields a finite dimensional integration which can be evaluated stochastically by generating an ensemble of representative configurations $[\phi]$ and averaging over them. To estimate continuum quantities simulations at several lattice spacings a and volumes V need to be extrapolated towards $a \to 0$ and $V \to \infty$, which is discussed in section 3.4. It will also turn out that the computation at physical quark masses - especially on large lattice volumes - is computationally expensive and that the computation is often carried out at heavier quark masses and then extrapolated towards physical values. The required theory is briefly described in section 2.4.2.

The remaining tasks are finding a suitable discretized version of gauge and fermion action and generating the representative ensemble of configurations. Afterwards lattice interpolators can be combined to build correlation functions which yield masses and matrix elements. All such operators suffer from discretization effects such as mixing and the breaking of rotational symmetry which is restored in the continuum limit. If operators mix with lower dimensional representations the continuum limit becomes especially difficult. The generation of configurations is discussed in section 3.2. The following paragraph addresses gauge invariance before the discretization of the QCD action S_{QCD} is introduced in section 3.1.2.

3.1.1. Gauge invariance

The $SU(3)$ gauge invariance of the fermion fields $\overline{\psi}, \psi$ - and therefore their action - can be assured if oriented link variables U_μ connect neighboring sites

$$\begin{aligned} \overline{\psi}(n) U_\mu(n) \psi(n+\hat{\mu}) \quad &\to \quad \overline{\psi}'(n) U'_\mu(n) \psi'(n+\hat{\mu}) \\ &= \quad \overline{\psi}(n) \Omega(n)^\dagger U'_\mu(n) \Omega(n+\hat{\mu}) \psi(n+\hat{\mu}) \end{aligned} \tag{3.5}$$

and the gauge transformation Ω of the links is defined by

$$U_\mu(n) \to U'_\mu(n) = \Omega(n) U_\mu(n) \Omega(n+\hat{\mu})^\dagger. \tag{3.6}$$

These links will become our new, compact degrees of freedom for the gauge fields. They are the discretized approximation

$$U(n) = \exp\big(\mathrm{i} a A(n)\big) \tag{3.7}$$

of path-ordered, continuum, gauge transporters

$$G(x,y) = P\exp\left(\mathrm{i}\int_{\mathcal{C}_{xy}} A\cdot \mathrm{d}s\right), \tag{3.8}$$

between two neighboring sites $x = an, y = an + a\hat{\mu}$. The approximation is correct up to order $\mathcal{O}(a)$, at which no path-ordering (P) is necessary.

The links obey the following relation

$$U_{-\mu}(x) = U_{\mu}^{-1}(x-\hat{\mu}) = U_{\mu}(x-\hat{\mu})^{\dagger} \tag{3.9}$$

because U_μ is unitary and directional. Note that any closed loop of links variables is automatically gauge invariant.

3.1.2. The discretized Dirac operator

For the fermion action the continuum Dirac equation has to be mapped onto the lattice. Its naive derivative discretization is

$$\partial_\mu\psi(x) = \frac{1}{2a}\big(\psi(x+\hat{\mu}) - \psi(x-\hat{\mu})\big). \tag{3.10}$$

Examining the Fourier transformed operator of this free, massless theory in a box with discrete spacetime points it is easy to see that the inverse of the operator $\gamma_\mu p_\mu$ has unphysical poles at the boundaries of the Brillouin zone $p_\mu = \pi/a$ which are called doublers. These doublers can be removed by an additional term that vanishes in the continuum. The result is the so-called Wilson Dirac operator

$$\mathcal{D}_W^{(f)}(y \leftarrow x) = \left(m^{(f)} + \frac{4}{a}\right)\delta_{xy} - \frac{1}{2a}\sum_{\mu=\pm1}^{\pm4}(\mathbb{1}-\gamma_\mu)\,U_\mu(x)\delta_{y+\hat{\mu},x} \tag{3.11}$$

which already incorporates the gauge links U_μ for gauge invariance. This non-unique choice of the Dirac operator lattice discretization is commonly rewritten as $\mathcal{D}_W = C(\mathbb{1} - \kappa H)$, where the normalization $C = m + 4/a$ is absorbed into the definition of the fields $[\bar{\psi}, \psi]$, $\kappa = (2(am+4)^{-1}$ is called the hopping parameter and the hopping term

$$H(y \leftarrow x) = \sum_\mu (\mathbb{1}-\gamma_\mu)\,U_\mu(x)\delta_{y+\hat{\mu},x} \tag{3.12}$$

collects all the derivatives. The additional term comes at a price since it does break chiral symmetry of the massless Dirac operator explicitly. A theorem by Nielsen and Ninomyia states that there cannot be a lattice regulated theory free of doublers and obeying chiral symmetry [71]. This is often referred to as the no-go theorem. A possible solution to this problem is to only require chiral symmetry restoration in the continuum

as expressed by the Ginsparg-Wilson equation

$$\mathcal{D}\gamma_5 + \gamma_5\mathcal{D} = a\,\mathcal{D}\,\gamma_5\,\mathcal{D}. \tag{3.13}$$

The relation, which was found in [72], was put to use in 1997/98, when two Dirac operators obeying above equation where found [73, 74].

An important property of all discretized Dirac operators which are discussed here is that they are γ_5 hermitian:

$$\mathcal{D}^\dagger(n,m) = \gamma_5\,\mathcal{D}(m,n)\,\gamma_5 \tag{3.14}$$

This property is also inherited by quark propagators $\mathcal{M}$ which are the inverse of the Dirac operator $\mathcal{M} = \mathcal{D}^{-1}$.

3.1.3. Gauge action

The field strength tensor in the continuum gauge action (eq. (2.10)) can be interpreted as a generalized curl of the gauge potential. This motivated Wilson to propose a gauge action made out of small loops. The smallest loop (illustrated in fig. 3.1)

$$\begin{aligned} P_{\mu\nu}(m) &= U_\mu(m)U_\nu(m+\hat{\mu})U_{-\mu}(m+\hat{\mu}+\hat{\nu})U_{-\nu}(m+\hat{\nu}) \\ &= U_\mu(m)U_\nu(m+\hat{\mu})U_\mu(m+\hat{\nu})^\dagger U_\nu(m)^\dagger \end{aligned} \tag{3.15}$$

is called the plaquette. The unique sum over all available plaquettes turned out to converge to the continuum gauge action in the limit $a \to 0$. This so-called Wilson plaquette action is defined by

$$S_G[U] = \frac{\beta}{3}\sum_{m\in V}\sum_{\mu<\nu}\mathrm{Re}\,\mathrm{tr}\,[\mathbb{1} - P_{\mu\nu}(m)] \tag{3.16}$$

with $\beta = 6/g_0^2$ and is equal to $\sum_m F_{\mu\nu}(m)^2$ up to corrections of $\mathcal{O}(a^2)$. Generalizations for different number of colors N_c are straight forward.

3.1.4. Improved actions

The gauge and fermion action presented before have cut-off effects of $\mathcal{O}(a^2)$ and $\mathcal{O}(a)$ respectively. These orders can be improved by following the Symanzik improvement program [75]. Please note that hadronic matrix elements and quark masses are also subject to discretization errors which can and should be improved following the same program.

The $\mathcal{O}(a)$ cutoff effects of the Wilson fermion action can be removed if the Sheikholeslami-Wohlert term [76]

$$S_F^{\mathrm{sw}}[\overline{\psi},\psi,U_\mu] = c_{\mathrm{sw}}a^5\sum_n\sum_{\mu<\nu}\overline{\psi}(n)\frac{1}{2}\sigma_{\mu\nu}\hat{F}_{\mu\nu}(n)\psi(n) \tag{3.17}$$

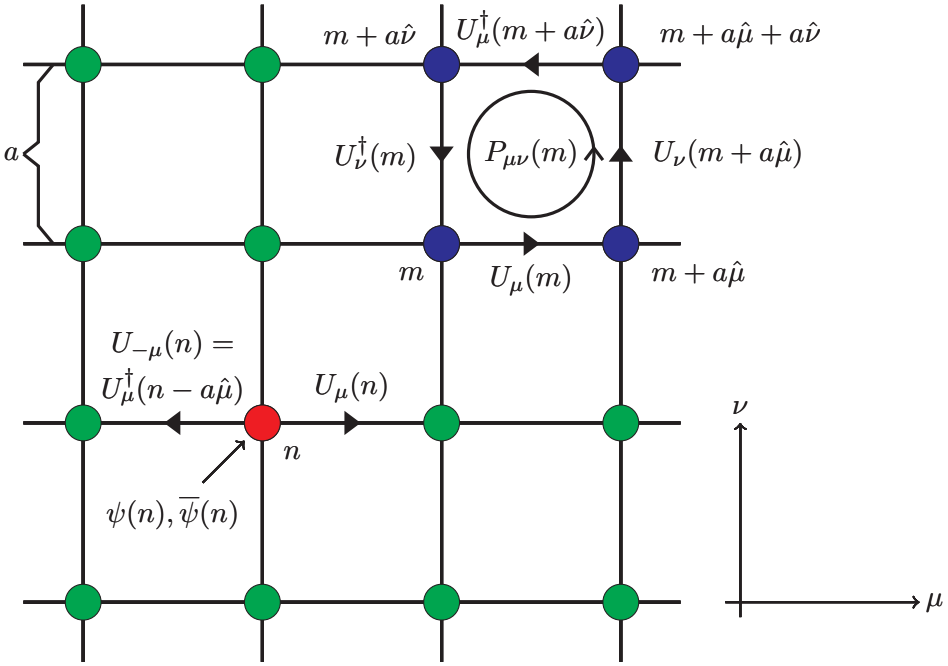

Figure 3.1.: Fermion fields $\psi(m)$, link variables $U_\mu(m)$, and the plaquette $P_{\mu\nu}(m)$ in the μ-ν-plane of the lattice Λ.

is added. A common choice for the discretization of the field strength tensor $\hat{F}_{\mu\nu}$ is

$$\hat{F}_{\mu\nu}(n) = \frac{1}{8a^2}\left[Q_{\mu\nu}(n) - Q_{\mu\nu}^\dagger(n)\right] \tag{3.18}$$
$$\text{with} \qquad Q_{\mu\nu}(n) = P_{\mu,\nu}(n) + P_{\nu,-\mu}(n) + P_{-\mu,-\nu}(n) + P_{-\nu,\mu}(n).$$

The variables $P_{\pm\mu,\pm\nu}$ refer to plaquettes (eq. (3.15)) of different orientations. Due to the pictorial representation (fig. 3.2) of $\hat{F}_{\mu\nu}$ the extra term is often called Clover term. The coefficient c_{sw} depends on gauge and fermion parameters. It can be determined perturbatively as well as non-perturbatively. The tree level value is 1.

Improved gauge actions incorporate extended plaquettes. The weights of the individual extended plaquettes are restricted by positivity of the action. The remaining degrees of freedom can be determined by different, non-unique criteria. Improvement of spectral quantities to first order in perturbation theory yields the so-called Lüscher-Weisz action S_{LW}[77]. Renormalization group considerations motivate other choices, e.g. the so-called Iwasaki action [78]. Note that this improvement does not remove leading order gauge action cut-off effects of any observable.

Fermion actions can be further improved by smearing the links (see section 3.3.3) of the covariant derivative. Smeared Wilson fermions break chiral symmetry in a much milder way than their thin link counterparts [79]. Furthermore smearing stabilizes the generation of configurations [80].

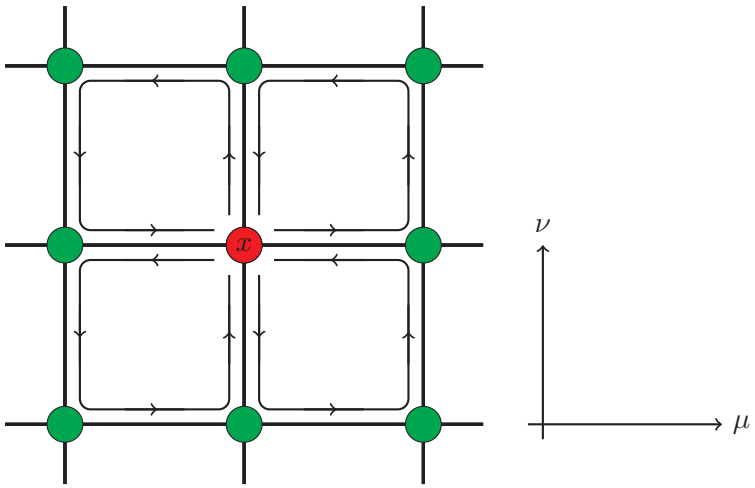

Figure 3.2.: Clover term

3.2. Gaugefield generation

So far the partition function is integrated over all possible discretized field configurations $[\bar{\psi}, \psi, U_\mu]$. Instead of performing the full integral over gauge and fermion fields, the fermion part of the lattice QCD action can be integrated out analytically [81] due to the fact that the fermion field variables are represented by Grassman variables $\eta_{m,f}$. The expectation value of an operator therefore becomes

$$\begin{aligned}\langle \mathbf{O} \rangle &= \frac{1}{Z} \int \mathcal{D}[\bar{\psi}, \psi, U_\mu] \cdot \mathbf{O}[\bar{\psi}^{f_1}, \psi^{f_2}, U_\mu] \cdot \mathrm{e}^{-S_G[U_\mu] - \sum_x \sum_f \bar{\psi}^f \mathcal{D} \psi^f} \\ &= \frac{1}{Z} \int \mathcal{D}[U_\mu] \cdot \mathbf{O}[\mathcal{M}^{f_1}, \mathcal{M}^{f_2}, U_\mu] \cdot \mathrm{e}^{-S_G[U_\mu]} \cdot \prod_f \det \mathcal{D}^f \end{aligned} \tag{3.19}$$

with the partition function

$$Z = \int \mathcal{D}[U_\mu] \cdot \mathrm{e}^{-S_G[U_\mu]} \cdot \prod_f \det \mathcal{D}^f \tag{3.20}$$

as normalization.

The remaining multi-dimensional integral over $[U_\mu]$ on all sites of the lattice is evaluated by means of importance sampling techniques: Samples are drawn from the finite-dimensional and continuous configuration space. Instead of directly generating suitable configurations an updating algorithm is used that transforms the current configuration into a new one. This is done with Monte Carlo methods. Several such methods are commonly used [82]:

- Metropolis: Loop over sites and apply probable transitions from the current value.

- Heatbath: Loop over sites and find suitable alternative values without using the current value.
- Hybrid Monte Carlo (HMC) [83]: Treat fields as generalized coordinates, introduce random conjugate momenta to the action and evolve this system in an additional Monte Carlo time. The conjugate momenta must be redrawn periodically. Accept reject steps are necessary.

The generation of a new ensemble can either start from a unit configuration or a random $SU(3)$. The first is commonly called a cold start and represents the free theory, whereas the latter is called a hot start representing infinite coupling. Both starting points require the trajectory to thermalize before measurements provide reliable data [68].

Also note that successive configurations are usually not independent. In theory, measurements should only be performed on configurations that are farther apart in Monte Carlo time than the integrated autocorrelation time τ_{int} of the most correlated variable or one should correctly account for the error [84]. Typically, the topological charge is assumed to have an appropriately large autocorrelation time.

In summary after choosing a suitable action an ensemble of lattice gauge configurations depends on a small number of important parameters. The gauge coupling β determines the approximate lattice spacing a and the hopping parameter κ or the bare mass m_0 for the individual quarks is responsible for the mass of the sea quarks. The lattice spacing and the volume $V = N_s^3 \times N_t$ set temperature T and physical volume. The action might include an ambiguous choice of improvement parameters. Note that the mapping between bare and physical values usually depends on all parameters: e.g. the mass of a sea quark depends on the choice of the action including the number of flavors, the lattice spacing (and therefore on β) and lastly on the bare mass parameter κ or m_0. In practice HMC simulations require additional parameters to set the length of a trajectory, separate the integration of low modes from high modes, tune the acceptance rate and ultimately influence the autocorrelation time.

3.3. Measurement of correlation functions

One of the most important quantities lattice QCD provides are hadronic correlators. They are measured by constructing hadronic creation and annihilation operators such as the local mesons interpolators

$$O_a(x) = \overline{\psi}^{f_1}(x)\,\Gamma_a\,\psi^{f_2}(x)\,, \quad \overline{O}_b(y) = \overline{\psi}^{f_2}(y)\,\Gamma_b\,\psi^{f_1}(y) \tag{3.21}$$

which are then combined into a suitable trace upon which the necessary wick contractions

$$\begin{aligned}\left\langle O_a(x)\overline{O}_b(y)\right\rangle &= \left\langle \overline{d}(x)\Gamma_a u(x)\overline{u}(y)\Gamma_b d(y)\right\rangle \\ &= \left\langle \mathcal{M}_d(x\leftarrow y)\Gamma_a\mathcal{M}_u(x\leftarrow y)\Gamma_b\right\rangle \\ &= \left\langle \gamma_5\mathcal{M}_d(y\leftarrow x)^\dagger\gamma_5\Gamma_a\mathcal{M}_u(x\leftarrow y)\Gamma_b\right\rangle \end{aligned} \tag{3.22}$$

are preformed. These correlators must be averaged over all color indices to become gauge invariant. Note that if the quark types are identical - as for a hypothetic $q\bar{q}$ meson - it is furthermore necessary to contract the quarks locally. The hadronic two point function then contains an additional disconnected contribution

$$\left\langle O_a(x)\overline{O}_b(y)\right\rangle_{\text{disc.}} \propto \left\langle \gamma_5\mathcal{M}_q(y\leftarrow y)^\dagger\gamma_5\Gamma_a\mathcal{M}_q(x\leftarrow x)\Gamma_b\right\rangle. \tag{3.23}$$

3.3.1. Quark sources and propagators

The full propagator $\mathcal{M}$ is a complex matrix of size $(N_c\times N_s\times V)^2$ which does not fit into the memory of current computer architectures at quark masses and volumes required to take the physical limit. Instead of inverting the full matrix, one uses the translational invariance (in the ensemble average) of the problem and inverts only a few suitably chosen columns

$$\mathcal{D}\psi=\eta \quad\rightarrow\quad \psi=\mathcal{D}^{-1}\eta \tag{3.24}$$

which will be referred to as quark sources η, where the Dirac operator $\mathcal{D}$ is a large sparse matrix, the source η is known and ψ is the desired solution. This is a common problem in linear algebra which can be solved by Krylov subspace based algorithms like `CG` [85], `BiCGStab` [86] or `GMRES` [87]. All of these show critical slowing down when the lattices become larger and the light quark masses approach physical values. Recently (algebraic) multigrid methods have been developed that overcome this problem [88, 89]. They require a (costly) setup that can be reused for arbitrarily many fast solves on the same configuration.

One-end trick

The signal to noise ratio of hadronic correlators can be improved by stochastic wall sources, most notably for momentum zero. The requirement to compute $N_sN_c=12$ sources can be circumvented for mesons by also seeding the color and spin indices. The combined method for a single specific spin contraction was first introduced in [90].

Consider a generic meson two-point function $C_\Gamma(\tau=t'-t,\mathbf{p})$ after Wick contraction. Instead of inverting only one column of the matrix - like for a local source - a stochastic

identity

$$\frac{1}{N_k}\sum_{k=1}^{N_k}\eta^k\eta^{k*} = \mathbb{1} + \mathcal{O}\left(N_k^{1/2}\right) \tag{3.25}$$

with complex $\mathbb{Z}_2$ noise vectors

$$\eta^k_{\alpha,c} = \frac{1}{\sqrt{2}}\left(r_{1,k} \pm \mathrm{i} r_{2,k}\right) \tag{3.26}$$

seeded on the source time slice t, is inserted between the desired propagators:

$$\begin{aligned} C_\Gamma(\tau,\mathbf{p}) &= \sum_{\mathbf{x},\mathbf{y}} \mathrm{e}^{-\mathrm{i}\mathbf{p}(\mathbf{y}-\mathbf{x})} \times \mathrm{tr}\left[\Gamma\mathcal{M}_1(\mathbf{y},t'\leftarrow\mathbf{x},t)\Gamma\mathcal{M}_2(\mathbf{x},t\leftarrow\mathbf{y},t')\right] \\ &= \frac{1}{N_k}\sum_{k,\mathbf{y}} \mathrm{e}^{-\mathrm{i}\mathbf{p}(\mathbf{y}-\mathbf{x})} \times \mathrm{tr}\left[\Gamma\mathcal{M}_1(\mathbf{y},t'\leftarrow\mathbf{x},t)\eta^k\eta^{k*}\Gamma\mathcal{M}_2(\mathbf{x},t\leftarrow\mathbf{y},t')\right]. \end{aligned} \tag{3.27}$$

The sum over $\mathbf{x}$ is replaced by an stochastic average, and after identifying

$$\begin{aligned} \chi^k_{1,\mathbf{0}} &= \mathcal{M}_1(\mathbf{y},t'\leftarrow\mathbf{x},t)\eta^k \\ \chi^{k,\Gamma}_{2,\mathbf{p}} &= \mathcal{M}_2(\mathbf{y},t'\leftarrow\mathbf{x},t)\Gamma\mathrm{e}^{\mathrm{i}\mathbf{p}\mathbf{x}}\eta^k, \end{aligned} \tag{3.28}$$

the contraction becomes a simple scalar product

$$C_\Gamma(\tau,\mathbf{p}) = \left\langle \chi^{k,\Gamma}_{2,\mathbf{p}} \,\middle|\, \Gamma\chi^k_{1,\mathbf{0}} \right\rangle. \tag{3.29}$$

Note that one can use different operators $\mathcal{M}_1 \neq \mathcal{M}_2$, insert smearing at source, sink or both, or use other noise (as long as eq. (3.25) is fulfilled). A generalization to compute all spin combinations by using an explicit spin is presented in [91]. This is also known as spin dilution.

3.3.2. Quark wave functions

Hadrons are extended objects and an improved overlap with physical quark wave functions demands extended quark sources. Approximately Gaussian wave functions can be constructed by iterating the following update procedure

$$\psi_{n+1}(x) = \frac{1}{1+2(N_d-1)\kappa}\left[\psi_n(x) + \kappa\sum_i U_i\psi_n(x+\hat{\imath}) + U_i\psi_n(x-\hat{\imath})\right] \tag{3.30}$$

where the number of iterations N and the parameter κ control the width. This is commonly called Wuppertal smearing [92]. Other methods include a superposition of different number of smearings [93], specialized smearing for momentum source [94], using low eigenmodes of the 3D Laplacian [95], and Jacobi smearing [96]. Jacobi smearing

provides wave functions with a sharper peak and longer tails than Wuppertal smearing.

3.3.3. Gauge Smearing

High frequency fluctuations of the gauge fields make the quark smearing techniques erratic and significantly distort the resulting source [97]. Using a smeared gauge field for quark smearing will damp these fluctuations which the wave function should anyway be insensitive to. There are several (iterative) methods most of which rely on the sum of alternate paths such as the staple

$$U_\mu^s(m) = \sum_{\pm\nu\neq\mu} U_\nu(m) U_\mu(m+\hat{\nu}) U_{-\nu}(m+\hat{\mu}+\hat{\nu}) \tag{3.31}$$

which is no longer $\in SU(3)$. Gauge smearing is slightly more complicated then quark smearing because the smeared gauge link $\tilde{U}_\mu$ must still remain in the group $SU(3)$. An APE link smearing iteration [98] just averages the original link and the attached staple

$$U_\mu^{(n)}(m) \to U_\mu^{(n+1)}(m) = \mathcal{P}_{SU(3)} \left(\alpha^{\mathrm{APE}} U_\mu^{(n)}(m) + U_\mu^{s,(n)}(m) \right) \tag{3.32}$$

with intermediate non-analytical back projection

$$\mathcal{P}_{SU(3)} V = X \in SU(3) \quad \text{for} \quad \max \mathrm{Re}\,\mathrm{tr} \left[X V^\dagger \right] \tag{3.33}$$

Another method called HYP smearing sums all paths within the hypercubes attached to the original link [99].

An alternative to the above are multiplicative smearing procedures whose fat links remain in the same group as the thin links. They require no projection, allow thin link derivatives (and forces) and can therefore be used to modify the dynamic fermions in the HMC. The simplest example Stout smearing [100] has the following iteration prescription

$$\begin{aligned} U_\mu^{(n+1)}(m) &= \mathrm{e}^{\mathrm{i}Q_\mu(m)}\, U_\mu^{(n)}(m) \\ \text{with} \qquad Q_\mu(m) &= \frac{\mathrm{i}}{2} \left(\Omega(m) - \Omega(m)^\dagger - \frac{\mathbb{1}}{3} \mathrm{tr} \left[\Omega(m) - \Omega(m)^\dagger \right] \right) \\ \text{and} \qquad \Omega(m) &= \sum_{\pm\mu\neq\nu} \rho_{\mu\nu} U_{\mu\nu}^{s,(n)}(m)\, U_\mu^{(n)}(m)^\dagger \end{aligned} \tag{3.34}$$

and uses the same staples as above. The coefficients $\rho_{\mu\nu}$ are real. A nested combination of Stout and HYP smearing that combines their advantages is called HEX smearing [79].

Note that the number of smearing iterations N and the other parameters depend on the application. Link smearing for the hopping term of quark smearing (eq. (3.30)) usually has many iterations and is only done in the spatial volume within the same time slice. Smearing of dynamic fermions includes all directions and uses comparatively little iterations N because many iterations require complicated and costly force terms.

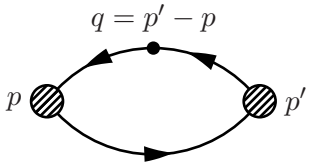

Figure 3.3.: Lattice three point function

3.3.4. Matrix Elements

Apart from masses LQCD can also provide matrix elements. Two point functions give information about hadronic decay constants [101] and moments of the hadron distribution amplitudes [102]. Suitable operators can be inserted between hadronic states, yielding insight about semileptonic decay, form factors (see for example [103]) and generalized parton distributions. Recently a second operator has been inserted testing factorization properties of various currents [104]. All such matrix elements have to be properly normalized, can be improved and should be renormalized for continuum extrapolation.

Decay constants

Decay constants give information about the coupling between hadron and the vacuum. The pseudoscalar decay constant can be extracted from the zero momentum relation

$$m_\pi f_\pi = \langle 0|\mathcal{A}_4|\pi\rangle \tag{3.35}$$

where the local axial current $\mathcal{A}_4$ is assumed to be renormalized and improved. The unrenormalized A_4 current appears in the large t limit of the correlator

$$\begin{aligned} C^{LS}_{A_4P}(t) &= \left\langle \bar{u}(t)\gamma_4\gamma_5 d(t)\bar{d}(0)\gamma_5 u(0)\right\rangle \\ &\overset{t\to\infty}{=} \langle 0|A_4(t)|\pi\rangle\langle\pi|P(0)|0\rangle\, \mathrm{e}^{-m_\pi t} = A^{LS}_{A_4P}\, \mathrm{e}^{-m_\pi t} \end{aligned} \tag{3.36}$$

where the superscripts L and S identify local and smeared interpolators. Using the source and sink smeared pseudoscalar correlator

$$C^{SS}_{PP}(t) \overset{t\to\infty}{=} |\langle 0|P(t)|\pi\rangle|^2\, \mathrm{e}^{-m_\pi t} = A^{SS}_{PP}\, \mathrm{e}^{-m_\pi t} \tag{3.37}$$

and the lattice normalization

$$\left\langle \pi_{\mathbf{p}}|\pi_{\mathbf{p}'}\right\rangle = (2\pi)^3\, 2p_0\delta(\mathbf{p}-\mathbf{p}') \tag{3.38}$$

yields the unrenormalized and unimproved decay constant in form of

$$m_\pi f^{(0)}_\pi = \frac{\sqrt{2m_\pi}A^{LS}_{A_4P}}{\sqrt{A^{SS}_{PP}}}. \tag{3.39}$$

Following [105] the renormalized and improved current is

$$\mathcal{A}_\mu = (1 + b_A a m_q)\, Z_A\, (A_\mu + c_A a \partial_\mu P) \tag{3.40}$$

where c_A is the improvement coefficient of the current and b_A describes the quark mass dependence (to first order in am) of the renormalization constant Z_A. There are perturbative [106, 107] and non-perturbative methods [108] for setting these coefficients. The improvement term can be evaluated with

$$a f_\pi^{(1)} = f_\pi^{(0)} \sinh(a m_\pi) \frac{A_{PP}^{LS}}{A_{A_4 P}^{LS}} \tag{3.41}$$

$$f_\pi = (1 + b_A a m)\, Z_A \left(f_\pi^{(0)} + c_A a f_\pi^{(1)} \right). \tag{3.42}$$

3.3.5. Analysis

On the lattice we (mostly) measure correlation functions. Extracting the physic quantities of interest in the continuum requires complicated analysis, which can roughly be split into two parts. The analysis of a single ensemble depending on the bare parameters β, m_q and the following extrapolation of multiple ensembles towards the physical point. There a several analysis methods generally used, which will be mentioned here or be detailed in appendix A.

Ground state masses and matrix elements of hadrons must be extracted from the large t behavior of correlators. Theses correlators are fitted to test functions in an appropriate t interval. A suitable choice can be found by examining so the called effective mass (illustrated in fig. 3.4) given by

$$m_{\text{eff,exp}}(t + 1/2) = \ln \frac{C(t)}{C(t+1)} \tag{3.43}$$

for states that decay sufficiently fast or by inverting

$$\frac{C(t)}{C(t+1)} = \frac{\cosh(m_{\text{eff,cosh}}(t - N_t/2))}{\cosh(m_{\text{eff,cosh}}(t + 1 - N_t/2))} \tag{3.44}$$

for (back propagating) mesons.

3.4. The physical limit

The physical limit consist in extrapolations of lattice spacing $a \to 0$ to the continuum, the quark masses m_q to their respective physical values and the volume V to infinity. Matrix elements and quark masses require renormalization and can be improved. Hadronic masses are on shell quantities which are automatically improved when the action is improved (see section 3.1.4). Before the extrapolation we need to relate the bare lattice parameters $\beta, \{m_q\}$ to values in physical units. The quark masses are usually related to

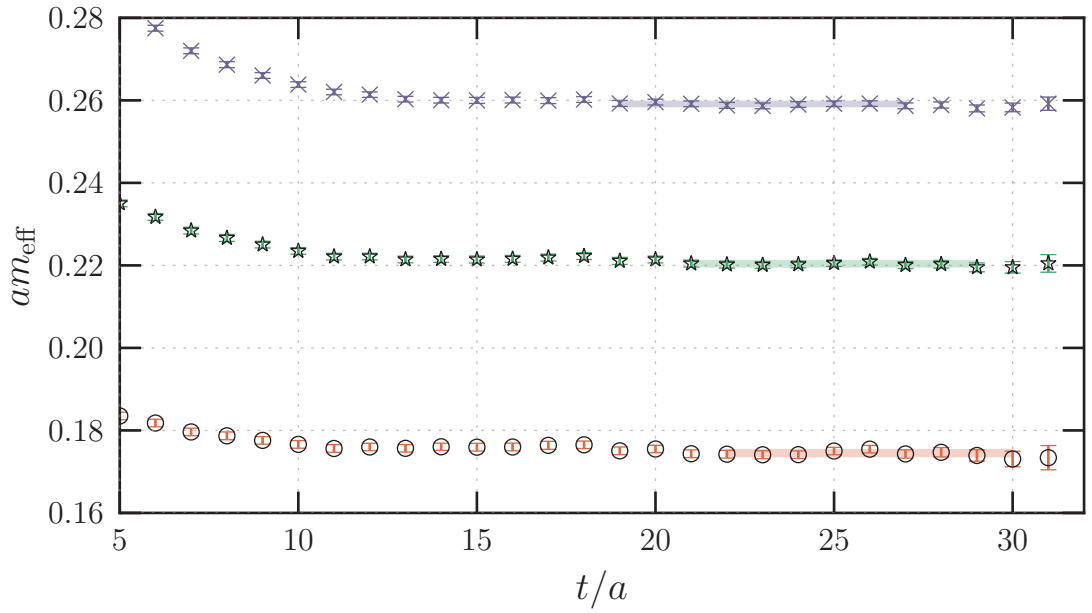

Figure 3.4.: Effective mass $m_{\text{eff,cosh}}$ of various light and strange pseudoscalar mesons on the ensemble `L0` (see table 5.1). The bands are masses m_i from cosh fits to corresponding correlators. The slopes on the left side are due to exited state contamination.

the masses of hadrons: The light quarks mass m_{ud} is set by the mass of the pion m_π and the strange quark can for example be tuned with the kaon mass m_K. Most of the time one does not calculate the quark masses but rather extrapolates in the aforementioned meson masses.

3.4.1. Scale setting

Dimensionless lattice QCD observables, such as masses am, must be converted to physical units with the lattice spacing a. There are several methods for determining the lattice spacing all of which depend upon extrapolation to physical or zero quark masses.

- The natural way is to use a hadron mass $\tilde{m}_x = am_x$ in the physical (or chiral) mass limit. The lattice mass ratio $r_x(m_q) = \frac{am_x(m_q)}{am_\pi(m_q)}$ is extrapolated to the physical value $r_{\text{exp.}} = r_x(m_q^*)$, where $m_x(m_q^*)$ can be identified as the experimental mass. The lattice spacing is then given by $a = \tilde{m}_x(m_q^*)/m_x^{\text{exp.}}$. Suitable choices include the nucleon, and Ξ- or $\Omega-$baryon masses [109] which require a simultaneous strange mass extrapolation.

- One can evaluate the static (infinitely heavy) quark-antiquark potential $V(r)$ on the lattice and fix the dimensionless product $r_i^2 \partial_r V(r)|_{r=r_i} = c_i$ at a reference scale

r_i to values c_i known from phenomenology. The two reference points commonly used are $c_0 = 1.65$ at $r_0 \approx 0.5$fm [110] and $c_1 = 1$ at $r_1 \approx 0.36$fm [111]. Note that these reference points are model dependent or can be set with lattice simulations that relate them to experimentally accessible observables in the continuum limit.

- Another secondary method uses the Wilson flow [112, 113]. The gauge fields are evolved in an extra flow time t until the action density $E(t)$ fulfills a dimensionless condition such as $t_0^2 \langle E(t_0) \rangle = 0.3$ or $t\partial_t \{t^2 \langle E(t) \rangle\}|_{t=w_0^2} = 0.3$. The experimental scales $\sqrt{t_0}, w_0$ must be determined by an initial continuum (and mass) extrapolation, which uses lattice spacings determined with for example hadron masses. The experimental values can then be used for future simulations.

3.4.2. Finite volume effects

Mass (and other) observables on the lattice suffer from finite size effects because the particle itself and other force mitigating particles may propagate around the periodic lattice [114]. Gluons are screened at large distances and their finite volume contribution can be neglected. The contribution of massive particles is exponentially suppressed with $\exp(-mL)$ making the leading finite size effects explicitly dependent on the lightest particles: the pion(s). Another possible effect is that large wave functions, e.g. exited states, might be squeezed, which results in power law finite size effects [115].

Finite volume effects can be integrated into the chiral extrapolations described below by replacing χPT continuum loop integrals with the sums over all discrete momenta. One assumes that LQCD finite size effects on a lot of observables can be neglected for $m_\pi L \geq 4$ [24]. In these cases it is sufficient to assert that the results are volume independent.

3.4.3. Operator improvement

Lattice interpolators $\mathbf{O}(g_0)$ can be $\mathcal{O}(a)$ improved in the same way as lattice actions (see section 3.1.4). One identifies all terms with the same quantum numbers at a fixed (the next) dimension. Then lattice EOM are used to remove redundant terms. The remaining terms can simply be combined with the naive term to obtain the improved interpolator

$$\mathbf{O}_x^I = \mathbf{O}_x^{(0)}(g_0) + \sum_{i=1} c_x^{(i)} \mathbf{O}_x^{(i)} \tag{3.45}$$

The improvement coefficients $c_x^{(i)}$ depend on the action S and on the coupling g_0^2. They are usually known to LO in *lattice perturbation theory* (LPT), where they are independent of the fermions [116]. Nonperturbative determination for specific cases show significant deviations from the LO results indicating that LPT is poorly convergent [108]. The improvement coefficient c_A for the axial current (eq. (3.42)) can be obtained by imposing the PCAC relation which will be covered in section 4.2.

3.4.4. Renormalization

A lattice simulation is a particular regulator that depends on the choice of fermion and gauge action. The resulting operators - such as quark bilinears $\bar{q}_1 \Gamma q_2$ - must be converted to a suitable continuum scheme for comparison. The matching can formally be given by

$$\left[\mathbf{O}_\Gamma^{\text{cont}}(g_R, m_R, \mu)\right]_R = \lim_{a\to 0}\left[Z_{\mathbf{O}_\Gamma}(g_0, a\mu)\mathbf{O}_\Gamma^{\text{lat}}(g_0, m)\right] \tag{3.46}$$

Perturbative determination of renormalization constants $Z_{\mathbf{O}}$ is in principle possible, but because lattice PT is unreliable the methods of choice are non-perturbative [117]. The most common of those is called RI/MOM (regularization independent momentum subtraction) [118]. It computes amputated lattice Green functions $\Lambda_{\mathbf{O}}(q^2)$ in a fixed gauge which are then - by virtue of the renormalization condition - matched with $Z_{\mathbf{O}}^{\text{RI}}$ to their tree level value at the renormalization scale $\mu^2 = q^2$. These results are then extrapolated to the chiral limit to become mass independent. Finally the ratio $R_{\mathbf{O}}(\mu)$ of renormalization constants in continuum momentum subtraction regularization and the desired continuum regulator can be calculated in perturbation theory at the order of choice. The renormalization scale μ is bounded by the so-called renormalization window

$$\Lambda_{\text{QCD}} \ll \mu \ll a^{-1} \tag{3.47}$$

which assures that perturbative matching calculations are possible and that the non-perturbative Green function is not affected by the lattice cutoff a^{-1}.

Mass independent renormalization requires us to scale the renormalization constants with the 'average' composite quark mass

$$am_q = \frac{1}{2}\left(am_{q_1} + am_{q_2}\right) = \frac{1}{4}\left(\frac{1}{\kappa_1} + \frac{1}{\kappa_2} - \frac{2}{\kappa_{crit}}\right) \tag{3.48}$$

The final $\mathcal{O}(am)$ renormalization prescription for composite operators in the $\overline{\text{MS}}$ scheme becomes

$$\mathbf{O}_R^{\overline{\text{MS}}}(\mu) = R_{\mathbf{O}}(\mu) Z_{\mathbf{O}}^{\text{RI}}(g_0, a\mu) \cdot \left(1 + b_m am_q + \bar{b}_m a\bar{m}\right) \mathbf{O}(g_0) \tag{3.49}$$

where b_m ($\bar{b}_m$) encodes the valence (sea) quark mass dependence. The sea quark mass effect for dynamical QCD ensembles is unknown and usually neglected. The valence quark contribution b_m is of $\mathcal{O}(1)$ causing substantial corrections for large (e.g. charm) quark masses. Note that the renormalization constants $Z_{S,P,T}(g_0^2, a\mu)$ are renormalization scale dependent whereas $Z_{V,A}(g_0^2)$ and the ratio $Z_s/Z_p(g_0^2)$ are not.

Alternative determination or restriction of renormalization constants $Z_{\mathbf{O}}$ and mass dependence b_m include the use of ward identities [117] or the Schrödinger functional (SF) [22].

3.4.5. Chiral and continuum extrapolation

After renormalization and determination of lattice quark masses and spacing a the remaining task is the extrapolation to physical mass values in the continuum. The mass extrapolation by virtue of χPT (see section 2.4.2) is formulated in the continuum and requires to extrapolate lattice observables to the continuum before it is performed. Alternatively combined extrapolations can be constructed which require integration of discretization effects into χPT. This can be done by constructing a continuum EFT of the lattice theory for $p \ll a^{-1}$. The terms in the Lagrangian of the so-called Symanzik theory [75] can be separated into the desired continuum contributions and discretization effects proportional to powers of a. The theory is truncated at the required order and then used to construct a modified χPT that includes explicit dependence on the lattice spacing a. The combined approach has the advantage that it simultaneously describes different discretization effects of multiple observables and that the polynomial extrapolation $a \to 0$ is extended by non-analytic cutoff dependent terms [60].

Although partially quenched QCD is unphysical and non-unitary most of the LECs of *partially quenched* χPT (PQχPT) are identical to normal χPT. Partially quenched lattice simulations therefore provide additional input to disentangle sea quark from valence quark effects. Furthermore unphysical observables can be used to determine specific LECs.

An alternative to χPT is a Taylor expansion in the quark masses m_q around the flavor symmetric point $m_{u,d,s} = \bar{m}$ which can be determined by using singlet mass combinations such as $X_\pi^2 = (m_\pi^2 + 2m_K^2)/3$. Keeping the light quarks degenerate and the sum of the quark masses fixed results in highly constrained extrapolations [119].

In practice often multiple approaches are used to estimate the systematic error of the extrapolation as for example done in [120]. The different approaches might vary extrapolation ordering, try different formulations of χPT ($SU(2)$ or $SU(3)$ and NLO or NNLO) or some alternative, fix parameters to values known or estimated from other sources and include cuts on the lattice spacing, pion masses or volumes. The mentioned possibilities are by no means complete. The individual results can additionally be weighted according to their likeliness.

4. QCD+QED

The following chapter intends to outline the methods required for QCD+QED simulations on the lattice. The current status of QED field generation and the main difficulties compared to pure QCD calculations will be covered: This includes gauge choices, different QED formulations, finite-size effects and the quark mass definition.

Wilson's initial lattice gauge theory paper [12] discusses compact lattice QED for the investigation of confinement. Subsequently, the first simulations studied its phase structure [121, 122] and the static potential [123]. It took more than 20 years to show that the confinement phase transition at $\beta \approx 1$ is of order one [124]. Amongst many other applications lattice QED can also be used to examine the triviality of QED [125, 126].

The simulations of QCD+QED on the lattice started in 1996, with fully quenched simulations performed by Duncan et al. [127, 128] yielding the first results on electromagnetic charge splittings of light hadrons. Their results also allowed to estimate the non-degenerate up- and down quark masses, which cannot be measured directly in experiments. This was further refined by [129, 130] with dynamic QCD fields, a first investigation of finite-size effects and chiral extrapolations. The first fully dynamical simulation used reweighting [131]. Systematic errors of quenching and finite-volume were discussed in [132]. The effects of electromagnetic charge on charmed mesons, which belong to the so-called gold plated observables, have not been investigated.

Recently all efforts have accumulated into a fully unquenched QCD+QED simulation, yielding post- as well as predictions of baryon octet splittings with controlled systematics from first principle [120].

The quark mass scale in QCD+QED simulation is determined by connected charge neutral pseudoscalars. Instead of dynamical QED fields, the effect of a large magnetic background is an alternate area of interest [133]: Corresponding physical systems can either be found in heavy ion collisions or are assumed in the big bang/neutron stars. Many of the required methods are the same and improvement as well as a better quark mass definition become desirable.

Until recently all QCD+QED simulations have only calculated masses and neglected matrix elements as well as the probably largely suppressed disconnected contributions. A current paper [134] outlines extended requirements and methods for the calculation of hadronic processes at $\mathcal{O}(\alpha_{\text{em}})$ in the background of QCD+QED.

4.1. Simulation

QCD+QED simulations on the lattice utilize a lot of techniques from pure QCD simulations, which have to be extended to meet the requirements of the modified theory

[120, 127, 129]. Commonly an additional non-perturbative[1] QED field $B_\mu(n)$ is incorporated into the calculation of hadron lattice correlators. An alternative are calculations that explicitly evaluate QED correction diagrams in the background of (isometric) QCD at fixed order $\mathcal{O}(\alpha_{\text{em}})$ [135]. The next section covers the most used partially quenched QED setup [136], which neglects the charge of the sea quarks. Unquenching of QED is either achieved in a full simulation [120], or via reweighting [131]. Regardless of the charge of the sea quark all previously mentioned options require to fix the QED gauge, either implicitly or explicitly. Gauge invariant lattice QED is possible with modified boundary conditions [137]. A further complication are severe finite-volume effects of the long ranged QED, which have power law dependencies in contrast to the exponential behavior of QCD [135, 138, 139].

The continuum QCD+QED fermion action (of a single quark flavor f) can be written as

$$S_F = \int \mathrm{d}^4x\, \overline{\psi}^{(f)}(x) \left[\mathrm{i}\gamma_\mu \left(\partial_\mu + \mathrm{i}A_\mu(x) + \mathrm{i}e^{(f)}B_\mu(x)\right) - m^{(f)}\right] \psi^{(f)(x)} \tag{4.1}$$

with fractional electric quark charge $e^{(f)}$ and the positron charge absorbed into B_μ. Following analogous compactification and discretization as for QCD

$$U_\mu^{em,(f)}(n) = \exp\left(\mathrm{i}e^{(f)}B_\mu(n)\right) \tag{4.2}$$

the QED field can be incorporated into the Symanzik improved fermion operator for a flavor f as

$$\begin{aligned}\mathcal{D}^{QCD+QED}\psi^{(f)}(n) = &\left(m_0^{(f)} + \frac{4}{a}\right)\psi^{(f)}(n) \\ &- \frac{\mathrm{i}a}{4}\left[c_{\text{sw}}\sigma_{\mu\nu}F_{\mu\nu}(n) + c_{\text{em}}\sigma_{\mu\nu}G_{\mu\nu}^{(f)}(n)\right]\psi^{(f)}(n) \\ &- \frac{1}{2a}\sum_{\pm\mu}(\mathbb{1}-\gamma_\mu)\, U_\mu^{(f)}(n)\,\psi^{(f)}(n+\hat{\mu})\end{aligned} \tag{4.3}$$

with

$$U_\mu^{(f)} = U_\mu^{QCD} \times U_\mu^{em,(f)}, \tag{4.4}$$

and either compact or non-compact QED field strength tensor $G_{\mu\nu}^{(f)}$. The same choice applies to the lattice gauge action. The coefficient c_{em} has the same the tree-level value 1 as its QCD equivalent c_{sw}.

[1] We hereby mean that QED is evaluated to all orders. Lattice QED itself is - unless it is compact and in the confined phase - still perturbative.

4.1.1. Partially quenched

The majority of QCD+QED simulations up to the present are partially quenched, meaning they employ dynamic sea quarks without charge [127–130, 140]. According to [136, 141] the effects of QED quenching on $\mathcal{O}(\alpha)$ corrections are at leading order proportional to $\mathrm{tr}[\hat{Q}\mathcal{M}]$. For $N_f = 2 + 1$ the charge matrix $\hat{Q}$ is traceless and $\mathcal{M}$ is the block diagonal QCD quark propagator that contains all three quarks. Quenching errors are therefore flavor breaking effects and comparison with flavor breaking observables amounts to quenching errors on the QED splittings which are maximally 10% in the physical mass limit. Another estimate relies on PQχPT: Pseudoscalar masses and pion mass splittings might have negligible errors, whereas kaon mass splitting errors are estimated to be 5% [132]. PQχPT predicts that Dashen term like differences have suppressed dependence on the charge of the sea quarks [142].

Ignoring the systematics of quenching and the possible complications of the unquenched HMC we believe that partially quenched calculation offer some systematic advantages:

- The QED coupling can be set to the exact physical value.
- The QED background does not break the $\pm B_\mu$ symmetry, which can be averaged over for a largely improved signal [129].
- More generally there a no singled out, 'correct' quark charges, making the use of unphysical charge combinations straight forward.
- For actions with explicitly broken chiral symmetry the quark masses can be easily tuned to known values from the QCD calculations.

Compact QED

The QED vector gauge potential can be discretized analogously to QCD: Instead of simulating the fields links become the degrees of freedom and one can apply the same methods for their generation and gauge fermion interaction as for the QCD links. The slightly modified methods are discussed in appendix C.2. The whole simulation is simply extended by a complex phase of the gauge links, for the individual quark families. The compact gauge action

$$S_G^{QED} = \frac{\beta_{QED}}{4} \sum_n \sum_{\mu,\nu} \mathrm{Re}\left[1 - P_{\mu\nu}(n)\right] \tag{4.5}$$

is given in terms of the corresponding $U(1)$ plaquette $P_{\mu\nu}(n)$.

In the authors opinion, there are certain disadvantages of the compact formulation:

- The coupling requires multiplicative renormalization because of implicit self-interaction in the action. The corresponding renormalization constant is close to 1 for physical electromagnetic coupling.

- Gauge fixing is not implicit in the configuration generation.
- Measurements are bound to integer charges e_q after the initial, free choice of the coupling.
- The generation by update schemes implies an additional autocorrelation time τ_{int}. Furthermore a Monte Carlo trajectory can be stuck in configuration space.

Non-compact QED

In contrast to the non-abelian QCD, it is straightforward for QED to discretize also the abelian vector gauge potential B_μ. The action of the fields B_μ is local and decouples in momentum space. The non-compact generation requires a specific gauge choice, but configurations can be transformed to other gauges after generation. Technical notes on the generation of quenched, non-compact QED gauge fields can be found in appendix C.1.1.

4.1.2. Full QCD+QED

Fully dynamic QCD+QED calculations are technically challenging and expensive. Some of the additional complications are

- It is necessary to renormalize α_{em} because of the effects of the sea quarks.
- Additional extrapolations due to two non-degenerate, light quark masses are required. Fermion actions that explicitly break chiral symmetry at finite lattice spacing require better tuning due to the unknown critical hopping parameter κ_c for the different charges $e_{u,d(,s,c)}$.
- Broken vB_μ symmetry (with $v \in \mathbb{R}$), making it impossible to cancel $\mathcal{O}(e)$ noise by averaging over $\pm B_\mu$.
- The Dirac operator for non-degenerate light quark masses is no longer protected from negative determinants and the applicability of RHMC must be validated after the simulation [120].

Nevertheless some simulations have already been carried out [131, 143, 144].

Recently an impressive effort culminated in the calculation of baryon splittings with fully controlled systematics [120]. Their simulations were performed at unphysically large electromagnetic coupling such that physical terms quadratic in the charge Q dominate over linear noise terms. The coupling was renormalized with the Wilson flow. Results were then extrapolated to physical coupling. Analytic higher order finite volume corrections were used.

Dynamic lepton loops that screen the QED vacuum can be safely neglected because the running of the QED coupling above $\mu = 2m_{e^+}$ is a (weak) $\mathcal{O}(\alpha_{\text{em}}^2)$ effect that would modify α_{em} by only approximately 1%.

4.1.3. Simulations at fixed $\mathcal{O}(\alpha_{\text{em}})$

Given that $\mathcal{O}(\alpha_{\text{em}}^2)$ corrections are decreased by approximately another factor 100, leading order QED corrections are currently sufficient to control QED systematics. Expanding the full QCD+QED path integral in $(e^2, \Delta m_{ud})$ around isometric $(e^2 = 0, m_u = m_d)$ QCD configurations and evaluating all contributing diagrams yields equally viable results for leading isospin breaking effects [135]. This setup can also be used to evaluate diagrams that do not factorize into hadronic and leptonic currents [134].

4.1.4. Gauge dependence

QED correlators and matrix elements of charged hadrons in a periodic box are not gauge invariant [120]. Their calculation therefore requires gauge fixing: Landau and Coulomb gauge conditions are easy to implement in compact QED, Feynman gauge is practical in non-compact QED. Note that all of these gauge choice have global gauge ambiguities. Furthermore Gauss' law

$$\nabla \cdot \mathbf{E}(\mathbf{x}) = \rho(\mathbf{x}) \tag{4.6}$$

is violated for a single charged particle on the torus [145, 146]: After volume integration of both sides the left side vanishes whereas the right side gives the charge.

This can be fixed by a uniform background charge density which cancels the charge and thereby removes the zero modes of the gauge field in momentum space

$$\tilde{B}_\mu(\mathbf{k} = \mathbf{0}, k_0) = 0. \tag{4.7}$$

Momentum volume integration no longer includes $\mathbf{k} = \mathbf{0}$ and therefore no degrees of freedom $\tilde{B}_\mu(\mathbf{0}, k_0) \propto \sum_{\mathbf{x}} B_\mu(\mathbf{x}, k_0)$. This condition is commonly referred to as QED$_L$.

QED$_C$

An alternative to periodic boundary conditions and quenching of zero modes is investigated in [137]: QED$_C$ implements C^* boundary conditions [147, 148] in one or more spatial directions. The gauge zero modes do not exist due to anti-periodicity of the gauge fields in spatial directions $B_\mu(x + \hat{L}_\mu) = -B_\mu(x)$. These boundary conditions break flavor symmetry, which is sufficiently suppressed by a factor $\mathrm{e}^{-\mu L}$, where μ is a function of hadron masses participating in the polluting mixing. The charge q is no longer a conserved quantum number, but it becomes quantized in units of an elementary charge q_{el} and $(-1)^{q/q_{el}}$ is still conserved, i.e. charge conservation is only violated in units of $2q_{el}$. The resulting theory is *local*, renormalizable, gauge invariant and has smaller finite volume effects then, e.g. QED$_L$. Modified quark field interpolators allow the computation of most particles of interest. The formalism is applicable in compact and non-compact formulation.

4.1.5. Finite size effects

When QED is simulated in a finite size box $L^{d-1} \times T$ with periodic boundary conditions charge dependent observables suffer from power law corrections L^{-n} because QED is a long range interaction. This makes explicit treatment by calculations on large volumes and extrapolations towards infinite-volume mandatory. Finite size effects of charged hadrons are gauge dependent [146] and the leading order is $1/L$ [135]. Further work calculated higher orders and revealed that LO and NLO coefficients are universal [138, 139]

$$m(T,L) \underset{T,L\to+\infty}{\sim} m\left\{1 - q^2\alpha_{\mathrm{em}}\frac{\kappa}{2mL}\left[1+\frac{2}{mL}\right] + \mathcal{O}\left(\frac{q^2\alpha_{\mathrm{em}}}{(mL)^3}\right)\right\} \tag{4.8}$$

with the analytic parameter $\kappa = 2.83729....$ Higher orders depend on the gauge and the structure of the hadron. The analysis in [120] established the necessity of NNLO corrections for the large coupling $\alpha_{\mathrm{em}} = 1$.

Finite volume effects of fixed order calculations as discussed in section 4.1.3 might be significantly improved by the considerations in [149]: They propose to couple finite-volume QCD configurations to infinite volume valence quarks and photons, which is achieved by averaging (stochastically) over twisted boundary conditions θ_μ.

Massive photons

Simulations with massive photons which screen the long range interaction and extrapolation towards zero photon mass can resolve the finite volume issues [150]. Hadron correlators have an additional t^2 dependence in the exponent due to the zero mode of the temporal gauge field.

4.1.6. Continuum limit of lattice QED

QED and electroweak $U(1)$ are UV trivial because the renormalized charge becomes zero if the cutoff Λ is removed. This is also expressed in the running coupling constant which has a so-called Landau Pole at some large scale Λ_L. This has been investigated on the lattice [125] where forbidden regions of renormalized fermion mass and charge were found.

Quenched, non-compact lattice QED has no running coupling and can therefore safely be extrapolated to the continuum. Dynamic QCD+QED is not protected from this. The limit $a \to 0$ can then be understood as an extrapolation to a scale Λ where discretization effects are negligible and low energy QCD observables are insensitive to. Furthermore this scale is 'safely' below Λ_L or the Planck scale such that one can always choose the renormalized coupling to be $\hat{\alpha} = \frac{1}{137}$. This procedure simply acknowledges that QED is just an effective theory and will need to be modified below Λ_L, e.g. unified at the Planck scale M_P.

4.2. Ward identities and PCAC masses

We repeat the GMOR relation (eq. (2.32)) of isometric QCD

$$(m_u + m_d)\langle\overline{\psi}\psi\rangle = F_\pi^2 m_\pi^2, \tag{4.9}$$

where the quark masses are assumed to be degenerate and renormalized. When the degeneracy is broken (either through QED charges or with different masses) this equation can no longer be used to calculate the individual quark masses $m_{u,d}$, not even in the chiral limit $m_\pi^2 \to 0$. Individual masses can be calculated with the use of Ward-Takahashi identities. The formula for the QCD+QED case with domain wall fermions were first given in [129].

For vector and axial vector flavor variations

$$\delta\psi(x) = \mathrm{i}[\alpha_V^j(x)\frac{\tau^j}{2}]\psi(x), \qquad \delta\bar{\psi}(x) = -\mathrm{i}\bar{\psi}(x)[\alpha_V^j(x)\frac{\tau^j}{2}] \tag{4.10}$$

$$\delta\psi(x) = \mathrm{i}[\alpha_A^j(x)\frac{\tau^j}{2}\gamma_5]\psi(x), \qquad \delta\bar{\psi}(x) = -\mathrm{i}\bar{\psi}(x)[\alpha_A^j(x)\frac{\tau^j}{2}\gamma_5] \tag{4.11}$$

Ward-Takahashi identities [151] assume that the expectation values of all suitable observables $\langle\mathbf{O}\rangle$ remain invariant under the transformations above. The invariance is expressed in terms of the identity

$$\frac{\delta}{\delta\alpha_Z^j(x)}\langle\mathbf{O}\rangle = \left\langle\frac{\delta\mathbf{O}}{\delta\alpha_z^j(x)}\right\rangle - \left\langle\mathbf{O}\frac{\delta S_F}{\delta\alpha_z^j(x)}\right\rangle = 0 \tag{4.12}$$

which can be used to deduce relations between operators from which one can obtain renormalization constants and fundamental parameters of the theory. Choosing local operators $\langle\mathbf{O}(x_1,\ldots,x_i)\rangle$ that are well separated from the $\delta a_z^j(x)$ variation reduces the condition to

$$\left\langle\mathbf{O}\frac{\delta S_F}{\delta\alpha_z^j(x)}\right\rangle = 0. \tag{4.13}$$

This is the axial (or vector) Ward-Takahashi identity for $\alpha_z^j(x)$ from eq. (4.11) (or eq. (4.10)). The variation of the QCD+QED lattice action S_F (eq. (4.3)) was worked out for meson spectroscopy in external magnetic field $\mathbf{B}$ [133]. Initial results showed inconsistencies of $\mathbf{B}$ field dependent meson masses between different fermion discretizations. This could be attributed to the charge and $\mathbf{B}$ field dependent critical mass of Wilson fermions and resolved by tuning of the bare quark mass with the external, electromagnetic field.

For the flavor base $\psi = (u,d)^T$ the QED links can be written as a flavor space matrix $U_\mu^{\mathrm{em}} = \mathrm{diag}(U_\mu^u, U_\mu^d)$ which do not commute with the flavor space rotation τ^j of the

transformations. The corresponding commutators evaluate to

$$\left[U_\mu^{\mathrm{em}}, \tau^j\right] = \mathrm{i}\epsilon_{3jk}\left[\exp(\mathrm{i}e_u a B_\mu) - \exp(\mathrm{i}e_d a B_\mu)\right]\tau^k = \mathrm{i}\epsilon_{3jk}\delta U^{em}\tau^k \tag{4.14}$$

$$\left[U_\mu^{\mathrm{em},\dagger}, \tau^j\right] = \mathrm{i}\epsilon_{3jk}\left[\exp(-\mathrm{i}e_u a B_\mu) - \exp(-\mathrm{i}e_d a B_\mu)\right]\tau^k = \mathrm{i}\epsilon_{3jk}\delta U^{\mathrm{em},\dagger}\tau^k \tag{4.15}$$

and appear in interpolators with non-degenerate charges. The flavor dependent plaquettes

$$U_{\mu,\nu}^{\mathrm{em},u/d}(x) = \exp\left(\mathrm{i}e_{u/d}\, a\left(B_\mu(x) + B_\nu(x+\hat{\mu}) - B_\mu(x+\hat{\nu}) - B_\nu(x)\right)\right) \tag{4.16}$$

in the clover term give rise to a similar difference for the vector Ward identity

$$\begin{aligned} \delta G_{\mu\nu} =& \frac{1}{8a^2}\left[\delta U_{\mu,\nu}^{\mathrm{em}} + \delta U_{\nu,-\mu}^{\mathrm{em}} + \delta U_{-\mu,-\nu}^{\mathrm{em}} + \delta U_{-\nu,\mu}^{\mathrm{em}} - \mathrm{h.c.}\right] \\ \text{with} \qquad \delta U_{\mu,\nu}^{\mathrm{em}}(x) =& U_{\mu,\nu}^{\mathrm{em},u}(x) - U_{\mu,\nu}^{\mathrm{em},d}(x). \end{aligned} \tag{4.17}$$

For axial transformations the anti-commutator the terms are summed to

$$\begin{aligned} \Sigma G_{\mu\nu} =& \frac{1}{8a^2}\left[\Sigma U_{\mu,\nu}^{\mathrm{em}} + \Sigma U_{\nu,-\mu}^{\mathrm{em}} + \Sigma U_{-\mu,-\nu}^{\mathrm{em}} + \Sigma U_{-\nu,\mu}^{\mathrm{em}} - \mathrm{h.c.}\right] \\ \text{with} \qquad \Sigma U_{\mu,\nu}^{\mathrm{em}}(x) =& U_{\mu,\nu}^{\mathrm{em},u}(x) + U_{\mu,\nu}^{\mathrm{em},d}(x). \end{aligned} \tag{4.18}$$

With these expression the final π^+ vector Ward identity becomes

$$\begin{aligned} -a^4\sum_\mu \nabla_x^\mu \tilde{V}_\mu^+(x) = a^4(m_u - m_d)\bar{d}(x)u(x) \\ - \frac{a^3}{2}\sum_\mu \quad & \Big[\bar{d}(x)U_\mu^{gl}(x)\delta U^{em}(x)u(x+\hat{\mu}) \\ & + \bar{d}(x)U_\mu^{gl,\dagger}(x-\hat{\mu})\delta U_\mu^{em,\dagger}(x-\hat{\mu})u(x-\hat{\mu})\Big] \\ - \frac{a^3}{2}\sum_\mu \quad & \Big[-\bar{d}(x)\gamma_\mu U_\mu^{gl}(x)\delta U^{em}(x)u(x+\hat{\mu}) \\ & + \bar{d}(x)\gamma_\mu U_\mu^{gl,\dagger}(x-\hat{\mu})\delta U_\mu^{em,\dagger}(x-\hat{\mu})u(x-\hat{\mu})\Big] \\ + \frac{\mathrm{i}}{2}c_{\mathrm{em}}a^5\bar{d}(x)\sigma_{\mu\nu}\delta G_{\mu\nu}(x)u(x), \end{aligned} \tag{4.19}$$

the axial Ward identity is

$$
\begin{aligned}
a^4 \sum_\mu \nabla_x^\mu \tilde{A}_\mu^+(x) = {} & a^4(m_u + m_d)\bar{d}(x)\gamma_5 u(x) + a^4 X^+(x) + \mathrm{i}c_{\mathrm{sw}} a^5 \bar{d}(x)\sigma_{\mu\nu}F_{\mu\nu}(x)\gamma_5 u(x) \\
& - \frac{a^3}{2}\sum_\mu \Big[\bar{d}(x)U_\mu^{gl}(x)\delta U^{em}(x)\gamma_5 u(x+\hat{\mu}) \\
& \qquad + \bar{d}(x)U_\mu^{gl,\dagger}(x-\hat{\mu})\delta U_\mu^{em,\dagger}(x-\hat{\mu})\gamma_5 u(x-\hat{\mu})\Big] \\
& - \frac{a^3}{2}\sum_\mu \Big[-\bar{d}(x)\gamma_5\gamma_\mu U_\mu^{gl}(x)\delta U^{em}(x) u(x+\hat{\mu}) \\
& \qquad + \bar{d}(x)\gamma_5\gamma_\mu U_\mu^{gl,\dagger}(x-\hat{\mu})\delta U_\mu^{em,\dagger}(x-\hat{\mu}) u(x-\hat{\mu})\Big] \\
& - \mathrm{i}c_{\mathrm{em}} a^5 \bar{d}(x)\sigma_{\mu\nu}\Sigma G_{\mu\nu}(x)\gamma_5 u(x),
\end{aligned}
\tag{4.20}
$$

where the structure of the first line of both equations is identical to the pure QCD (or flavor symmetric result) with (partially) conserved QCD point split currents on the left hand side and the contribution of the Wilson term X^+ for axial transformations. Note that here the QCD currents contain the electromagnetic links of the conjugate quark. The lines after the first contain the contribution terms of the coupling to the electromagnetic field.

The axial (vector) identities of unimproved Wilson fermions were calculate with $\mathbf{O} = P\,(S)$ for (static) external magnetic field $\mathbf{B}$ and dynamic $\alpha_{\mathrm{em}} = 1$ QED$_L$ configurations. Up and down quark masses could be tuned with the approximate PCAC relation of electromagnetically neutral correlators

$$
m_f^{\mathrm{PCAC}} = \frac{\partial_0 \left\langle \left(\tilde{A}^{+,ff}\right)_0(x_0)\, P^{ff}(0)\right\rangle}{\left\langle P^{ff}(x_0)\, P^{ff}(0)\right\rangle}. \tag{4.21}
$$

which neglects disconnected diagrams, and QCD and QED anomaly terms. Nevertheless this approximate tuning was found to be equivalent to tuning with the mass of connected neutral pseudoscalars. All individual, unimproved correlators of eqs. (4.19) and (4.20) were evaluated. Charged correlators can be averaged over $\pm B_\mu$ for the dynamic QED background. The charged vector Ward-Takahashi identity was to noisy due to the corresponding scalar operator $\mathbf{O} = S$. The axial identity did not yield well behaved plateau that could be fitted. A publication including the contribution of improvement terms is in preparation [152].

5. QED splittings of pseudoscalar quantities

This chapter will describe the simulation of QCD + quenched QED, on $N_f = 2 + 1$ SLiNC configurations at physical electromagnetic coupling. Compact and non-compact lattice QED actions are investigated. The subsequent analysis of charge splittings of pseudoscalar masses and decay constants provides results of the isospin breaking effects, and discusses the challenges of matrix element lattice calculations of charged hadrons.

5.1. Simulation

The goal of our simulation was to calculate electromagnetic corrections to pseudoscalar decay constants. The simulations were started with a compact QED action, which is described in the following section and appendix C. Analysis yielded results inconsistent with the expected charge dependent splittings $\delta f(Q^2, \Delta^2)$. Mass dependence and analysis of finite volume effects led to the suspicion that the generated QED ensembles were not thermalized, or that the chosen gauge was exhibiting large finite volume effects, or both. The simulation therefore continued with the non-compact QED action, that was used in [120]. We will first describe the dynamical QCD ensembles, before turning to the compact and non-compact QED specifics.

5.1.1. QCD ensembles

The QCD ensembles used in this study employed a $N_f = 2 + 1$ SLiNC (**S**tout **Li**nk **N**on-perturbative **C**lover) fermion action and a Symanzik improved gauge action S_G. The Sheikoleslami-Wohlert coefficient $c_{\text{sw}} = 2.65$ was determined non-perturbatively in [153]. Stout smeared gauge links in the fermion action are supposed to remedy the increase of exceptional configurations due to a large clover contribution [80]. The quark masses of the corresponding ensembles were chosen in a way that the sum of their bare masses remained fixed to the value at the flavor symmetric point defined by a dimensionless singlet quantity such as

$$\left(\frac{aX_\pi}{aX_N}\right)^2 = \left.\frac{X_\pi^2}{X_N^2}\right|^* = \left.\frac{(M_\pi^2 + 2M_K^2)/3}{(M_N + M_\Sigma + M_\Xi)^2/9}\right|^*, \tag{5.1}$$

which is in contrast to the usual strategy of fixing the strange quark mass to its approximate physical value and varying the light quark masses for the chiral extrapolation. The modified strategy has the advantage that the strange mass is always smaller than the physical strange mass and extrapolation can be constrained to fewer (flavor breaking) parameters [119]. The lattice spacing used for tuning the symmetric hopping parameter

label	β	κ_l	κ_s	$L \times T$	m_π(MeV)	Lm_π	N_{cfg}
S0	5.50	0.12090	0.12090	16×32	(689)	4.2	366
M0		0.12090	0.12090	24×48	476	4.3	567
M1		0.12100	0.12070	24×48	405	3.6	667
M2		0.12104	0.12062	24×48	370	3.3	716
L0		0.12090	0.12090	32×64	460	5.6	684
L1		0.12104	0.12062	32×64	352	4.3	549
L2		0.121145	0.120413	32×64	237	3.0	549

Table 5.1.: The ensembles used for our analysis. Details about their generation and action are described in [119]. Note that $\beta = 10/g_0^2$ because the improvement coefficient $c_0 = 5/3$ is included into the definition. We used $a = 0.075\,\text{fm} = (2.631\,\text{GeV})^{-1}$. The ensemble S0 was only used to investigate FV effects and does not enter into final results because its pion mass was found to be inconsistently large. The number N_{cfg} refers to the number of configurations that entered into our analysis. Most of the ensembles contain more configurations than were used here.

$\kappa_{\text{sym.}} = 0.12090$ of the ensembles listed in table 5.1, was too large [154], yielding heavier than physical singlet masses, and an unphysically large strange quark mass at the physical pion mass [155].

5.1.2. Compact QED configurations

The electrically charged fermion action included a smeared QED field multiplied by a charge factor into the hopping term. The coupling was rescaled such that the quark charges have integer values, because taking the third root of the compact field for rescaling is ambiguous.

$$\beta_{QED} = \frac{1}{g^2_{QED}} = \frac{\alpha_{QED}}{4\pi} = \frac{137}{4\pi} \quad \xrightarrow{q'=3q} \quad \beta_{QED} \simeq 99 \tag{5.2}$$

The QED contribution to the clover term was neglected because c_{em} for QED is different than for QCD and there was no planned continuum extrapolation. It would have been viable to set c_{em} to the tree level value 1 since higher orders are assumed to be small. In compact formulation of the electromagnetic gauge action the degrees of freedom suffer from a (small) self-interacting contribution. This requires multiplicative renormalization of the electromagnetic coupling constant, which can be applied at the end of the analysis. This renormalization factor Z_e can be determined by measuring $U(1)$ Wilson loops $W(r,t) \sim \exp(-V(r)t)$ to obtain the Coulomb potential $V(r)$ in a box which can be fitted to perturbative lattice QED predictions [138, 156] with the coupling and an irrelevant self-energy as only free parameters.

The generation of a compact $U(1)$ is described in appendix C.2. Using a scheme

proposed in [157] we fixed the QED field to Landau gauge without global zero modes $\sum_m B_\mu(m) = 0$ because charged correlators are not gauge invariant. The resulting $U(1)$ field facilitated our first observation of pseudoscalar decay constant splitting [158] on a relatively heavy QCD ensemble (`b5p29kp13550-24x48` mentioned in [159]). A more detailed analysis, with lots of unphysical charge combinations on the SLiNC QCD ensembles listed in table 5.1, did not show a Q^2 dependent scaling of the splitting. The QED gauge initially proposed in [146] and employed in [120] was therefore used in the following measurements on a non-compact QED background.

5.1.3. Non-compact QED

The following results were obtained by simulation with QED_L background configurations at physical coupling $e = \sqrt{4\pi\alpha}$. Details of the QED gauge field generation in momentum space can be found in appendix C.1.1. It shall be noted that successive QED configurations are uncorrelated.

5.1.4. Quark mass tuning

Equivalently to the QCD background, the QED field exhibits an axial anomaly (eq. (2.29)). Wilson fermions violate chiral symmetry and therefore suffer from charge dependent, additive quark mass renormalization. This effect can be damped by smearing [120].

The hopping parameters $\kappa(e_q^2)$ for charged propagators were tuned in such a way that all connected, symmetric and charge neutral pseudoscalars have the same mass as the pure QCD meson. The measurements included charged valence quarks matched to the masses of all sea quarks. Furthermore, (charged) valence quarks with masses corresponding to physical strange and charm values were added. Their masses were tuned by matching lattice quantities to

$$(am_{s\bar{s}})^2 = \left(m_{K^+}^2 + m_{K^0}^2 - m_{\pi^+}^2\right)_{\text{exp.}} \tag{5.3}$$

$$am_{\eta_c} + 3\,am_{J/\psi} = \left(m_{\eta_c} + 3\,m_{J/\psi}\right)_{\text{exp.}} \tag{5.4}$$

with a lattice spacing $a = 0.075\,\text{fm} = (2.631\,\text{GeV})^{-1}$ as determined in [160]. The resulting uncharged κ values are listed in table 5.2.

In the non-compact production measurements the charged strange and charm masses were set by applying the same mass shift as for the light quarks, because additional corrections at larger masses turned out to be small. The simulation was performed with three slightly detuned kappas which allows to adjust for the remaining mistuning in the analysis.

5.1.5. Details of the Measurements

As mentioned previously, we calculated light and optional strange propagators with the same pseudoscalar mass as the QCD sea quarks and valence strange and charm propagators with approximate physical masses. For each of these 4 or 3 mass classes, we

Ensemble	κ_S	κ_C
M0	0.12048	0.111553
M1	0.12048	0.111553
M2	0.12048	0.111553
L0	0.12048	0.111553
L1	0.120466	0.111540
L2	0.120466	0.111540

Table 5.2.: Hopping parameters κ for the partially quenched valence quarks at physical strange and charm quark mass. We denote them with uppercase subscripts $_{S,C}$. Note that for the lightest ensemble L2 the kappa of the strange sea quark $\kappa_s = 0.120413$ is smaller than the one of the physical κ_S indicating that extrapolating from that symmetric point does not hit the physical point [155].

performed inversions at 2 additional κ values, with a fixed detuning of $\delta\kappa = \pm 0.00002$ which allowed precise quark mass matching in the final analysis. We did inversions for the charge $q \in e/3 \times [0, \pm 1, \pm 2]$ and performed (almost[1]) all available, non-redundant contractions. The required meson correlators were calculated with zero momentum spin explicit one-end sources. We used one source on a randomly chosen timeslice per configuration. Smeared and point interpolators were contracted at source and sink. This amounted to up to 120 one-end propagators and approximately 7000 contractions per configuration and source. The final statistics for all ensemble can be found in table 5.1. The used configurations were distributed evenly in Monte Carlo time.

5.2. Analysis

The following chapter will provide an analysis of pseudoscalar mass and decay constant splittings. The mass splitting analysis reproduces previous results and validates our approach for the following decay constant analysis. Note that we excluded up to five exceptional configurations on ensembles M2 and L2 which were identified by the extreme deviation of the uncharged QCD pion correlator at their respective light quark masses. We attribute their existence to the low Lm_π of the ensembles.

At first the extraction and analysis of decay constant observables on single ensembles is described. Then the chiral and finite volume analysis yield results at our single lattice spacing a. A discussion of neglected systematics will conclude this section.

[1] We did not contract mass detuned propagators with the same absolute charge value within the same meson mass class.

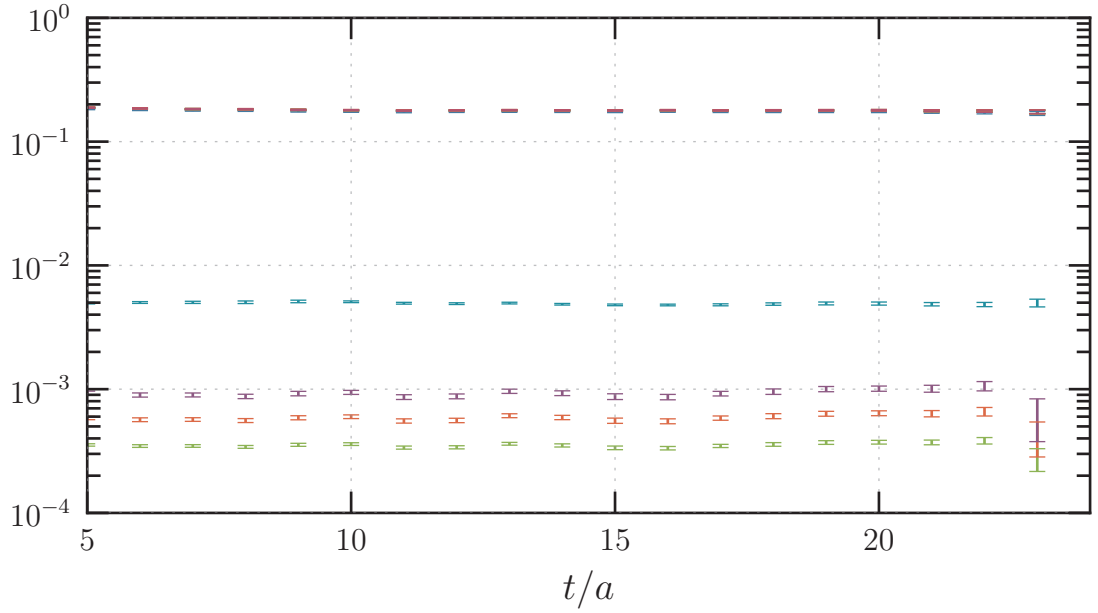

Figure 5.1.: Effective mass of light pseudoscalars on ensemble `M0` and their difference. The top line are (overlapping) effective masses of various detunings and mass combinations. The lines below are their difference to the uncharged sea quark effective mass. Note the log scale on these plots indicating that we can resolve differences 3 orders of magnitude below the absolute value.

5.2.1. Masses

Initial pseudoscalar masses

$$m_{f_1\bar{f}_2}\left(q_1, q_2, \delta\kappa_1, \delta\kappa_2\right) \tag{5.5}$$

were extracted by correlated cosh fits to smeared-point or smeared-smeared correlators. The variables q_i and $\delta\kappa_i$ are the charge and the hopping parameter detuning. The charge of the anti-quark $\bar{f}_2$ is taken to be $-q_2$ such that the meson charge is given by $Q = q_1 - q_2$. Quark types f_i only refer to the approximate quark mass of a specific flavor and specifically not to the charge. All correlators of the same meson type $f_1\bar{f}_2$ (e.g. light-light or strange-charm) had the same fit range to propagate their correlation for the necessary subtractions and correlated fits. Suitable fit ranges were identified by the criteria described in appendix A.3. The χ^2/dof values of these fits typically varied between 0.7 and 1.5 and are stable for different charge combinations on the same fit range. The fit ranges were also inspected by *effective mass difference* plots (see fig. 5.1) as used in [150].

Instead of including the mass of all detuned data into global fits, which proved to be highly unstable, we match all data within the same meson type (f_1, f_2) at the quark

mass parameters

$$\{x_i\} = \left(m^2_{f_1\bar{f}_1}, m^2_{f_2\bar{f}_2}\right) \tag{5.6}$$

of the uncharged and not detuned quark types $f_{1,2}$. This comes at the expense of ignoring quark mass slope information and ignores the violation of the GMOR relation (eq. (2.32)) at large quark masses. The matching at the same quark masses was performed according to appendix B.2. In principle the following options were considered:

- Using a linear model $M^2(\{\tilde{x}_i\})$ to describe the charged mass in the vicinity of $\{x_i\}$. The resulting ordinary least squares problem can be solved without reweighting due to errors. Note that the error is propagated nonetheless since this procedure is performed on all (resampled) samples.
- Diagonal or correlated fits that described the linear dependence of the data in the vicinity of $\{x_i\}$. This requires a somewhat complicated inclusion of the error on the predictors.

The first and simpler choice yielded reasonable results giving us no reason to investigate the second possibility. The resulting set of pseudoscalar masses

$$M^2_{\mathrm{PS}}\left(q_1, q_2, \{x_i\}, \{\kappa_{\mathrm{sea}}\}, L \times T\right) \tag{5.7}$$

can then either be used directly or be subtracted (due to the matched $\{x_i\}$) for further analysis. The meson type is implicit in the quark mass parameters $\{x_i\}$.

Finite volume corrections

As discussed in section 4.1.5 masses of charged particles have leading order $1/L$ dependence on the volume. Given that this analysis only uses 2 volumes we choose to explicitly correct masses of charged mesons up to NLO which is universal [120, 138]. Note that the correction on the mass is small but that effects on splittings like ΔM^2 might be as large as 100%. Remaining corrections

$$m(T, L) \underset{T,L\to+\infty}{\sim} m\left\{1 + \mathcal{O}\left(\frac{q^2\alpha_{\mathrm{em}}}{(mL)^3}\right)\right\} \tag{5.8}$$

are incorporated into the chiral extrapolation equations of the splitting

$$\begin{aligned}\Delta m^2(q^2, L) &= m^2(q^2, L) - m_0^2 = m^2(q^2, \infty) - m_0^2 + \mathcal{O}\left(\frac{q^2\alpha_{\mathrm{em}}}{m(q^2, \infty)L^3}\right) \\ &\simeq \Delta m^2_\infty(q^2, \infty) + \mathcal{O}\left(\frac{q^2\alpha_{\mathrm{em}}}{m(q^2, L)\, L^3}\right),\end{aligned} \tag{5.9}$$

where m_0 is the mass of the corresponding QCD meson. The replacement $m(q^2, \infty) \to m(q^2, L)$, in the last transformation, is justified because the total correction is small and correct at $\mathcal{O}(\alpha_{\mathrm{em}}/L^3)$.

PQχPT

Partially quenched χPT has been used to calculate the following $SU(3)$+QED formulae (extracted from [142]) where the pseudoscalar mass dependence is parametrized as

$$M^2_{\text{phys}} = \chi_{e,ij} + \frac{\delta^{(4)vs}}{F_0^2} + \mathcal{O}(p^6, e^2p^4) \tag{5.10}$$

with v and s being the number of mass degenerate valence and sea quarks. The splittings

$$\begin{aligned}
\delta^{(4)13} &= \left[48L_6^r - 24L_4^r\right]\chi_1\bar{\chi}_1 + \left[16L_8^r - 8L_5^r\right]\chi_1^2 \\
&- 48e^2Z_EF_0^2L_4^rq_{12}^2\bar{\chi}_1 - 16e^2Z_EF_0^2L_5^rq_{12}^2\chi_1 \\
&- 12e^2F_0^2\left[K_1^{Er} + K_2^{Er} - K_7^{Er} - K_8^{Er}\right]\overline{Q}_2\chi_1 \\
&- 4e^2F_0^2\left[K_5^{Er} + K_6^{Er} - K_9^{Er} - K_{10}^{Er}\right]q_p^2\chi_1 \\
&+ 12e^2F_0^2K_8^{Er}q_{12}^2\bar{\chi}_1 \\
&+ 8e^2F_0^2\left[K_{10}^{Er} + K_{11}^{Er}\right]q_{12}^2\chi_1 - e^2F_0^2\left[8K_{18}^{Er} + 4K_{19}^{Er}\right]q_1q_2\chi_1 \\
&- 1/3\bar{A}(\chi_m)R_{n11}^m\chi_1 - 1/3\bar{A}(\chi_1)R_1^c\chi_1 \\
&+ e^2F_0^2\left[\bar{A}(\chi_1) + 2Z_E\bar{A}(\chi_{1s})\right]q_{12}^2 \\
&- 1/3\bar{B}(\chi_1,\chi_1,0)R_1^d\chi_1 \\
&+ 4e^2F_0^2\left[\bar{B}(\chi_\gamma,\chi_1,\chi_1) - \bar{B}_1(\chi_\gamma,\chi_1,\chi_1)\right]q_{12}^2\chi_1
\end{aligned} \tag{5.11}$$

and

$$\begin{aligned}
\delta^{(4)23} &= \left[48L_6^r - 24L_4^r\right]\bar{\chi}_1\chi_{13} + \left[16L_8^r - 8L_5^r\right]\chi_{13}^2 \\
&- 48e^2Z_EF_0^2L_4^rq_{13}^2\bar{\chi}_1 - 16e^2Z_EF_0^2L_5^rq_{13}^2\chi_{13} \\
&- 12e^2F_0^2\left[K_1^{Er} + K_2^{Er} - K_7^{Er} - K_8^{Er}\right]\overline{Q}_2\chi_{13} \\
&- 4e^2F_0^2\left[K_5^{Er} + K_6^{Er}\right]q_p^2\chi_{13} + 4e^2F_0^2\left[K_9^{Er} + K_{10}^{Er}\right]q_p^2\chi_p \\
&+ 12e^2F_0^2K_8^{Er}q_{13}^2\bar{\chi}_1 \\
&+ 8e^2F_0^2\left[K_{10}^{Er} + K_{11}^{Er}\right]q_{13}^2\chi_{13} - e^2F_0^2\left[8K_{18}^{Er} + 4K_{19}^{Er}\right]q_1q_3\chi_{13} \\
&- 1/3\bar{A}(\chi_m)R_{n13}^m\chi_{13} - 1/3\bar{A}(\chi_p)R_{q\pi\eta}^p\chi_{13} \\
&+ e^2F_0^2\bar{A}(\chi_{13})q_{13}^2 + 2e^2Z_EF_0^2\bar{A}(\chi_{1s})q_{1s}q_{13} - 2e^2Z_EF_0^2\bar{A}(\chi_{3s})q_{3s}q_{13} \\
&+ 4e^2F_0^2\left[\bar{B}(\chi_\gamma,\chi_1,\chi_1) - \bar{B}_1(\chi_\gamma,\chi_1,\chi_1)\right]q_{13}^2\chi_{13}
\end{aligned} \tag{5.12}$$

provide a large number of QCD and QED low energy constants (L_i^r and K_j^{Er}) that must be determined. The parameters $\chi_i = 2B_0m_{qi}$ parametrize the quark mass dependency, and q_i the fractional quark charges. The indices $i = 1, 2, 3$ refer to valence and $i = 4, 5, 6$ to sea quarks. The quantity $q_{ij} = q_i - q_j$ is the meson charge. An index p implies summation over all valence quarks (of the meson). The bared variables $\overline{Q}_2$ and $\bar{\chi}_1$ indicate summation over all sea quarks, and are therefore $\overline{Q}_2 = 0$ and $\bar{\chi}_1 \approx$ const. $\approx \bar{\chi}_{1,\text{phys.}}$ on our dynamic, SLiNC QCD ensembles. Furthermore A and B are loop integrals

containing chiral logs, R are mass ratios and a photon mass χ_γ regulates IR divergences. We refer the reader to the original paper [142] for the exact definitions.

Global fits including all of the LECs above are unstable and possibly contain a large number of irrelevant parameters. They furthermore do not include FV corrections. A parametrization with a reduced set of parameters which includes FV corrections may provide more intuitive insight.

$SU(3)$ χPT might be poorly convergent and fits to a $\mathrm{tr}M$ = const quark mass trajectory are insufficiently constrained. Alternative extrapolation formalisms include $SU(2)$+kaon+QED χ-PT [130], and simple polynomial fits in m_π^2, m_K^2 [132] which could be customized to fit the (strange) mass extrapolation scheme of our ensembles.

Light quark masses and pion mass splitting

A low energy description of pseudoscalar meson masses depending on (renormalized) quark masses m_q and the meson charge Q^2 can be used to calculate the light quark mass splitting at a convenient scale μ. Quark masses are renormalized and $\mathcal{O}(a)$ improved by

$$m_q^{\overline{\mathrm{MS}}}(\mu) = Z_m(g^2, a\mu)(1 + b_m(g_0^2)am_q)m_q \tag{5.13}$$

$$b_m = b_m^{(0)} + b_m^{(1)} \times C_F\, g_0^2 + \mathcal{O}(g_0^4) \simeq -0.6387 \tag{5.14}$$

with a non-perturbative $Z_m^{-1} = Z_s^{\overline{\mathrm{MS}}} = 0.6822(061)(176)$ from [161] at $\mu = 2\,\mathrm{GeV}$, $b_m^{(0)} = -1/2$ inferred from the relation $b_s = -2b_m$ [162] and the LO coefficient $b_m^{(1)} = -0.05722$ from [116]. The dependence on the average sea quark mass parametrized by $\bar{b}_m$ is ignored.

For the estimation of the individual light quark masses, quark and meson masses are transformed to physical units and eq. (5.13) is applied to the quark masses. The improved and renormalized data is fitted to (χPT) extrapolation formulae yielding a set of parameters. These parameters will in the following be referred to as LECs although they do not belong to a specific and complete χPT formulation. An example of an extrapolation formula is

$$M^2 = \left[A_0 Q^2 + \left(B_0 + B_1 Q^2\right)(m_q + m_{\bar{q}})\right]. \tag{5.15}$$

These expressions are then matched to experimental meson mass values - we use the masses m_{π^+}, m_{K^0} and m_{K^+} - yielding renormalized quark masses in the $\overline{\mathrm{MS}}$ scheme.

To (partially) account for the systematic error, the following considerations and variations entered into the analysis:

- The different fit range criteria mentioned above often gave the same fit range which we was only counted once. The fit ranges were complemented by a fit range $t/a \in [T/2 - 7, T/2 - 1]$.
- To investigate QCD and remaining QED FV effects we used an optional cut on Lm_π which excludes the ensembles `M2` and `L2`.

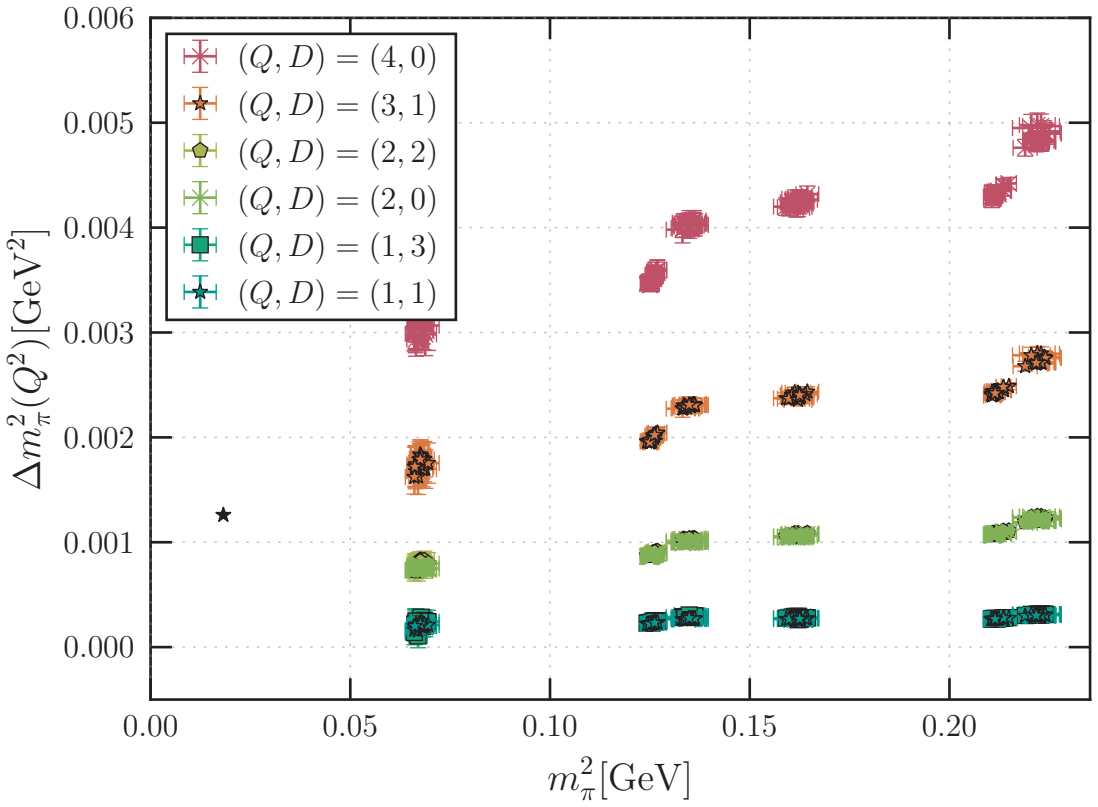

Figure 5.2.: Light pseudoscalar mass splitting for various charge combinations. Shown are all ensembles and multiple fit ranges. Note the fit range dependence at the lightest pion mass which hints at problems due to the low Lm_π. The finite volume contributions of the charged masses are removed up to NLO. The ensembles are (left to right) `L2`, `L1`, `M2`, `M1`, `L0` and `M0`. The steps between $L = 24$ and $L = 32$ lattices are due to higher order finite volume contributions. The black star is the physical point.

- We use the lattice spacing $a = 0.075\,\mathrm{fm}$, which was given without quoting an error [160]. An error value ($0.002\,\mathrm{fm}$) was estimated by comparison to the determination in [163]. To account for lattice spacing effects the three values $a = 0.073, 0.075$ and $0.077\,\mathrm{fm}$ were used.

- The parameter b_m describing the quark mass dependence of the renormalization constant Z_m might be subject to large non-perturbative contributions. To account for this the analysis was performed with the LO value $b_m = -0.5832$ and approximately twice that value: $b_m = -1$.

- We choose to neglect the kaon mass data on the individual ensembles and assume that our fit formulae are valid up to the strange mass. This assumption is motivated

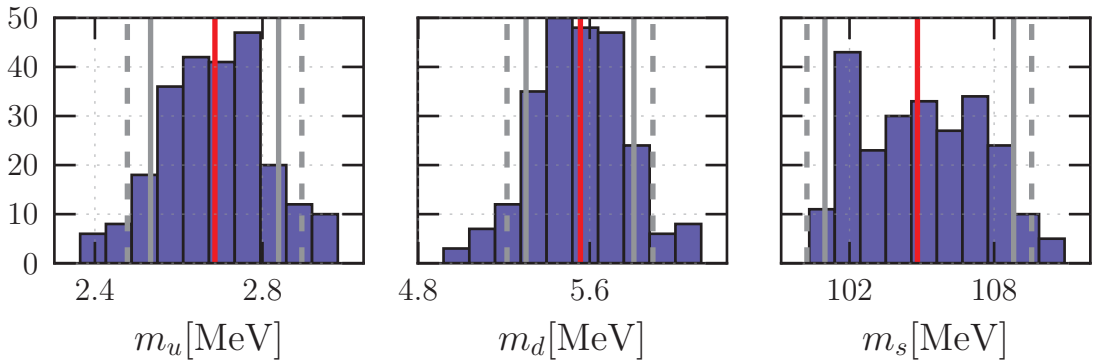

Figure 5.3.: Histogram of light and strange quark mass results. The median is marked by the red, the systematic error by the grey and linearly added statistical and systematic error by the grey dashed line. Most of the width in the m_s histogram is due to the lattice spacing variation.

by the impressive success of early quenched QCD+QED simulations with large quark masses [127, 128]. A fully controlled analysis would need to include the kaon and rigorously address this.

- To determine the coefficients A_0, B_0, B_1 and optionally C_0 (for the m_q^2 term) we fit the squared splittings $\Delta M^2(Q^2, m_{q,\text{sea}}, L \times T)$ and the sea pseudoscalar $M^2(Q^2 = 0, m_{q,\text{sea}}, L \times T)$ individually. Therefore eq. (5.15) is split and the sea pseudoscalar fit is complemented by an additional term $\propto m_q^2$.

- As previously discussed the mistuning of the lattice spacing a lead to singlet quantities (eq. (5.1)) that are heavier than their physical values. In light of the fact that we do not include kaon data into our chiral fits, the effect causes the extrapolation to a strange sea quark that is approximately 25% too heavy [160]. Strange and (degenerate) light quark masses from $N_f = 2 + 1$ measurements are roughly 10% lighter than on $N_f = 2$ [14]. Assuming a $\frac{1}{m_s}$ interpolation for $m_s \in [m_s^{\text{phys}}, \infty]$ yields a 2% deviation. We therefore add 2.5% in quadrature to account for higher order terms in the inverse mass expansion. The effect on the previously determined LECs is highly correlated with the quark masses and approximately cancels in the products $B_{0,1} m_q$. The Dashen terms and the pion mass difference only contain such products and should therefore be unaffected. We conservatively add the same 2.5% as for the quark masses. An extended analysis including kaon masses could be corrected along the lines of [160].

- To account for electromagnetic quenching errors we use the conservative estimate discussed in section 4.1.1: Quenching is assumed to maximally cause 10% corrections to the $\mathcal{O}(\alpha)$ splittings which is incorporated by adding uncorrelated noise to the resampled splittings. The error is thereby propagated to our final results: The

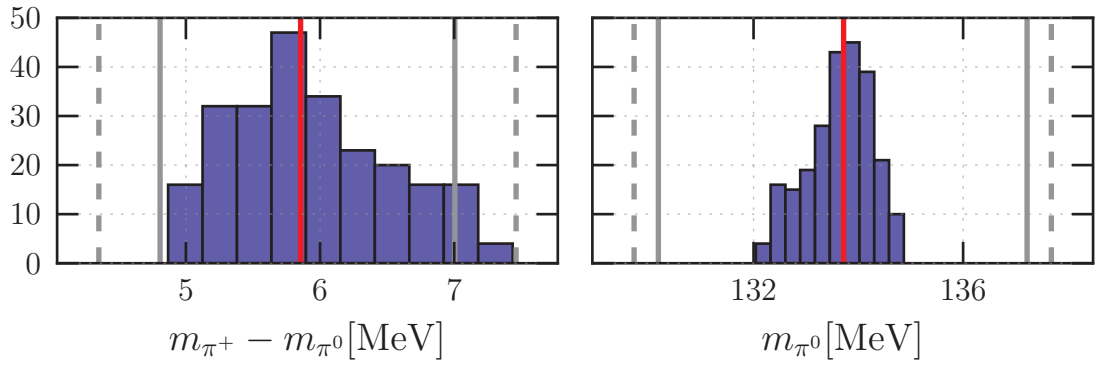

Figure 5.4.: Histogram of light pion mass (splitting) results. The vertical lines have the same meaning as in fig. 5.3.

quark masses are only mildly affected, whereas pion mass splitting and Dashen terms show a large dependence.

Our estimates at $\mu = 2\,\mathrm{GeV}$ in the $\overline{\mathrm{MS}}$ scheme become

$$\boxed{\begin{aligned} m_u &= (2.69 \pm 0.06_{\mathrm{stat.}} \pm 0.15_{\mathrm{sys.}})\,\mathrm{MeV}, \\ m_d &= (5.56 \pm 0.09_{\mathrm{stat.}} \pm 0.25_{\mathrm{sys.}})\,\mathrm{MeV}, \\ m_s &= (105 \pm 1_{\mathrm{stat.}} \pm 4_{\mathrm{sys.}})\,\mathrm{MeV} \end{aligned}} \tag{5.16}$$

The center value is the median of the results shown in the histograms of fig. 5.3 and the statistical error is conservatively taken as the median of the corresponding statistical errors. The error propagation utilized Jackknife and Bootstrap, which agree within statistical errors. The systematic error is determined from the appropriate 1-σ quantiles and the additional contributions discussed above. It does however not account for the necessary continuum extrapolation or possible QCD autocorrelations. Nevertheless these results and the PDG averages [23] agree within their respective errors. The PDG values are mostly based on other lattice calculations such as [130, 135] and [164].

Following the analysis of [127] the determined quark mass values can be used to approximate the neutral pion mass

$$m_{\pi^0} = \frac{m_{u\bar{u}} + m_{d\bar{d}}}{2} \tag{5.17}$$

which yields the pion mass splitting

$$\boxed{m_{\pi^\pm} - m_{\pi^0} = (5.9 \pm 0.5_{\mathrm{stat.}} \pm 1.1_{\mathrm{sys.}})\,\mathrm{MeV}.} \tag{5.18}$$

Center and error values were determined as above. The result is within its error slightly too large compared to the (experimental) PDG value 4.5936(5) MeV [23] which can

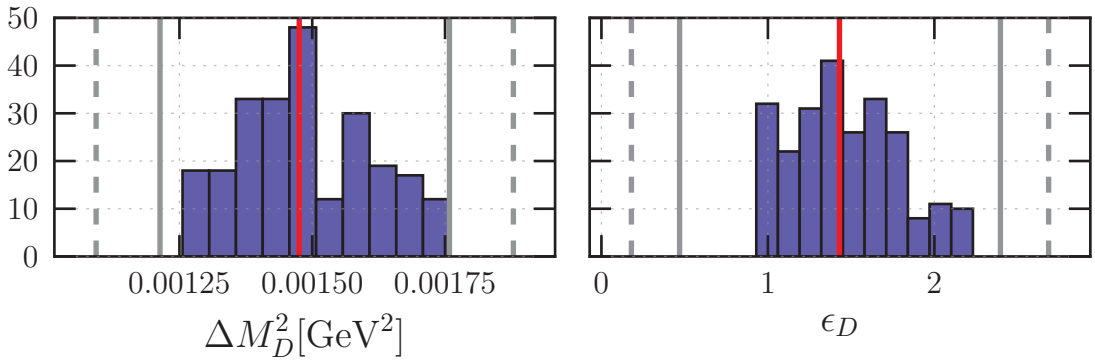

Figure 5.5.: Histogram of absolute and relative Dashen term results. The vertical lines have the same meaning as in fig. 5.3.

probably be attributed to our chiral approximations.

Dashen term

The Dashen term is another benchmark observable for partially quenched simulations proposed in [142]. Its quenching errors should be suppressed because most of the sea quark charge contributions in eq. (5.10) cancel. The term which is the absolute correction to Dashen's theorem [165] is defined as the difference of the electromagnetic kaon and the pion mass splitting

$$\Delta M_D^2 = \left(m_{K^+}^2 - m_{K^0}^2\right) - \left(m_{\pi^+}^2 - m_{\pi^0}^2\right) \tag{5.19}$$

at symmetric light quark masses $m_u = m_d = m_{ud}$ and interesting because of higher order electromagnetic isospin breaking. This can be generalized to arbitrary mass scales $\chi_{1,3}$

$$\begin{aligned}\Delta M^2 = {} & M^2(\chi_1, \chi_3, q_1, q_3) - M^2(\chi_1, \chi_3, q_3, q_3) \\ & - M^2(\chi_1, \chi_1, q_1, q_3) + M^2(\chi_1, \chi_1, q_3, q_3).\end{aligned} \tag{5.20}$$

A widely used alternative is to give the correction to Dashen's theorem in its relative form given by

$$\epsilon_D = \frac{m_{K^+}^2 - m_{K^0}^2}{m_{\pi^+}^2 - m_{\pi^0}^2} - 1 \tag{5.21}$$

These numbers can be evaluated with the LECs determined above yielding

$$\boxed{\begin{aligned}\Delta M_D^2 &= (0.00148 \pm 0.00012_{\mathrm{stat.}}(^{+0.00028}_{-0.00026})_{\mathrm{sys.}})\,\mathrm{GeV}^2, \\ \epsilon_D &= (1.43 \pm 0.29_{\mathrm{stat.}}(^{+0.97}_{-0.96})_{\mathrm{sys.}})\end{aligned}} \tag{5.22}$$

where center and error values were determined following the same procedure as in the quark mass analysis. These results are large in comparison to current lattice averages [14, 24] which indicate the lack of predictive power of our extrapolation formula eq. (5.15) and variations of it. This also shows that the values of m_{ud}/m_s or B_1 are problematic or additional terms are necessary. More sophisticated formulae require more data which is currently not available to us.

Another possibility of calculating these quantities on our data set would be the direct measurement of the splitting with equal up and down masses. This splitting is then naively extrapolated to the physical point defined by the pion and kaon masses, where the singlet and therefore strange quark mistuning has to be taken into account. The pion mass splitting requires the neutral pion mass which can be approximated in terms of the connected $u\bar{u}$ and $d\bar{d}$ correlators at symmetric light quark mass:

$$C_{\pi^0}(t) = \frac{1}{2}\left(C_{u\bar{u}}(t) + C_{d\bar{d}}(t)\right) \propto \mathrm{e}^{-m_{\pi^0}t} \tag{5.23}$$

This method should yield comparable numbers within errors. Similar and extended analysis of QED effects on the Dashen terms, pseudoscalar and quark masses can be found in [135, 141].

5.2.2. Pseudoscalar decay constants

Lattice decay constants can be extracted from two point functions following the procedure described in section 3.3.4. They belong to the so-called gold plated observables which can be measured with percent precision where QED effects become relevant. Decay constants are necessary for the determination of CKM matrix elements and checks of the unitary triangles. Recently a method was outlined in [134] for the calculation of $\mathcal{O}(\alpha_{\mathrm{em}})$ corrections to hadronic matrix elements. The π^0 decay constant f_{π^0} appears in effective formulae for the dominant decay rate $\Gamma(\pi^0 \to \gamma\gamma)$ and may provide insight into (isospin violating) π^0, η, η' mixing.

We therefore measure smeared-point pion-axial current $C^{LS}_{A_4P}(t)$ and pion-pion $C^{LS}_{PP}(t)$ as well as smeared-smeared pion-pion $C^{SS}_{PP}(t)$ correlators and perform combined fits with the same mass parameter and identical fit ranges. A second analysis uses point sources. We use the matrix element convention in which f_{π^+} is approximately 130 MeV. After renormalization and improvement charged decay constants are matched at the same quark masses $\{m_{f_i}\}$ (parametrized by the symmetric uncharged pseudoscalar masses $M^2(Q^2 = 0, m_1 = m_2 = m_{f_i})$) within their respective meson (mass) types $f_1\bar{f}_2$. We subtract the corresponding uncharged QCD decay constants and analyzed their mass and finite volume dependence across multiple ensembles.

Renormalization and improvement

The decay constant is calculated according to eq. (3.40). For this we use a renormalization constant Z_A determined using the RI-SMOM scheme [161] and b_A and c_A determined in one loop PT [107]. At this order these are independent of the fermion action. The

(a) vertex correction (b) propagator correction

Figure 5.6.: QED contributions at $\mathcal{O}(\alpha_{\text{em}})$ to QCD+QED renormalization constants. The sign of fig. 5.6a depends on the relative sign of the quark charges. The total LO QED corrections to charge neutral vertices can be obtained with an appropriately scaled coupling from the analogous QCD formula. General charge combinations do not obey the same symmetries and would require to disentangle the QED contributions.

used values are

$$Z_A = 0.8728(006)(027) \tag{5.24}$$

$$b_A = b_A^{(0)} + b_A^{(1)} g_0^2 + \mathcal{O}(g_0^4) \simeq 1.21358 \tag{5.25}$$

$$\text{with} \qquad b_A^{(0)} = 1, \quad b_A^{(1)} = 0.0881(13) \times C_F, \quad C_F = \frac{N_c^2 - 1}{2N_c}$$

and

$$c_A^{PT} = c_A^{(1)} g_0^2 + \mathcal{O}(g_0^4) \simeq -0.01097 \tag{5.26}$$

$$\text{with} \qquad c_A^{(1)} = -0.004525(25) \times C_F$$

Note, however, that perturbative and non-perturbative values of c_A for a similar action (Clover + LW) differ by $300 - 400\%$ [108]. Similarly the higher order corrections to b_A are commonly also large [166]. For this reason we also performed the analysis with the large values $c_A = -0.05$ and $b_A = 2$ to estimate possible NP corrections. A comparison is illustrated in fig. B.3.

Since all of these values are in principle subject to QED modifications we furthermore perform the complete analysis with $b_A = c_A = 0$ and $Z_A = 1$ to assert that variations of these parameters do not influence the splitting signal significantly. All of these values depend in principle on the fractional charges $e_{1,2}$. The effects on the renormalization constant Z_A are especially troubling which can be seen by considering the LO contributions (as shown in fig. 5.6) in LPT

$$Z_A^{\text{QED,LO}}(e_1, e_2) = e_1 e_2 \tilde{Z}^{(2)}_{A,\text{vertex}} + \left(e_1^2 + e_2^2\right) \tilde{Z}^{(2)}_{A,\text{propagator}} \tag{5.27}$$

which clearly distinguish attraction and repulsion and do not allow for a simple rescaling of the normal QCD results if the meson is charged. The vertex contribution is of the

same order $\mathcal{O}(\alpha_{\text{em}})$ as the leading contribution to the signal, it is not suppressed by any other small factors and might therefore cancel the observed signal.

The charge dependence of the improvement coefficient c_A has the same form

$$c_A^{\text{QED,LO}}(e_1, e_2) = e_1 e_2 \tilde{c}_{A,\text{vertex}}^{(2)} + \left(e_1^2 + e_2^2\right) \tilde{c}_{A,\text{propagator}}^{(2)} \tag{5.28}$$

which can determined from the analogous determination for QCD in LO LPT [167, 168]. The remaining parameter b_A does not contain a $e_1 e_2$ term such that we can model the charge dependence of the improvement coefficient b_A by the replacement

$$b_A am \to b_A am + \tilde{b}_{A,\text{QED}}^{(2)} \left(e_1^2 am_1 + e_2^2 am_2\right). \tag{5.29}$$

Instead of determining these coefficients we can test the stability of our signal by varying the unknown parameters $\tilde{b}_A^{(2)}$ and $\tilde{c}_A^{(2)}$ in a suitable range (see eq. (5.37)). Note that QCD+QED renormalization constants for QED_L might be volume dependent as pointed out by [137].

Parameterization of QED effects on decay constants

A χPT prediction for the decay constant splitting truncated at $\mathcal{O}(p^6, e^2p^4)$ can be found in [142]

$$F_{\text{phys}} = F_0 \left[1 + \frac{f^{(4)vs}}{F_0^2} + \mathcal{O}(p^6, e^2p^4)\right], \tag{5.30}$$

where (4) is the order we are working at and v and s are the number of non-degenerate valence and sea quark masses. The higher order terms are given by

$$\begin{aligned} f^{(4)13} &= 12L_4^r \bar{\chi}_1 + 4L_5^r \chi_1 + 1/4 \bar{A}(\chi_{e,ps}) \\ &+ 6e^2F_0^2 \left[K_1^{Er} + K_2^{Er}\right] \overline{Q}_2 + 2e^2F_0^2 \left[K_5^{Er} + K_6^{Er}\right] q_p^2 \\ &+ 2e^2F_0^2 K_{12}^{Er} q_{12}^2 + e^2F_0^2 \left[4K_{18}^{Er} + 2K_{19}^{Er}\right] q_1 q_2 \\ &+ 2e^2F_0^2 \left[\bar{B}'(\chi_\gamma, \chi_1, \chi_1) - \bar{B}_1'(\chi_\gamma, \chi_1, \chi_1)\right] q_{12}^2 \chi_1 \\ &- e^2F_0^2 \bar{B}_1(\chi_\gamma, \chi_1, \chi_1) q_{12}^2 \end{aligned} \tag{5.31}$$

and

$$\begin{aligned} f^{(4)23} &= 12L_4^r \bar{\chi}_1 + 4L_5^r \chi_{13} + 1/4 \bar{A}(\chi_{e,ps}) \\ &- 1/12 \bar{A}(\chi_m) R_{mn13}^v + \bar{A}(\chi_p) \left[1/6 R_{q\pi\eta}^p - 1/12 R_p^c\right] \\ &+ 6e^2F_0^2 \left[K_1^{Er} + K_2^{Er}\right] \overline{Q}_2 + 2e^2F_0^2 \left[K_5^{Er} + K_6^{Er}\right] q_p^2 \\ &+ 2e^2F_0^2 K_{12}^{Er} q_{13}^2 + e^2F_0^2 \left[4K_{18}^{Er} + 2K_{19}^{Er}\right] q_1 q_3 \\ &+ 2e^2F_0^2 \left[\bar{B}'(\chi_\gamma, \chi_{13}, \chi_{13}) - \bar{B}_1'(\chi_\gamma, \chi_{13}, \chi_{13})\right] q_{13}^2 \chi_{13} \\ &- e^2F_0^2 \bar{B}_1(\chi_\gamma, \chi_{13}, \chi_{13}) q_{13}^2 - 1/12 \bar{B}(\chi_p, \chi_p, 0) R_p^d, \end{aligned} \tag{5.32}$$

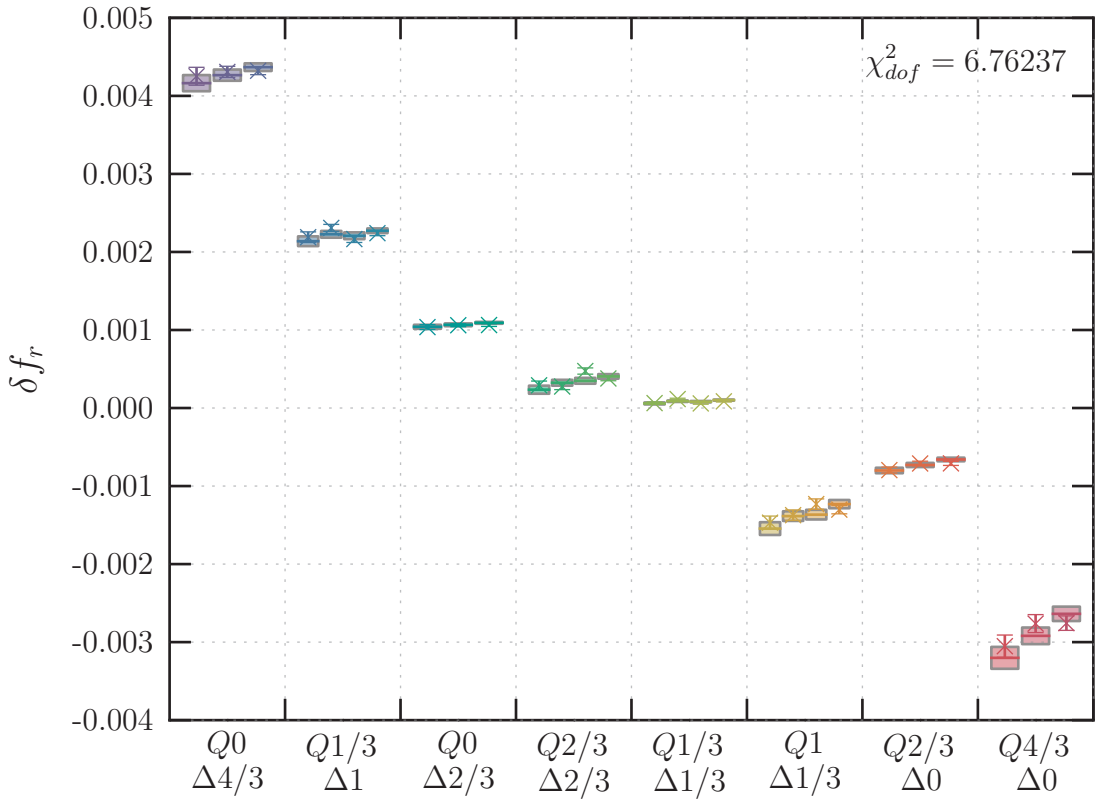

Figure 5.7.: Light and strange pseudoscalar decay constant splitting on the ensemble `L0`. The data in the individual charge channel columns corresponds left to right to doubly light, light-strange (, strange-light) and doubly strange mass combinations. The crosses are the original splittings. The bands are the fit results with errors. The fit function is $\delta f_r = (B_0 + B_1\chi_{ij})Q^2 + D_0\Delta_q^2 + S_0 Q\Delta_q\chi_{ij}$. The large χ^2_{dof} is due to the unaccounted finite size effects and large correlations between all data points. Fits with a diagonal covariance matrix yield χ^2_{dof} values of approximately 1.

where the parameter definitions are the same as for eqs. (5.11) and (5.12).

Given the number of free parameters and that these formulae do not include finite size effects we will not try to fit them directly but rather identify individual dependencies and combine them with various finite volume parametrizations. For this we compare the absolute difference

$$\delta f(q_1, q_2) = f(q_1, q_2) - f(0, 0) \tag{5.33}$$

of charged and pure QCD decay constants $f(0,0)$ at matched quark masses. The difference cancels all terms of eqs. (5.31) and (5.32) which do not depend on the valence

quark charges. This motivated the following parametrization for global fits of the absolute splitting

$$\begin{aligned}\delta f(q_1, q_2) = &\left(B_0 + B_1 M^2(q_1, q_2)\right) q_{12}^2 \\ &+ \left(P_0 + P_1 M^2(q_1, q_2)\right) q_p^2,\end{aligned} \tag{5.34}$$

which neglects the logarithmic dependencies and can be extended by FV terms. The $q_i q_j$ terms of eqs. (5.31) and (5.32) are dropped from the fits because they are a linear combination of q_{ij}^2 and q_p^2. The term is furthermore undesirable because its finite volume effects are rather unintuitive since the term can be nonzero for both charged and uncharged decay constants.

We also performed extrapolations of the relative splitting

$$\delta f_r(q_1, q_2) = \delta f(q_1, q_2)/f(0, 0), \tag{5.35}$$

which introduces an additional quark mass dependence in the denominator, leading for example to a q_p^2/χ_1 term which complicates the necessary extrapolations. For these we chose a natural and intuitive parametrization within a meson (mass) type: On a single ensemble the splittings depend on the meson charge[2] $q_{12} = Q = q_1 - q_2$ and quark charge difference $\Delta_q = q_1 + q_2$, and can be parametrized by

$$\delta f_r^{(i)}\left(Q^2, \Delta_q^2\right) = B^{(i)} Q^2 + C^{(i)} \Delta_q^2, \tag{5.36}$$

which can easily be observed in the light-light channel (i) on the ensemble `L0` of fig. 5.7. Note that the meson charge dependence is quite noisy in comparison to the splittings of neutral channels. The inclusion of strange channels hints at the fact that $B^{(i)}$ might be quark mass dependent as also indicated by $q_{ij}^2 \chi_{ij}$ terms in eq. (5.31) and eq. (5.32) or that large finite volume effects are present. Mass dependencies of $C^{(i)}$ could not be observed, neither by eye nor by the inclusion of corresponding terms and fitting with a nonzero coefficient.

The effect of charge dependent renormalization and improvement parameters Z_A, b_A and c_A was investigated by varying the $\mathcal{O}(\alpha_{\text{em}})$ contributions of eqs. (5.27) to (5.29) in a 5% range of a corresponding QCD parameter:

$$\begin{aligned}\tilde{b}_{A,\text{QED}}^{(2)} &= \pm\, 0.05(b_A - 1) \approx \pm 0.0107 \\ \tilde{c}_{A,x}^{(2)} &= \pm\, 0.05\, c_A \approx \pm 5.49 \times 10^{-4} \\ \tilde{Z}_{A,x}^{(2)} &= \pm\, 0.05(1 - Z_A) \approx \pm 0.00636\end{aligned} \tag{5.37}$$

where x indicates either the vertex or propagator contribution and the values for b_A, c_A and Z_A from eqs. (5.24) to (5.26) were used. The effect is shown in figs. 5.8 and 5.14. These ranges can be understood as a worst case since we would naturally assume that such QED effects are approximately 1%. It shall also be noted that the signs of the in-

[2] Again $-q_2$ is the charge of the anti-quark $\bar{f}_2$.

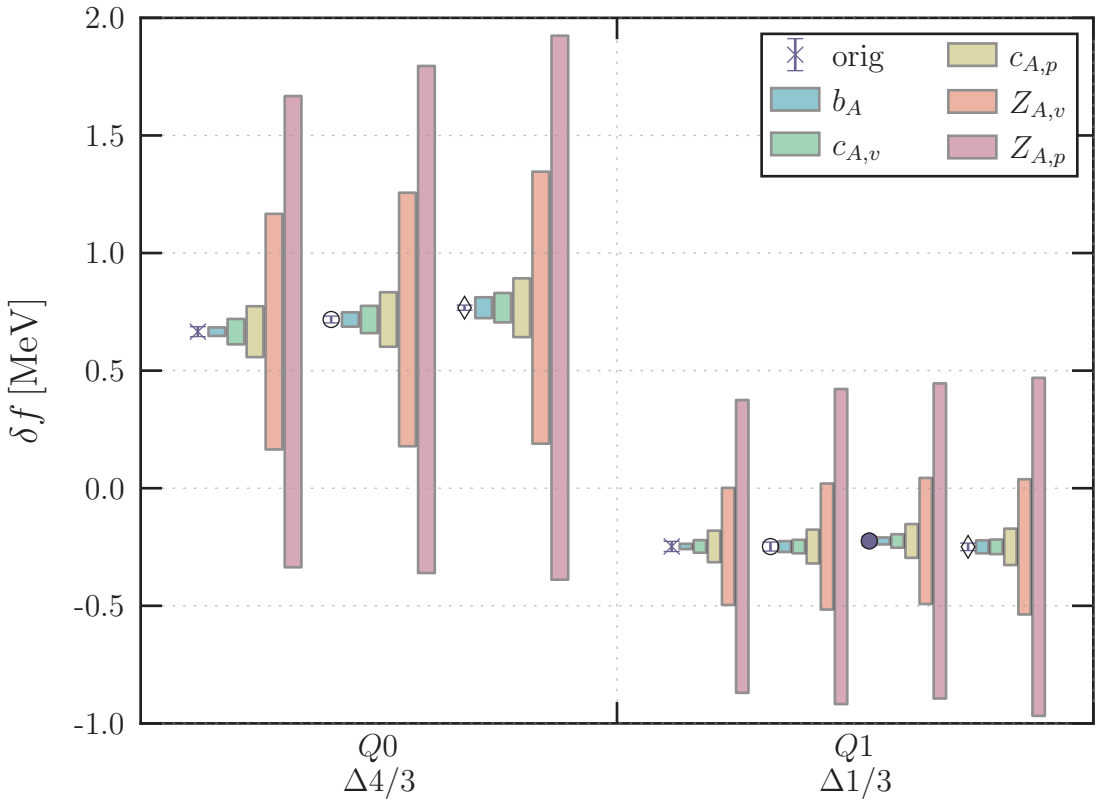

Figure 5.8.: Effects of a hypothetical charge dependence of renormalization and improvement parameters b_A, c_A and Z_A on the extracted splittings on ensemble `L0`. The effects were modeled by varying the $\mathcal{O}(\alpha_{\text{em}})$ coefficients of eqs. (5.27) to (5.29) in a 5% range of an equivalent QCD parameter. Vertex and propagator components may cancel. The cross is the doubly light, the circle the light-strange and the diamond the doubly strange channel. Full (open) symbols indicate physical (unphysical) charge combinations. There is also a zoomed plot without the Z_A variations (fig. 5.14).

dividual components are unknown and that vertex and propagator contributions might partially cancel (or sum up). Given that the 5% variation is probably largely overestimating the individual contributions, we expect the effects of $b^{(2)}_{A,\text{QED}}$ and $c^{(2)}_{A,x}$ to be roughly of the same size as our statistical error and ignore them in the following for light observables. The substantial effects on Z_A motivated us to examine ratios of charged renormalization constants where the renormalization constant drops out. For this purpose we calculated

$$R_{M,\text{rel}} = \frac{f_M(Q^2 = 1)}{f_{\pi^+}} \left(\frac{f_\pi}{f_M}\right)_{\text{QCD}} - 1 \tag{5.38}$$

which is shown in fig. 5.9. The result indicates permille QED corrections to the kaon-pion decay constant ratio before the physical limit. The D meson ratios are too noisy for any conclusions. They are furthermore also substantially affected by remaining b_A-QED artifacts due to the charm mass which can be seen in the splitting in fig. 5.14.

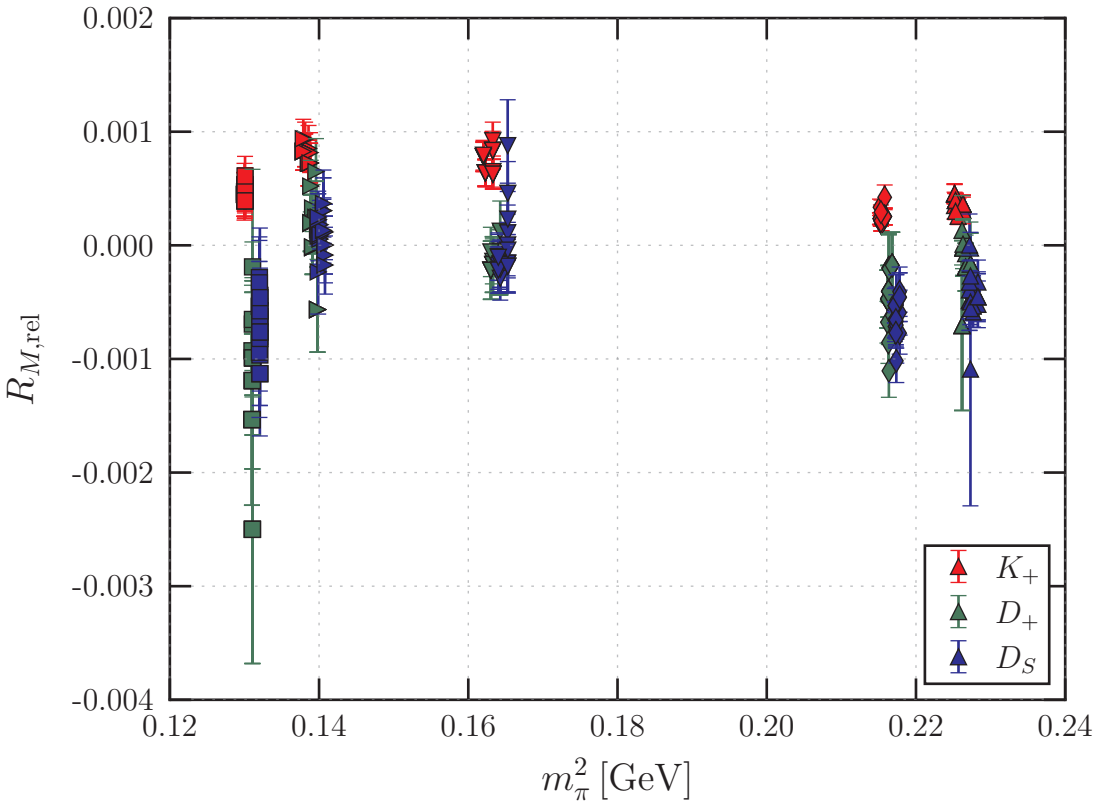

Figure 5.9.: Decay constant ratios which are independent of QCD+QED renormalization. Shown are (left to right) ratios of the ensembles `L1`, `M2`, `M1`, `L0` and `M0`. Multiple data points with the same color and symbol correspond to different fit ranges, bin sizes and covariance matrix estimations. The D meson ratios are slightly shifted for better visibility.

Although not predicted at the order of eq. (5.30) it is interesting to compare channels where the light quark charge q_l is larger than the heavy quark charge q_h to the case where the order is reversed: $\Delta f_{|q_l|>|q_h|} \neq \Delta f_{|q_l|<|q_h|}$. Parameterizing this effect could be done by a new term that is antisymmetric under quark exchange like

$$Q\Delta_q \cdot \Delta^k m = (q_1^2 - q_2^2) \cdot (m_1^k - m_2^k). \tag{5.39}$$

This effect is not directly observable because appropriate quarks are missing in nature.

Finite size effects

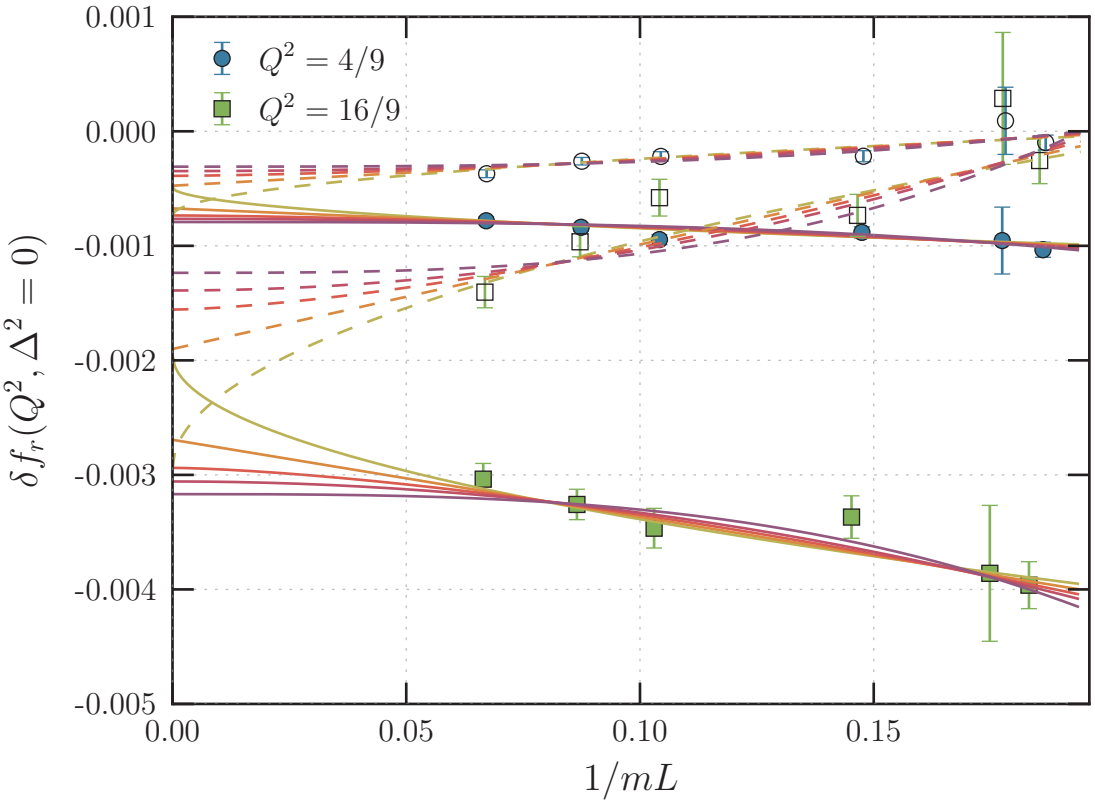

Figure 5.10.: Comparison of the doubly light and doubly strange decay constant splittings with (full symbols) and without (open symbols) removal of LO and NLO mass finite volume contributions. Note that the improvement is only partial. The solid (dashed) lines are $f(L) = f_0 + \tilde{f}_{1,p}/L^p$ fits to FV improved (unimproved) data of both charge combinations with powers $p \in [1/2, 1, 3/2, 2, 3]$. Additional meson mass m dependence of the splitting is ignored. The data from the smallest ensemble is rather unstable. Plotted is data from the ensembles `M0`, `L0`, and `S0`.

Given the definition $\langle 0|A_4|\pi\rangle = m_\pi f_\pi$, the severe QED finite volume effects of $m_\pi(Q^2)$ and that f_π has sizable QCD finite volume effects [103] it is very likely that $\delta f(Q^2 \neq 0)$ (or δf_r) and the matrix element suffer from comparable effects.

To better understand the origin of the finite volume effects we compare two cases which should yield the same infinite volume value after appropriate extrapolation: The first does not correct $m_\pi(Q^2)$ and all FV dependence is therefore absorbed into $\delta f_r(Q^2, \Delta_q^2)$. The second corrects $m_\pi(Q^2)$ up to NLO using eq. (4.8). Hypothetically an independent mass analysis could be used to subtract even higher terms or the corrections could only be

performed to LO yielding even more cases to compare. The QCD effects should generally cancel in the ratio in eq. (5.35). The effect of the subtraction is illustrated in fig. 5.10 and fig. 5.18: A substantial amplification of the splitting signal is observed. Additionally the remaining volume correction of the charged signal seems to change its sign in accordance to the relative sign of NLO and NNLO corrections to the mass [138]. We perform somewhat arbitrary polynomial two parameter fits to purely repulsive systems to show the compliance of the data with various extrapolation formulae and that they might extrapolate towards the same value in infinite volume. Both charge combinations are fitted simultaneously. A systematic analysis would most likely reveal that a sum of analogous terms has to be used[3], but we have far too few data points or theoretical input to try more sophisticated fits. Furthermore ignoring the possible quark mass dependence both $1/L$ and $1/mL$ are tested as predictors yielding no clear preference. For appropriately large volumes and heavy masses the negative QED contribution of the charged decay constant becomes almost as large as the contribution to the corresponding attractive system. This agrees with the naive expectation that the effect of attraction and repulsion should approximately have the same absolute value. Although the slope of the current data suggests otherwise, remaining FV effects might account for the (now decreased) difference.

Above we have shown PQχPT parametrizations. These are rather involved. A generic fit formula that incorporates finite volume corrections for the splitting should have the general structure

$$\begin{aligned}\delta f_r(Q^2, \Delta_q^2, m_{\mathrm{PS}}^2, L) = Q^2 \left(\delta f_r^{(0,Q)} + \delta f_r^{(1,Q)} m_{\mathrm{PS}}^2 + \dots\right) \cdot \left(1 + \sum_{i=1} \frac{c_i}{(mL)^i}\right) \\ + \Delta_q^2 \left(\delta f_r^{(0,\Delta)} + \delta f_r^{(1,\Delta)} m_{\mathrm{PS}}^2 + \dots\right) \cdot \left(1 + \sum_{j=1} \frac{d_j}{(mL)^j}\right). \end{aligned} \tag{5.40}$$

We choose to ignore the strange sea quark contribution given that the sea quarks are not sensitive to the QED field anyway and that the flavor breaking effects are probably small at our heavier ensembles. Given the low number of data points this can be further reduced by ignoring the volume dependence of the attraction term ($d_j = 0$) and terminating the c_i sum at the first order $i = 1$. Similarly, the absolute splitting eq. (5.33) can be extended and becomes

$$\begin{aligned}\delta f(q_1, q_2) = \left(B_0 + B_1 M^2(q_1, q_2)\right) q_{12}^2 \cdot \left(1 + \sum_{i=1} \frac{L_b^{(i)}}{(mL)^i}\right) \\ + \left(P_0 + P_1 M^2(q_1, q_2)\right) q_p^2 \cdot \left(1 + \sum_{j=1} \frac{L_p^{(j)}}{(mL)^j}\right). \end{aligned} \tag{5.41}$$

We also replaced the $1/mL$ predictor by $1/L$ in both parametrizations.

For the extrapolation of uncharged combinations we can neglect finite volume effects.

[3] The FV extrapolation of the charged kaon mass at coupling $\alpha_{\mathrm{em}} = 1$ in [120] required $\mathcal{O}(1/L^3)$ terms.

Physical charged quark combinations are more complicated. The QED corrections in the parametrization above splits into two parts, one which is highly sensitive to FV effects and one that is not. Resolving the increased number of parameters either requires additional information in form of unphysical charge combinations or using a different parametrization such as

$$\delta f_r(Q^2 = 1, m_{\mathrm{PS}}^2, L) = (\delta f_r^{(0)} + \delta f_r^{(1)} m_{\mathrm{PS}}^2 + \dots) \cdot \left(1 + \sum_{k=1} \frac{c_k}{m^k L^k}\right) \tag{5.42}$$

that combines both terms. Suitable unphysical charge combination for the first option are purely repulsive $q_1 = q_2$ (or attractive) channels. Fits to two volumes do not have enough information to distinguish or weight different ansatz' but will rather just match the input data. To account for this ambiguity we always compare fits with and without finite volume improved meson mass. The two options are not independent and should not be combined in fits.

We tried to determine the lowest order of finite volume effects and their magnitude in a *non-relativistic* (NR) setup where the decay rate of quarkonium ($c\gamma_i\bar{c} \equiv J/\psi$) given by eq. 3.18 of [169],

$$\Gamma = \frac{16\pi\hbar^3 \alpha_{\mathrm{em}}^2 e_Q^2 |\Psi(0)|^2}{m_{J/\psi}^2}, \tag{5.43}$$

is proportional to the norm of the quarkonium wave function Ψ at its origin. NRQED is feasible because the electromagnetic effects are small compared to the mass of the meson. The Schrödinger equation with perturbing QED becomes

$$0 = \left[-\frac{\nabla^2}{2m_\pi} + V_S(\mathbf{r}) + V_{em}(\mathbf{r}) - E\right] \Psi(\mathbf{r}) \tag{5.44}$$

where we assume that $V_{em} \ll V_S$. Following textbook perturbation theory (in for example [170]) for quantum mechanics the LO correction to the unperturbed ground state $|\psi_1^{(0)}\rangle$ is given by

$$|\psi_1^{(1)}\rangle = \sum_{k \neq 1} \frac{\langle \psi_k^{(0)} | V_{em} | \psi_1^{(0)} \rangle}{E_1^{(0)} - E_k^{(0)}} |\psi_k^{(0)}\rangle \tag{5.45}$$

which clearly depends on the unknown, unperturbed set of states $\{|\psi_k^{(0)}\rangle\}$ for $k > 1$. The dominant FV contribution therefore probably comes from the electromagnetic potential in finite volume in the matrix elements

$$\langle \psi_k^{(0)} | V_{em} | \psi_1^{(0)} \rangle \tag{5.46}$$

of energetically low states $|\psi_k^{(0)}\rangle$ with support at $\mathbf{r} = 0$. The periodic potential could be expressed as a function of L according to [138] but approximating the FV asymptotics

of all relevant, unperturbed states for $(r \to 0)$ is difficult because many states such as $\pi\pi$ states or low radial excitations could significantly contribute. The lack of suitable choices led us to abandon this approach.

Light and strange observables

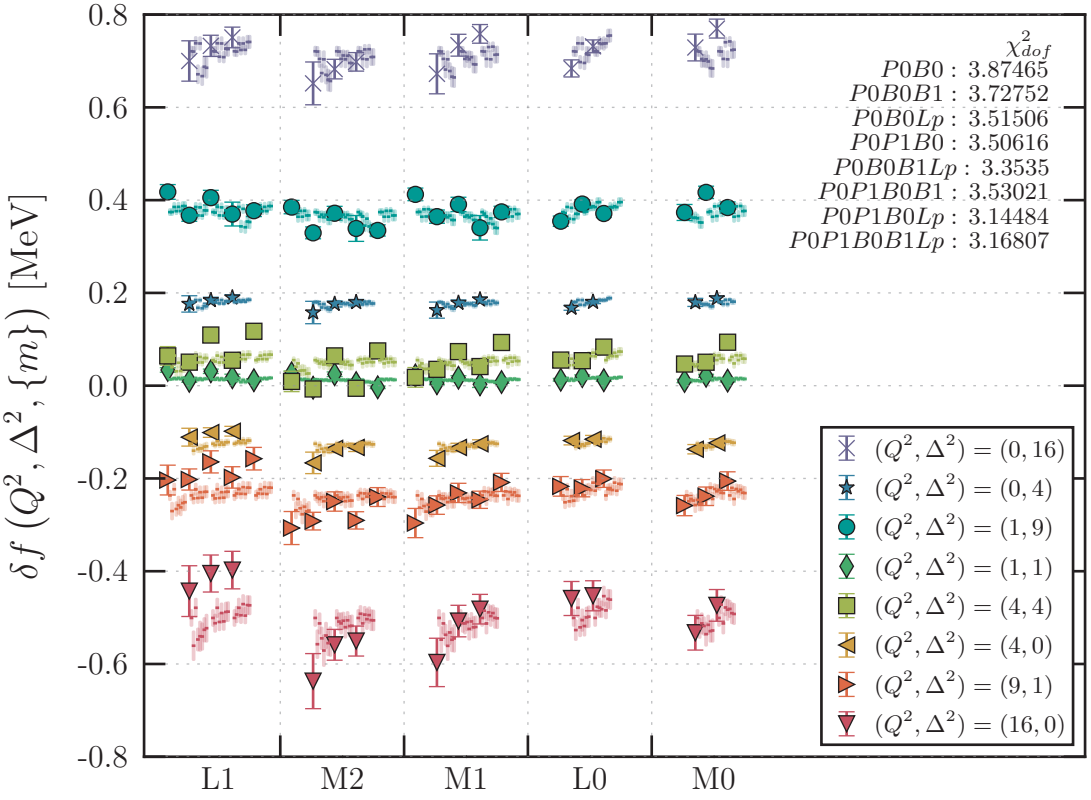

Figure 5.11.: Global fits to decay constant splitting on multiple ensembles. The symbols are the original splittings of doubly light and light-strange pseudoscalars. The predictions of the converged fits with a L^{-1} FV term are shown as bars to the right of the original data. Most combinations of fit parameters did not converge. The original data is specific to a fit range choice, bin size, renormalization choices etc. The parameter Lb corresponds to the amplitude of the finite volume term c_1 in the text. The multiple data points of one charge channel within a single ensemble are left to right: Doubly light, (light-strange$^{\text{sea}}$,) and light-strange$^{\text{phys}}$. If the quarks carry different absolute charges the light-strange channels are doubled by switching the charges.

Observables with physical charge combinations include the light pions π^0,π^+ and the

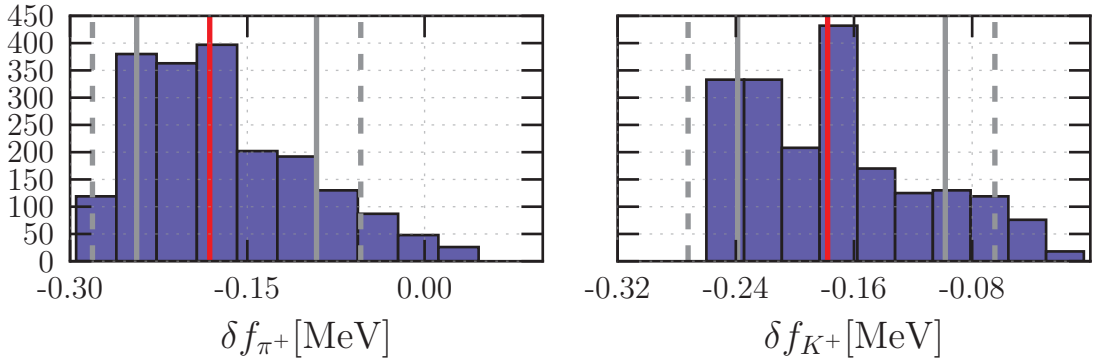

Figure 5.12.: Histogram of the extrapolations of pion decay constant splitting for $Q^2 = 1$. Fits with less free parameter converge more often and the histogram therefore shows a natural bias towards them. The median is marked by the red, the systematic error by the grey and the total linearly added error by the dashed vertical line.

kaons K^0 and K^+. Instead of direct extrapolation of appropriate charge combinations our mass and FV extrapolations utilized fits to eq. (5.34) which were optionally extended by independent L^{-1} (or $(mL)^{-1}$) finite volume corrections on all different charge terms. In the absence of more volumes this should give slightly more data to match finite volume terms. In most cases only fits with no FV term or only FV effects in the charge term q_{12}^2 converged. Due to the size of the input and the slightly too large χ^2/dof of fully correlated fits, the covariance matrix was always estimated to be diagonal.

Given the quality and quantity of our data the up to 8 parameters of the ansatz above were impossible to resolve by nonlinear minimization techniques. Instead we always keep the parameters B_0 and P_0 free and loop over all other (non-redundant) possible combinations of free parameters. All converged fits contribute to the final result. Certain combinations of free fit parameters shift and widen the distribution of extrapolated splittings but still overlap with all narrower distributions. Note that fits with less free parameters converged more often and the results include a bias towards them.

Two datasets were used for the global fits of charged pseudoscalar decay constants: The first consisted only of doubly light and light-strange pseudoscalars whereas the second additionally included doubly strange pseudoscalars. Here "strange" refers to the two quark masses tuned to the approximate physical strange quark mass and to the strange sea quark mass of the particular ensemble. Exemplary fit results for the first dataset are shown in fig. 5.11.

In addition to the cuts on the dataset and the loop over sets of free fit parameters we used variations of our input to estimate the systematic error. The initial correlator fit ranges were chosen according to the same criteria as for the mass analysis. Furthermore point and shell sources were employed to exclude excited state contamination. The correlator fits were performed with naive covariance matrix estimation, the shrinking

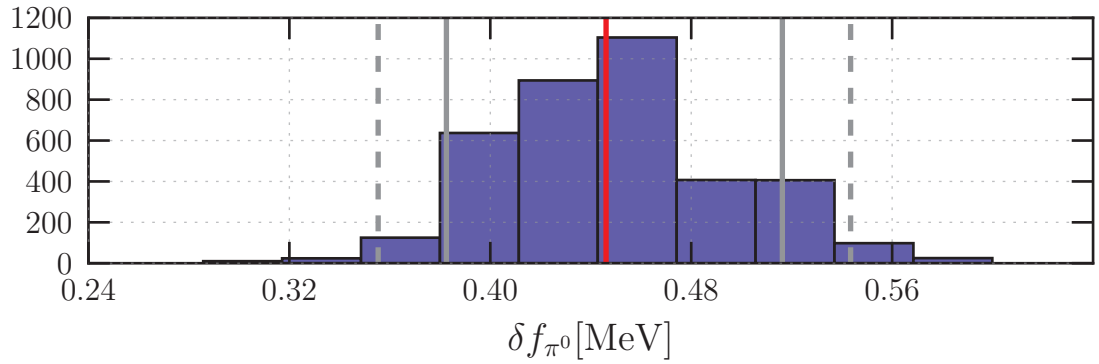

Figure 5.13.: Histogram of π^0 decay constant splitting results. The results were obtained from the same fits as for the charged extrapolation in fig. 5.12 and complemented by fits to data sets restricted to $Q^2 = 0$ data. The vertical lines have the same meaning as in fig. 5.12.

method described in appendix A.2.2 and diagonal fits. We found no significant differences and used the first two methods for our final results. Finally we employed multiple bin sizes to exclude autocorrelation. All different extrapolations are summarized/visualized in fig. 5.12. Theoretically these results could be reweighted by goodness of fit or comparable measures which was omitted due to our lack of control over the FV effects and possible other systematic errors. The final result is taken to be the median of the distribution. For the statistical error we take the median of statistical errors of the individual extrapolations. The systematic error is the standard 1σ quantile of the bootstrap error to which we add in quadrature 10% to account for the electromagnetic quenching and 2.5% for the mistuning of the strange sea quark. The error due to the missing continuum extrapolation is unknown and omitted.

Results for QED effects on the decay constant of the charged π^+, K^+ pseudoscalars can be straight forwardly obtained by inserting fit parameters, physical mass and charges into the fit function. The final numbers become

$$\boxed{\begin{aligned} \delta f_{\pi^+} &= (-0.199\,(^{+0.034}_{-0.031})_{\text{stat.}}\,(^{+0.092}_{-0.048})_{\text{sys.}})\,\text{MeV}, \\ \delta f_{K^+} &= (-0.188\,(^{+0.031}_{-0.037})_{\text{stat.}}\,(^{+0.073}_{-0.053})_{\text{sys.}})\,\text{MeV} \end{aligned}} \tag{5.47}$$

The QED contribution to the neutral pion π^0 decay constant can be approximated by

$$\delta f_{\pi^0} = \frac{\delta f_{u\bar{u}} + \delta f_{d\bar{d}}}{2} \tag{5.48}$$

for equal up and down quark masses which is again motivated by the overall weak quark mass dependence. The extrapolation of the "uncharged" decay constant used two additional data sets, which were obtained by restricting the data sets used for the charged results to $Q^2 = 0$ data. For those the fit parameters describing the Q^2 dependence were

set to zero. Extrapolating the connected $u\bar{u}$,$d\bar{d}$ pseudoscalars as above yields

$$\boxed{\delta f_{\pi^0} = (0.452\,(^{+0.015}_{-0.010})_{\text{stat.}}\,(^{+0.074}_{-0.067})_{\text{sys.}})\,\text{MeV}.} \tag{5.49}$$

Charm meson decay constants

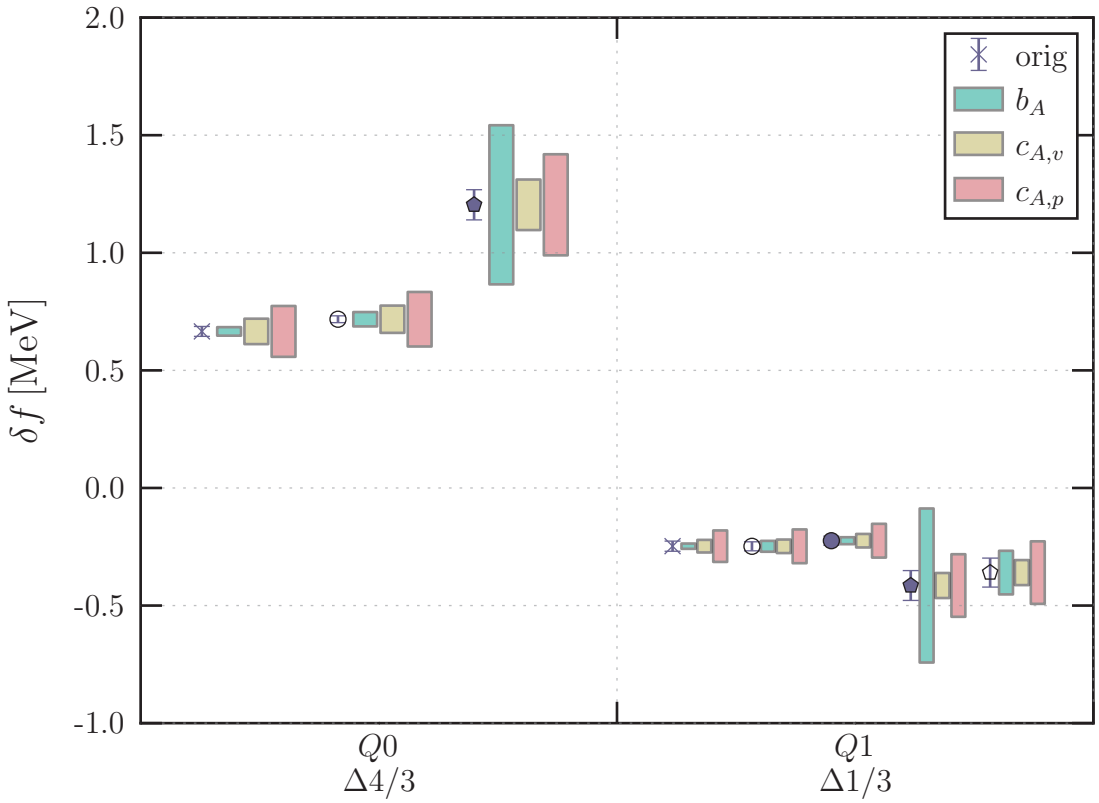

Figure 5.14.: Effects of a hypothetical charge dependence of improvement parameters b_A & c_A on the extracted splittings on ensemble `L0`. The effects were modeled by varying the $\mathcal{O}(\alpha_{\text{em}})$ coefficients of eqs. (5.28) and (5.29) in a 5% range of an equivalent QCD parameter. Vertex and propagator components may cancel. The cross is the doubly light, the circle the light-strange and the pentagon the light-charm channel. Full (open) symbols indicate physical (unphysical) charge combinations.

The calculation of QED corrections to the charmed pseudoscalars D_+, D_s and D_0 were mostly performed with the same methods as the extrapolation of light and strange pseudoscalars above. One difference being that we only require fits to one global data set consisting of light-charm and strange[4]-charm pseudoscalars. The extrapolation of

[4]With the strange quark mass tuned to both its physical value and to the sea quark value.

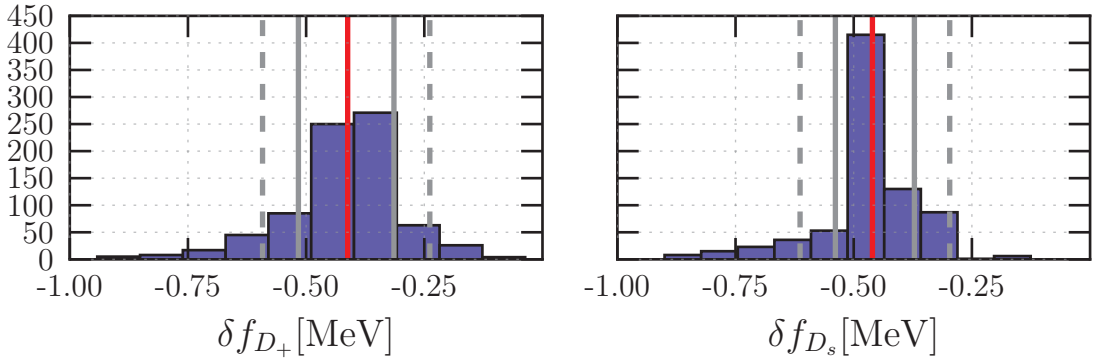

Figure 5.15.: Histogram of extrapolated charged D meson decay constant splittings. The results were obtained following the same considerations as for the charged pion and kaon extrapolations (see fig. 5.12) except that the dataset solely consisted of light-charm and strange-charm pseudoscalars. The vertical lines have the same meaning as in fig. 5.12.

the uncharged D_0 splitting also used a data set that was restricted to $Q^2 = 0$ data. The charm quark mass was individually tuned for all ensembles and given that the quark mass dependence of the splitting is generally observed to be weak, we assume the charm mass to be sufficiently matched across all our ensembles. This - although not in accordance with χPT - allows a naive extrapolation to use $m_{cc}^2 + m_{xx}^2$ as the only mass scale for extrapolations to physical light and strange quark masses.

Discretization artifacts are an enhanced source of systematic error for charmed mesons. We omit the extraction of the η_c decay constant due to the possibly large artifacts for mesons with $m \gg a^{-1}$. Furthermore for singly charmed pseudoscalars we investigated the effects of a charge dependent b_A due to the large $b_A am$ contribution at the charm quark mass. The same variation as described by eq. (5.37) yielded fig. 5.14, which clearly shows that b_A charge effects have to be taken into account. It also showed that the improvement coefficient c_A becomes more important at larger quark masses. We hope to include $\mathcal{O}(\alpha_{\text{em}})$ contributions in future work and neglect these variations in the following estimation of our systematic error.

As for the light and strange extrapolations we ignore the quark sea content and therefore neglect the missing charm quark, the absence of electromagnetic charge and the mistuning of the strange quark mass. We add the same factors in quadrature to the systematic error as before yielding the final results

$$\boxed{\begin{aligned} \delta f_{D_+} &= (-0.42\,(\pm 0.08)_{\text{stat.}}\,(\pm 0.10)_{\text{sys.}})\,\text{MeV}, \\ \delta f_{D_s} &= (-0.461\,(\pm 0.075)_{\text{stat.}}\,(^{+0.089}_{-0.078})_{\text{sys.}})\,\text{MeV}. \end{aligned}} \tag{5.50}$$

These results are also illustrated in fig. 5.15.

5.3. Summary & discussion

The decay constant splittings were extracted from combined fits to pion-pion correlators and pion-axial current correlators. The variation of the fit range and a second analysis with point sources suggest that excited states are sufficiently suppressed. The matching procedure at ensemble level described in appendix B solves the quark mass matching problem, takes correlations into account and provides measurable splittings. These decay constant splittings on a single ensembles show the phenomenologically expected behavior.

The infinite volume and therefore also the mass extrapolation of charged decay constant splittings where found to be problematic because finite size effects are far from under control: More ensembles with different and larger volumes, especially at small quark masses are required. An additional obstacle proved to be the lack of theoretical prediction of the functional form and coefficients of the finite volume effects. Nevertheless explicit subtraction of mass finite volume effects seem to improve the signal to noise ratio of the splitting and suggest to verify results by individual extrapolation of improved and unimproved splittings that approach the same value in infinite volume. This led us to believe that an extended study, possibly using twisted boundary conditions, as proposed in [149] should enable a controlled extrapolation of the splitting.

Decay constants of uncharged pseudoscalar are not measurable due to the fact that there are no flavor changing neutral currents. The exception due to the axial anomaly being the decay constants of π^0, η and η'. The decay constant f_{π^0} appears in formulae for the pion decay width and the approximate Goldberger-Treiman relation (eqs. (2.30) and (2.31)). It is affected by the electromagnetic attraction of the quarks and not subject to LO infrared divergences. QED finite size effects on the uncharged pseudoscalar mass vanish up to NNLO [138] and therefore cannot be improved. The decay constant itself does not show a finite volume dependence comparable to the charged case. The extrapolation nevertheless included FV terms to demonstrate that they are irrelevant. The π_0 result used the approximation $f_{\pi_0} = \frac{1}{2}(f_{\bar{u}u} + f_{\bar{d}d})$ and neglected disconnected contributions. We did not insert physical non-degenerate up and down quark masses into our extrapolations but used the approximation $m_{ud} = (m_u + m_d)/2$ instead, which is again motivated/justified by the small observed mass dependence.

Outlook

Meaningful predictions with full control of all systematic errors obviously require multiple lattice spacings and more ensembles at different volumes and quark masses. Further analysis should first focus on a controlled infinite volume limit and investigate the QED dependence of renormalization constant and improvement coefficients which is discussed below. Then charges can be added to sea quarks requiring a sound definition of the mass of a charged quark which might be provided by the PCAC considerations in section 4.2. Lastly, disconnected terms for the π^0 should be included which is also discussed below.

5.3.1. Missing systematics

In the following we will shortly address disconnected contributions to the π^0 correlator and QED effects on renormalization constants and improvement coefficients. Before that the reader shall be reminded that our results ignore effects due to QED quenching, light quark mass degeneracy and the continuum limit. The systematic error only accounts for the QED quenching and ignores the latter effects.

Renormalization and improvement

As mentioned previously QCD+QED renormalization constants depend on the individual quark charges and might be volume and/or gauge dependent. Theoretically QCD+LO QED renormalization constants for charge zero vertices could be obtained from lattice (QCD) perturbation theory results by rescaling the coupling. This was not possible due to the combination of actions[5] used in this work. The dominant LO QED contribution to charged QCD+QED renormalization constants is of the same order as the splitting itself. The QED vertex term has opposite sign than the QCD (color singlet) term. Additional QED renormalization might therefore reduce the observed QED splittings or even invert them.

The QED renormalization constant is possibly volume dependent due to the QED_L removal of the zero modes. This gauge transformation is *non-local* which violates the locality condition of renormalizability [137].

QED effects on the improvement coefficients are further suppressed and hence less troublesome: The mass dependent improvement parameter b_A of the renormalization constant depends on the quark charge q_i and is at least for light quark masses suppressed by the quark mass and therefore another order of magnitude. Future D meson studies require the calculation of the modifications either by rescaling LPT results or non-perturbatively as described in [166]. Similarly we can assume that the contribution from the improvement term eq. (3.41), consisting of QED corrections to a higher dimensional operator, is small for light quarks and can be neglected. The effects for the charm quark could be evaluated with LPT.

Disconnected contributions

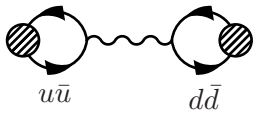

Figure 5.16.: The leading order π^0 disconnected diagram on the lattice with two electromagnetic vertices

[5] SLiNC fermions in combination with the QED Wilson gauge action.

The disconnected contribution (fig. 5.16) to the π^0 correlator is at leading order $\mathcal{O}(\alpha_{\mathrm{em}} m_{ud})$ and therefore largely suppressed for physical quark masses. Such disconnected contributions are difficult and expensive to calculate, generally have large errors and were therefore neglected in all studies up to the present. Recently, noise reduction techniques proposed in [171] have been extended to fermionic correlators [172], which might make them at least computationally feasible.

Decay rates

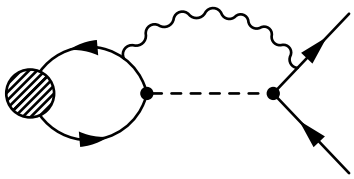

Figure 5.17.: The decay rate $\Gamma_{ps\to l+\nu_l}$ at $\mathcal{O}(\alpha_{\mathrm{em}})$ has contributions that break the factorization into currents [134, 135, 173]. The here calculated QCD+QED decay constant does not account for those.

Decay rates Γ of charged pseudoscalars can be used for the determination of CKM matrix elements. The calculation of QED corrections at fixed order of α_{em} is complicated by the fact that the process no longer factorizes into leptonic and hadronic currents. Already leading order processes like the one shown in fig. 5.17 contribute and diminish the predictive power of the matrix element $f_{\pi^\pm}$. Our $f_{ps^\pm}$ results therefore only partially account for $\mathcal{O}(\alpha_{\mathrm{em}})$ corrections to $\Gamma_{ps^\pm}$.

A further complication is that the illustrated process is infrared divergent. This divergence cancels when the rates of $\pi^+ \to l^+ + \nu_l$ and radiative $\pi^+ \to l^+ + \nu_l + \gamma$ are combined [28, 134]. A method to calculate $\mathcal{O}(\alpha_{\mathrm{em}})$ corrections to the π^+ decay rate $\Gamma(\pi^+ \to l^+ + \nu_l + (\gamma))$ is proposed in [134] and preliminary results are shown in [174]. It utilizes electroweak effective theory with four fermion interaction in combination with lattice QCD without a QED background. Instead, an explicit photon propagator is inserted into all relevant diagrams and correlation functions.

QCD+QED background calculations of hadronic matrix elements as ours cannot be complemented with explicit insertion of photon propagators into radiating and factorization breaking diagrams [174]. This is due to the cancellation requirement at all orders: If we inserted a single photon propagator the $\mathcal{O}(\alpha_{\mathrm{em}})$ divergences cancel, but higher order divergences remain because we are missing diagrams with two (or more) real photons and two (or more) photons between lepton and the quarks.

Neutral pions dominantly decay into two photons. The associated partial decay rate $\Gamma(\pi^0 \to \gamma\gamma)$ requires the axial anomaly. Its approximate prediction eq. (2.30) does not suffer from infrared divergent photons and contains the decay constant f_{π^0}. Effective theories provide an improved prediction by including π^0, η, η' mixing [175–177]. The splitting determined in this work could provide QED corrections to a $f_\pi \simeq f_{\pi^0}$ determination from lattice and experimental data [178, 179] that would be independent of V_{ud}

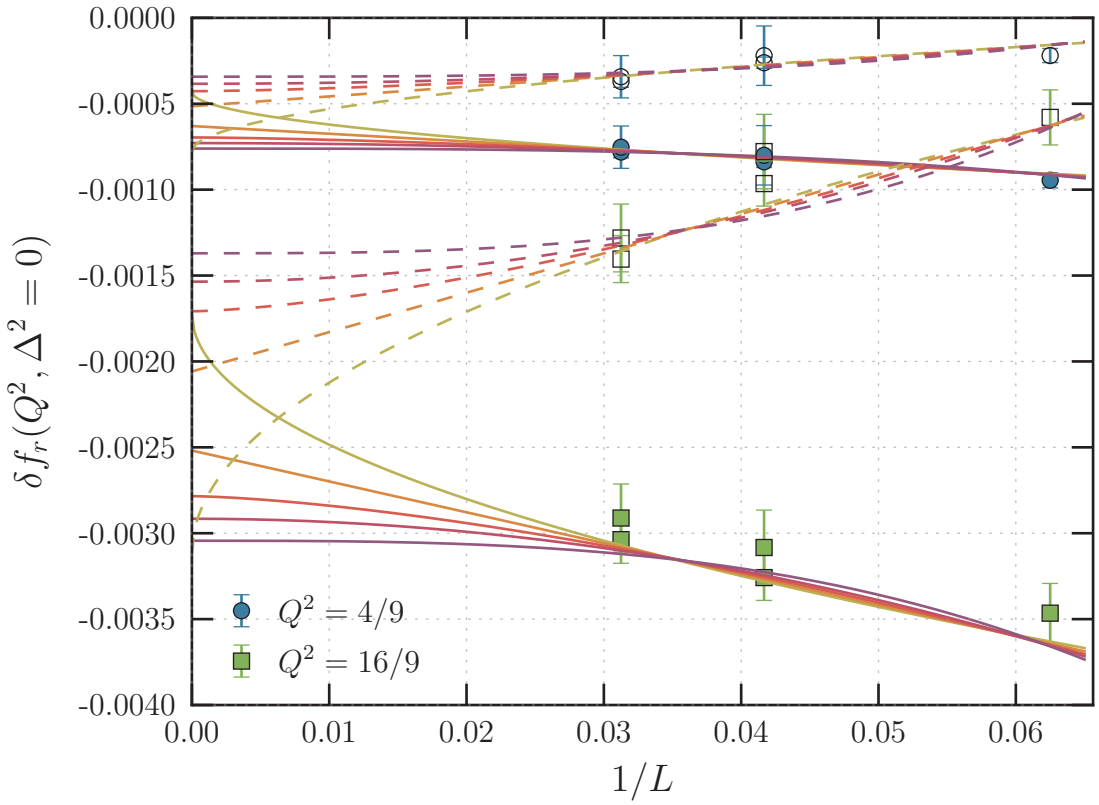

Figure 5.18.: Comparison of the doubly strange decay constant splittings with (full symbols) and without (open symbols) removal of LO and NLO mass finite volume contributions. The solid (dashed) lines are $f(L) = f_0 + \tilde{f}_{1,p}/L^p$ fits to FV improved (unimproved) data of both charge combinations with powers $p \in [1/2, 1, 3/2, 2, 3]$. Possible meson mass m dependence of the splitting ignored. Plotted is data from all ensembles except for `M2` and `L2`.

[177]. This can resolve differences between f_{π^+} and f_{π^0} which could be attributed to new physics, e.g. right handed currents [180].

Matrix elements described by other uncharged, non-anomalous, pseudoscalar decay constants do not appear in predictions of any physical processes. Their calculation in this work therefore only provides input to disentangle the FV effects and to stabilize the (chiral) fits.

6. Conclusion

The Standard model is enormously successful in describing the vast majority of particle physics. Various observations have established that it is nonetheless just an effective low energy description and will eventually need to be extended or replaced. Neither the observed *baryon number*, nor dark matter, which is only observable by its gravitational effects, can currently be explained by the SM. Additionally the SM does not include gravity, a theory that has gained prominence due to the recent terrestrial detection of gravitational waves. The investigation of the underlying theory is difficult because experimental energies are limited and may never reach the magnitude to directly observe new interactions and particles. The indirect detection by observing tiny modifications to low energy quantities requires extremely accurate standard model predictions. The QCD coupling constant is increasing with decreasing energy causing perturbation theory to fail at low energies: Hadron masses and matrix elements can only be computed by non-perturbative methods such as Lattice QCD (see chapter 3). High precision predictions are required to account for all sources of isospin breaking. QED corrections to hadron masses have recently yielded impressive results [120], and the determination of light and strange quark masses is dominated by lattice QCD+QED calculations [14, 23]. Other high precision observables from lattice QCD include pseudoscalar decay constants which can be used for unitary test of the CKM matrix.

After reviewing the current state of QCD+QED calculations on the lattice in chapter 4 we described the setup and analysis of a benchmark calculation for QED corrections to pseudoscalar decay constants on the lattice in chapter 5. The validity of the QCD+QED formulation has been confirmed by reproducing light quark masses and corrections to Dashen's theorem. We confirm the naive expectation of an increased (decreased) decay constant for QED attractive (repulsive) systems. Positive permille corrections of the uncharged π^0 decay constant to pure QCD quantities were calculated. Charged particles on the lattice are more problematic. They require special gauge choices and suffer from large finite volume corrections. The lattice sizes employed in this work were not sufficient for a fully controlled infinite volume limit. It also turned out that it is beneficial to improve matrix elements and meson mass independently. A further unresolved source of systematic errors are charge dependent QED modifications to renormalization constants and improvement coefficients. It also must be proven that QED renormalization constants are volume independent if a global gauge freedom is broken as in QED_L.

Outlook

The QCD+QED calculations of pseudoscalar decay constants presented in this thesis can be extended by focusing on improved (chiral) extrapolations, finite volume effects,

and explicit calculation of QCD+QED renormalization constants and improvement coefficients. Improved extrapolations may include input from other - possibly experimental - sources and constrain fits by phenomenological considerations. These extrapolations could address mass isospin violation and specific QCD+QED LECs. D meson extrapolation can be extended by *heavy quark effective theory* (HQET). It is obvious that all extrapolation would benefit from more data and statistics. Finite volume effects can be controlled by various techniques proposed in the literature: Combining large or infinite volume valence quarks and a smaller lattice volume [149], using massive photons [150], or using a formulation (like QED_C) that is naturally less affected by FV effects [137]. Analytical calculations of leading and higher order contributions in *nonrelativistic QCD* (NRQCD) or χPT will be useful. QED corrections to renormalization constants and improvement coefficients can be calculated non-perturbatively or in PT, since $\mathcal{O}(\alpha_{\text{em}})$ corrections would be sufficient for desirable error budgets. The mass improvement coefficients b_x can be easily obtained using spatial correlators as outline in [166]. The coefficients c_x of the higher dimensional improvement term can be determined in LPT. Calculations for the modified renormalization constant could be performed non-perturbatively in RI-SMOM. Renormalization constants also need to be proven to be volume independent unless a purely local QED formulation, such as QED_C, is used.

QCD+QED decay constant calculations beyond the framework of this thesis are critical to address further systematics. Disconnected contributions to π^0 (η, η') observables could be calculated (more) economically with the methods presented in [172]. Most importantly fixed $\mathcal{O}(\alpha_{\text{em}})$ calculations, that include IR divergent diagrams which violate QCD+QED factorization, are required to obtain full LO QED corrections [134]. The IR divergences cancel if diagrams containing real and virtual photons are combined. Unquenched calculations have been performed and could be extended to matrix element computations. Unquenched fixed $\mathcal{O}(\alpha_{\text{em}})$ results require multiple disconnected diagrams. These are expensive because they do not benefit from the method mentioned above. Other hadronic matrix elements have larger errors and are therefore less affected by systematic QED corrections. Nevertheless their calculation is possible and the next natural step would be the measurement of corrections to vector meson decay constants.

Lastly, precise experimental data for $\pi^0 \to \gamma\gamma$ should become available within the next few years [178, 179] and allow for a f_π determination that is independent of V_{ud} [177].

A. Analysis

The following appendix intends to give a short summary on general definitions and methods used in the analysis of lattice data. Some methods are not strictly necessary or can be replaced by alternative procedures in which cases it is beneficial to confirm that the analysis yields consistent results for all possible cases.

Measurements were performed on the computer clusters `iDataCool` [181], `qpace2` [182] and `athene` in Regensburg [183] as well as on the tier-0 computers `fermi` and `superMUC`.

The measurement code was a modified version of `chroma` [184], with data files partly utilizing `hdf5` [185, 186]. Depending on the computer architecture either the domain decomposed + deflated solver by [88] or the adaptive algebraic MG [89, 187] and `BiCGStab` implemented in `chroma` was used.

The analysis was performed with the analysis library `Woiperdinger` developed in Regensburg, which utilizes `armadillo` and `Minuit2` [188–190]. The data plots were produced with the python library `matplotlib` [191] and Feynman diagrams with the latex package `feynmp` [192].

A.1. Definitions and notation

Throughout this thesis I am using natural units in which the following constants are set to unity

$$c = \hbar = 1. \tag{A.1}$$

Energies and lengths can be related using

$$\hbar c = 197.3\,\mathrm{MeV\ fm} = 1. \tag{A.2}$$

Repeated occurrence of indices indicate summation according to the Einstein summing convention. Lattice units are indicated by the lattice spacing a. Some acronyms that are repeatedly used throughout this document are listed in table A.1.

A.2. Error estimation

The analysis of lattice QCD often requires iterative methods such as fitting to non-linear functions. This makes defining differentiable transformations and therefore analytical error propagation either impossible or vastly expansive for a large raw dataset and a complicated analysis chain. The error of the raw data is therefore propagated with resampling methods to the final quantity of interest.

Acronyms	
EOM	equation(s) of motion
FV	finite volume
HMC	hybrid Monte Carlo
IR	infrared
UV	ultra-violet
LO	leading order
NLO	next-to LO
NNLO	next-to-next-to LO
QCD	quantum chromodynamics
NRQCD	non-relativistic QCD
QED	quantum electrodynamics
QFT	quantum field theory
SM	standard model
PT	perturbation theory
LPT	lattice perturbation theory
χPT	chiral perturbation theory

Table A.1.: Acronyms used throughout the thesis.

The situation is further complicated by the fact that measurements on an HMC trajectory are correlated. Methods to quantify the effects of the so-called autocorrelation are described in appendix A.2.1.

Jackknife

One commonly used resampling method is called *Jackknife* [193, 194]. It replaces measurement samples by jackknife samples that are defined by

$$\tilde{x}^{(n)} = \frac{1}{N-1} \sum_{m \neq n}^{N} x^{(m)} \tag{A.3}$$

The mean $\bar{x} = \langle \tilde{x} \rangle$ is the trivial average of all jackknife samples $\tilde{x}^{(n)}$. Transformations of the data $f(x)$ are simply applied to all jackknife samples. Then the error of the mean of primary and all derived results $f_{\bar{x}}$ can be calculated by a simple rescaling of ordinary statistical analysis:

$$\tilde{\sigma}_{f_{\bar{x}}} = \sqrt{\frac{N-1}{N} \sum_{n}^{N} \left(f_{\tilde{x}^{(n)}} - f_{\bar{x}} \right)^2} \tag{A.4}$$

Covariance estimation is treated analogously. Jackknife is known to be extremely stable and to overestimate the error.

Bootstrap

A generalized method is called *Bootstrap* and uses stochastic resampling [195]. Given N initial measurements we construct M samples

$$\tilde{x}^{(m)} = \frac{1}{N'} \sum^{N'} x^{(r)} \tag{A.5}$$

where $r \in [1, N]$ is a random index and N' should ideally be equal or larger then N [1]. The error of the mean is also given by an adjustment of the ordinary formula:

$$\tilde{\sigma}(\langle \tilde{x} \rangle) = \sqrt{\frac{1}{M} \sum_{m}^{M} \left(x^{(m)} - \langle \tilde{x} \rangle \right)^2} \tag{A.6}$$

One can alternatively use the common $1\,\sigma$ quantiles to obtain even better and asymmetrical errors.

Bootstrap is possibly slightly more unstable than Jackknife but it has the advantage of more realistic errors. It can handle large number of measurements N by using $M < N$. or alternatively it may provide a more stable estimation of the inverse covariance matrix if M is sufficiently large.

A.2.1. Autocorrelation

As described earlier in section 3.2 successive measurement on a Monte Carlo trajectory are correlated. This can be quantified by the so-called *integrated autocorrelation time* τ_{int}, which is $1/2$ if the measurements are uncorrelated. Once the autocorrelation time is determined the errors of the naive results must be rescaled by

$$\sigma_{\bar{x}} = \sqrt{2\tau_{\text{int}}} \sigma_{\bar{x},\text{naive}}. \tag{A.7}$$

Naively one can check that autocorrelations are negligible by performing the analysis for various different bin sizes N_b and asserting that the resulting error is independent. If this is not the case then the variance σ^2_{x,N_b} grows as a function of N_b and saturates for large enough values. The saturation value of the variance can be used to estimate τ_{int}. An advanced method to calculated τ_{int} is described in [84].

Note that $\tau_{x,\text{int}}$ is different but approximately of the same order of magnitude for every observable x. Conservatively one can use the largest auto correlation time the value x can depend on. An example in LQCD is the topological charge.

A.2.2. Covariance estimation

The analysis described in chapter 5 is highly dependent on correlations within the measured data. Fitting requires the inversion of the square covariance matrix cov_{ij} of N_{var}

[1] Or at least be of the same order

data points. Limited statistics destabilizes the inversion (for large matrices) because naive covariance estimators have unreliable, small eigenvalues. The inversion of the covariance matrix was shown to be unsafe [196] unless

$$N_{meas} > \max\left(N_{var}^2, 10(N_{var}+1)\right). \tag{A.8}$$

The problem is known within the lattice community and various solutions such as discussed in [197] have been used. A particularly cheap solution to this problem is proposed in [198]. It consists of rescaling the off-diagonal elements of the covariance matrix with a single coefficient $c_{shrink} \in [0,1]$. This coefficient depends on the size of our statistics N_{meas}, the size of the matrix N_{var}^2 and the fluctuation of the data. In our analysis this factor was usually $c_{shrink} > 0.95$. The resulting fits are more stable and give parameters between fully covariant $c_{shrink} = 1$ and diagonal fits $c_{shrink} = 0$.

The coefficient can be calculated out of the correlation matrix, which makes the application to resampled datasets straight forward. Note that an ambiguity arises for bootstrap resampling when the size of the dataset is changed. Naively larger resampled sets result in less shrinking. We assert that the resampled set is always larger and choose to rescale the procedure such that the resulting coefficient remains approximately constant.

A.3. Fitting

Data points y_i with covariance matrix cov_{ij} can be described by a model function $f_i(\mathbf{p})$ with parameters $\mathbf{p}$. The best parameters $\mathbf{p}$ are found my minimizing the functional

$$\chi^2 = \sum_{i,j} \left(y_i - f_i(\mathbf{p})\right) \mathrm{cov}_{ij}^{-1} \left(y_j - f_j(\mathbf{p})\right). \tag{A.9}$$

Most non-linear functions $f_i(\mathbf{p})$ require the use of iterative minimization algorithms which converge to local minima. A good starting guess $\mathbf{p}_0$ for the location of the global minimum or testing of multiple starting positions in the space of $\mathbf{p}$ become imperative.

Fitting correlators to exponential decay requires a careful choice of the fit range. Ground states can be extracted in the large t limit of lattice QCD correlators where all heavier states are insignificant. The required large t limit might be in contradiction to the limited time extent T of the lattice or the (increasing) signal to noise ratio. A possible numerical criteria to compare fit ranges k is given in [199]

$$\begin{aligned} Q_k^{(a)} &= \left(1 - \mathrm{cdf}(\chi_k^2, dof_k)\right) \frac{dof_k}{dof_{\max}} \frac{p_i}{\sigma_{p_i}} \\ &= \left(1 - \mathrm{cdf}(\chi_k^2, dof_k)\right) \frac{dof_k}{dof_{\max}} \sqrt{\mathbf{p}^T \,\mathrm{cov}^{-1}\, \mathbf{p}} \qquad \text{(generalized)} \end{aligned} \tag{A.10}$$

A larger Q_k signifies a better fit quality. Note that this is only a combination of assumably good characteristics and not mathematically rigorous. Its is therefore also possible

to neglect individual components or weight them differently. For our analysis we tested two additional variations of the criteria above:

$$Q_k^{(b)} = \left(1 - \mathrm{cdf}(\chi_k^2, dof_k)\right) \frac{dof_k}{dof_{\max}} \tag{A.11}$$

$$Q_k^{(c)} = \mathrm{cdf}(\chi_k^2, dof_k) \left(1 - \mathrm{cdf}(\chi_k^2, dof_k)\right) \frac{dof_k}{dof_{\max}} \tag{A.12}$$

Criteria (b) ignores the relative error of the fit parameters and criteria (c) prevents over fitting by also cutting the χ^2 that are to small.

Chiral fits provide a large number of possible fit parameters. Dimensional analysis may be provide additional models and extensions. The relative significance of a model j with n_j parameters can be described with the Akaike Information Criteria [120]

$$AIC_j = \chi_j^2 + 2n_j. \tag{A.13}$$

This value can be used to weight individual models j with $\exp(-(AIC_{\min} - AIC_j)/2)$.

B. U(3) Analysis

B.1. Meson channels

Apart from spin structure mesons are mainly characterized by their quark masses m_i, respectively hopping parameters κ_i and charges q_i. All possible combinations are given by the product of $c_i = (\kappa_i, q_i)$ and $c_j(\kappa_j, q_j)$. We are ignoring different discrete representations, exited states and smearing choices and think of mesons solely as the ground state of a correlator.

Interchange of propagators in the meson contraction just yields the complex conjugate correlator. As in [130] correlators can be averaged over $\pm B_\mu$ or $\pm(q_i, q_j)$ respectively.

$$c_i \times c_j \to \frac{1}{2}\left(c_i \times c_j + \tilde{c}_i \times \tilde{c}_j\right) = \frac{1}{2}\left((\kappa_i, q_i) \times (\kappa_j, q_j) + (\kappa_i, -q_i) \times (\kappa_j, -q_j)\right) \tag{B.1}$$

What we indeed do want and can distinguish is whether a specific charge is on the lighter or on the heavier quark.

B.2. Quark mass matching

In the analysis of lattice QCD+QED data using Wilson discretization for fermions a quark mass matching problem for different quark charges emerges. The mis-tuning can be corrected by measuring all channels at n slightly detuned masses and matching in the analysis. This requires to separate all observables into different groups characterized by the approximate quark mass type (e.g. light, charm, ...) and the absolute quark charge of both individual quarks.

For matching, 4 different "meson" types can be distinguished:

- Groups with both quark charges $q_{1,2}$ equal to zero.
- In groups where exactly one quark charge q_i is zero, we only need to extrapolate the mass parameter of the charged quark and have exactly n points.
- Groups where the quark mass type of both quarks and the absolute quark charge $|q_1| = |q_2|$ are the same only require one extrapolation parameter since the mass parameters of quark and anti-quark are the same. Although there are $n(n-1)/2$ independent combinations of the mass parameter, we only use the n mass symmetric points and avoid higher order artifacts due to unequal masses.
- All other cases, where we have to extrapolate in two quark mass parameters and n^2 points available.

To match the $n^2 \geq 4$ points of a "meson" type we assume that the mass dependence of their decay constant can be parametrized locally by

$$f_{\mathrm{PS}} = A + B_1 m_{\mathrm{PS}}{}^2_{sym}(\kappa_1, q_1) + B_2 m_{\mathrm{PS}}{}^2_{sym}(\kappa_2, q_2) \tag{B.2}$$

$$= A x_0 \hat{e}_0 + B_1 x_1 \hat{e}_1 + B_2 x_2 \hat{e}_2 = \mathbf{X} \cdot \mathbf{P} \tag{B.3}$$

Note that this ansatz can be modified for charm quarks, where a better extrapolation parameter might be the unsquared symmetric meson mass. The interpolating parameters $\mathbf{P} = (A, B_1, B_2)^T$ can be determined when we have 3 or more different equations, by minimizing the norm

$$\|X\mathbf{P} - \mathbf{f}_{\mathrm{PS}}\|_2 = \sum_i (\mathbf{X}_i \cdot \mathbf{P} - f_{\mathrm{PS}i})^2 \tag{B.4}$$

This is a *ordinary least squares* (OLS) [200] problem, which is is solved by the equation

$$X^T X P = X^T \mathbf{f}_{\mathrm{PS}}. \tag{B.5}$$

Using all n^2 equations yields an overdetermined system which is solved by *singular value decomposition* (SVD). We neglect all errors since they are highly correlated and of the same order in f_{PS} and $m_{\mathrm{PS}}{}^2$ anyway. Finally the decay constant of the charged meson are matched at

$$\bar{X} = \left(1, m_{\mathrm{PS}}{}^2_{sym}(\kappa_1', 0), m_{\mathrm{PS}}{}^2_{sym}(\kappa_2', 0)\right) \tag{B.6}$$

where κ_i' is the kappa of the corresponding uncharged meson.

A conservative estimate for the error introduced by this extrapolation can be obtained by comparing the normalized value of eq. (B.4)

$$\frac{\|X\mathbf{P} - \mathbf{f}_{\mathrm{PS}}\|_2}{n^2} \tag{B.7}$$

to the desired splitting δf (eq. (5.33)). This values were spot checked and found to be at most 5% of δf for physically interesting parameter choices like improved meson masses, reasonable fit range choices and naive improvement parameters. The value becomes large in comparison to δf for (unphysical[1]) channels with small splittings ($< 0.1\,\mathrm{MeV}$). The error should be propagated correctly since the extrapolation is performed on all resampled datasets individually. One could nevertheless exclude such channels from the global fits. The largest deviations were found for mesons containing light and charm quarks, which might be resolved by using the unsquared meson mass as X parameter for the charm quarks. We furthermore remark that for critical channels the extrapolated values $\mathbf{X}_i \cdot \mathbf{P}$ in the summands of eq. (B.4) deviated at most by 0.05% from the measured value $f_{\mathrm{PS}i}$.

[1] e.g. $Q^2 = \Delta_q^2$

B.2.1. Additional plots

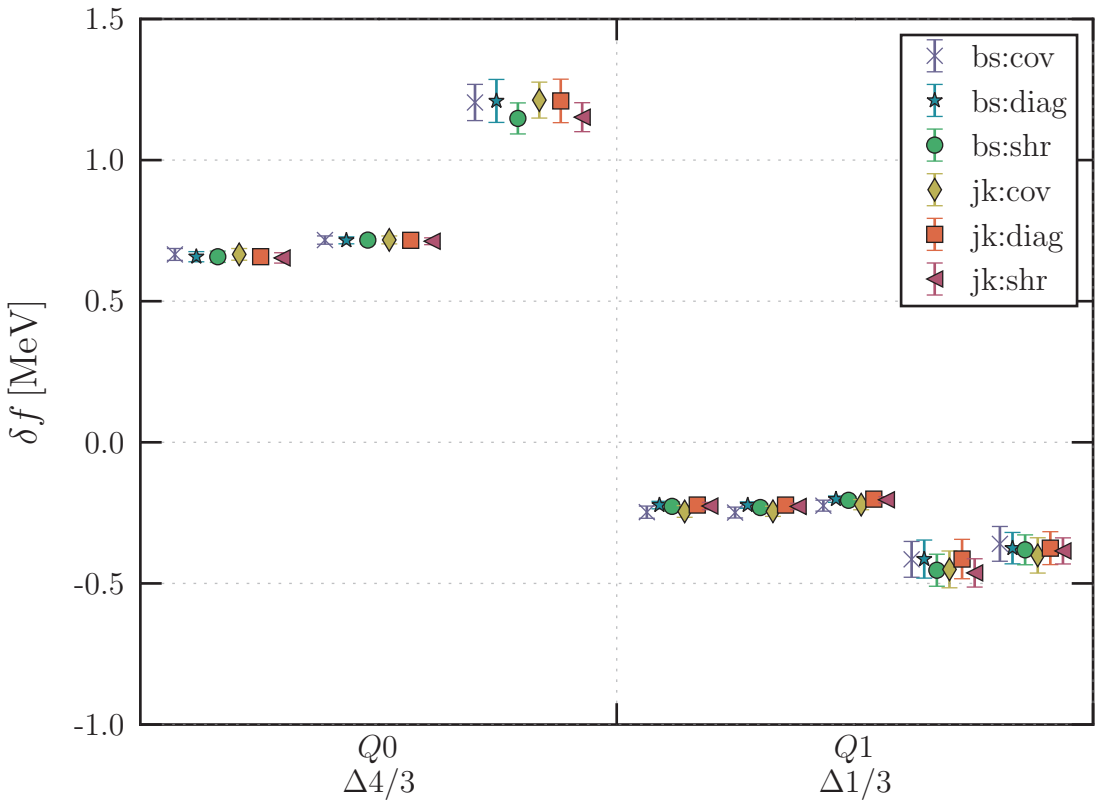

Figure B.1.: Doubly light, light-strange and light-charm data on ensemble `L0`. Shown are results for bootstrap(bs) and jackknife(jk) resampling and three covariance estimation methods for the correlator fits. It is noteworthy that shrinking (shr) covariance estimation is more consistent across both resampling methods whereas the naive (cov) covariance estimation is less so.

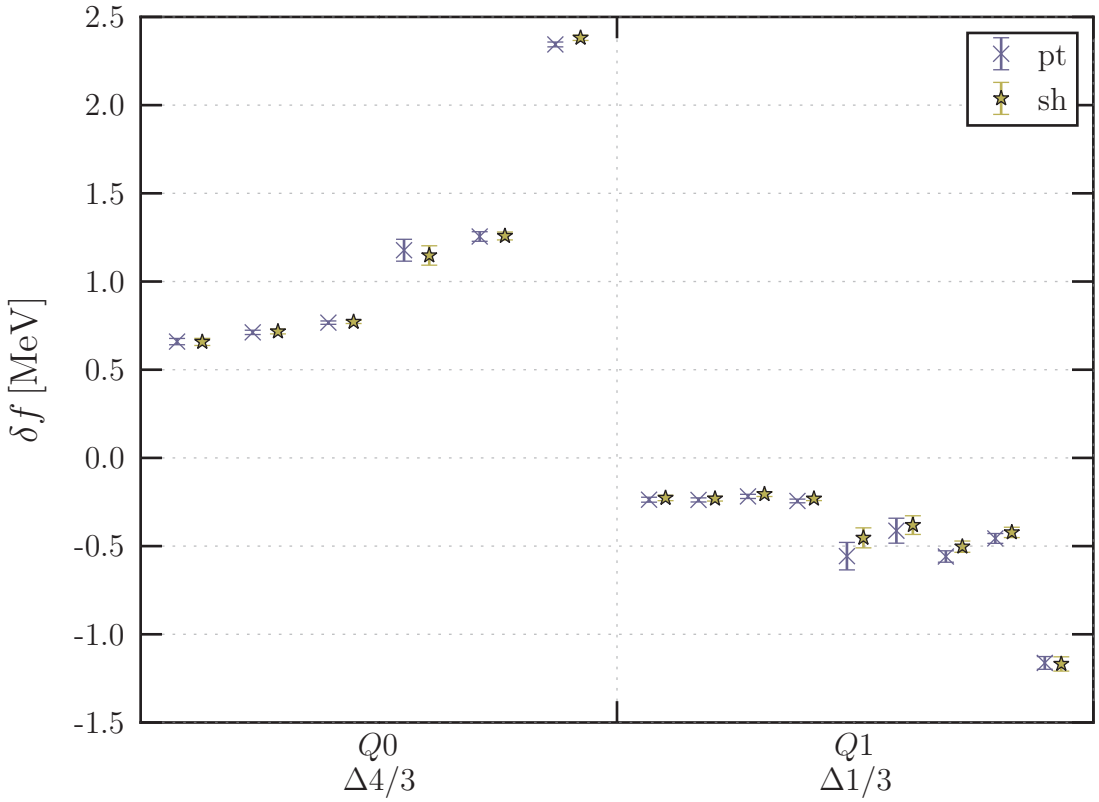

Figure B.2.: Extracted splittings for point and shell sources on ensemble `L0`. Shown are splittings of all quark mass combinations. The fit ranges where adjusted individually. There is no significant difference.

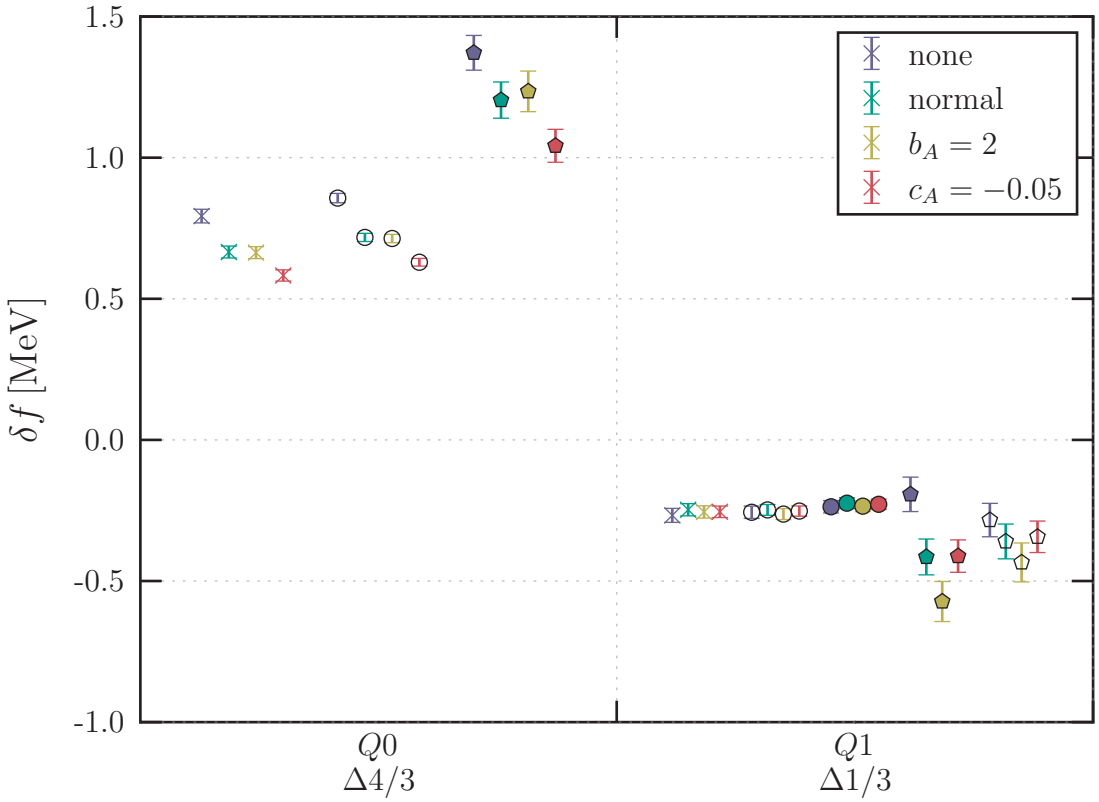

Figure B.3.: Effect of hypothetical higher order corrections to the coefficients b_A and c_A on ensemble `L0`. The *normal* data was obtained with our default values whereas the *none* data used $b_A = c_A = 0$ and $Z_A = 1$. Corrections on c_A consistently only affect uncharged splittings δf whereas corrections to b_A are only relevant for charged splittings of charmed mesons. The cross is the doubly light, the circle the light-strange and the pentagon the light-charm channel. Full (open) symbols indicate physical (unphysical) charge combinations.

C. Discretized QED generation

The following appendix only covers the quenched methods used in this work. Methods for the generation of fully dynamical QED(+QCD) were not used and are therefore only briefly referred to in section 4.1.2.

C.1. Non-compact

The non-compact QED (ncQED) gauge action is given by

$$S_G^{\text{ncQED}} = \frac{1}{4}\sum_n \sum_{\mu,\nu} \left(\hat{\partial}_\mu B_\nu(n) - \hat{\partial}_\nu B_\mu(n)\right)^2 \tag{C.1}$$

with the forward derivative

$$\hat{\partial}_\mu f(n) = a^{-1}\big(f(n+\hat{\mu}) - f(n)\big). \tag{C.2}$$

and real vector fields $B_\mu(n)$. Upon transformation to momentum space the new degrees of freedom $\tilde{B}_\mu(k)$ decouple. This reduces the generation of a QED configuration to drawing appropriately reweighted, uncorrelated Gaussian random numbers and a Fourier transform to obtain the position space fields. Assuming a perfect parallel random number generator, non-compact gauge fields with different seeds are completely uncorrelated.

C.1.1. Generation

The generation itself is most practical in Feynman gauge [120, 201] in which the action can be written as

$$S_G^{\text{ncQED}}(k) = \frac{1}{2}\sum_\mu \big|\hat{k}\big|^2 \big|B_\mu(k)\big|^2 \tag{C.3}$$

$$\text{with} \qquad \hat{k}_\mu = \frac{\exp(\mathrm{i}ak_\mu) - 1}{a} \quad \text{and} \quad k_\mu \in [0, L-1]\frac{2\pi}{L}.$$

The fields $\tilde{B}_\mu(k)$ therefore simply are complex Gaussian random numbers divided by $|\hat{k}|$. The division by zero and free choice of $\tilde{B}_\mu$ at $|\hat{k}| = 0$ is prevented by our 'global' gauge choice, which requires $\tilde{B}_\mu(|\mathbf{k}| = 0, k_0) = 0$ (eq. (4.7)). Note that the action above differs

by an irrelevant gauge dependent term from the gauge independent formulation

$$S_G^{\mathrm{ncQED}}(k) = \frac{1}{4}\sum_{\mu,\nu}\left|\hat{k}_\mu \tilde{B}_\nu - \hat{k}_\nu \tilde{B}_\mu\right|^2 \tag{C.4}$$

which can be used throughout the generation to assert the correctness of all transformations and in fact does yield the same value as the position space action.

Performing a naive discrete Fourier transform

$$B_\mu(n) = \frac{1}{\sqrt{V}}\sum_k \mathrm{e}^{\mathrm{i}kx}\tilde{B}_\mu(k) \tag{C.5}$$

gives complex instead of real position space fields. This can be remedied by explicitly setting the imaginary part to zero [202], which is equivalent to the involved treatment described in [129].

The reduced fields are transformed back to momentum space where the (non-iterative) operator

$$P_{C,\mu\nu} = \delta_{\mu\nu} - \frac{1}{\hat{\mathbf{k}}^2}(0,\hat{\mathbf{k}})^\dagger_\mu k_\nu \tag{C.6}$$

is used to obtain the fields in Coulomb gauge. After the final Fourier transform to position space the fields $B_\mu(x)$ can be used to multiply the $SU(3)$ links with the complex phase $U(1)_{\mu\,\mathrm{QED}} = \exp(\mathrm{i}e_q e_{\mathrm{QED}} B_\mu)$, where e_q is the fractional quark charge and e_{QED} the electromagnetic coupling.

Finally the coupling can be checked by comparing the plaquette for $e_q = e_{\mathrm{QED}} = 1$ to its asymptotic value in infinite volume $P_\infty = \exp(-1/4)$ [203].

C.2. Compact lattice QED

The compact QED action is given eq. (4.5). Its effective degrees of freedom are four angles θ_μ.

C.2.1. Generation

In the absence of charged sea quarks $U(1)$ configurations can be generated by heatbath updates. A single update draws a replacement angle $\theta_\mu \in [0, 2\pi)$ from the probability distribution

$$p(\theta_\mu) \propto \exp\left(w\cos(\theta_\mu - \theta_{\mathrm{staple}})\right) \tag{C.7}$$

where w and θ_{staple} depend on the attached staple and on the coupling β_{QED}. This angle can therefore be drawn simultaneously for one direction on all odd (respectively even) sites of the lattice.

The distribution itself cannot be mapped analytically by a coordinate transformation to the uniform or normal (Gaussian) distribution. The most efficient way of generating appropriate random numbers is therefore to find a distribution that is very similar and to stochastically correct for the difference. The scheme proposed in [204] was used for our compact $U(1)$ generation. We furthermore employed over relaxation [205]. Further details about the generation can be found in [158]. The updated configuration is in a random gauge and needs to be gauge fixed for the study of charged hadrons.

C.2.2. Properties

Compact lattice QED requires a small multiplicative renormalization due to the implicit self-interaction of the QED fields. The required renormalization constant can be determined by measuring $U(1)$ Wilson loops, which yield the periodic potential $V(an)$ that in turn can be fitted to lattice (QED) perturbation theory results. The fit yields the renormalized charge e^r and an irrelevant self energy.

The reader shall be reminded that compact QED restricts the quark charges to integer values. This is due to the fact that upon exponentiation the links U_μ are effectively restricted to local phase information. The extraction of the fields B_μ and the rescaling of the original links are therefore ambiguous.

C.3. Smearing

Both compact QED links as well as non-compact QED fields can be smeared. The non-compact smearing is given by

$$B_\mu^{smr}(n) = \alpha^{\mathrm{nc}} \cdot B_\mu(n) + \frac{1-\alpha^{\mathrm{nc}}}{2N_d - 2} \sum_{\nu\neq\mu}^{\pm N_d} B_\nu(n) + B_\mu(n+\hat{\nu}) - B_\nu(n+\hat{\nu}), \tag{C.8}$$

where it is important that all weights sum up to one. We employed $\alpha^{\mathrm{nc}} = 0.9$ in contrast to the simulation described in [120], which effectively uses $\alpha^{\mathrm{nc}} = 0.9/1.5 = 0.6$. This non-compact prescription is approximately equivalent (up to non-linear terms) to APE smearing of the $U(1)$ links

$$U_\mu^{smr}(n) = \left(\alpha^{U(1)\text{-APE}} U_\mu(n) + U_\mu^s(n)\right), \tag{C.9}$$

where U_μ^s is the $U(1)$ analogue to the QCD staple (eq. (3.31)) and the trivial backprojection to $U(1)$ is implied. The APE smearing parameter $\alpha^{U(1)\text{-APE}}$ is not equivalent to the corresponding non-compact coefficient. Either procedure can be performed iteratively.

D. Bibliography

[1] M. K. Gaillard, P. D. Grannis, and F. J. Sciulli, "The Standard model of particle physics", *Rev. Mod. Phys.* **71** (1999) S96–S111, arXiv:hep-ph/9812285.

[2] J. Ellis and T. You, "Updated Global Analysis of Higgs Couplings", *JHEP* **06** (2013) 103, arXiv:1303.3879 [hep-ph].

[3] S. L. Glashow, "Partial Symmetries of Weak Interactions", *Nucl. Phys.* **22** (1961) 579–588.

[4] A. Salam and J. C. Ward, "Electromagnetic and weak interactions", *Phys. Lett.* **13** (1964) 168–171.

[5] S. Weinberg, "A Model of Leptons", *Phys. Rev. Lett.* **19** (1967) 1264–1266.

[6] G. 't Hooft, "Renormalizable Lagrangians for Massive Yang-Mills Fields", *Nucl. Phys.* **B35** (1971) 167–188.

[7] H. Fritzsch, M. Gell-Mann, and H. Leutwyler, "Advantages of the Color Octet Gluon Picture", *Phys. Lett.* **B47** (1973) 365–368.

[8] M. Shaposhnikov, "Baryogenesis", *J. Phys. Conf. Ser.* **171** (2009) 012005.

[9] J. L. Feng, "Dark Matter Candidates from Particle Physics and Methods of Detection", *Ann. Rev. Astron. Astrophys.* **48** (2010) 495–545, arXiv:1003.0904 [astro-ph.CO].

[10] A. Djouadi, "The Anatomy of electro-weak symmetry breaking. I: The Higgs boson in the standard model", *Phys. Rept.* **457** (2008) 1–216, arXiv:hep-ph/0503172.

[11] The **LEP** collaborations and the **LEP** Electroweak Working Group, "A Combination of preliminary electroweak measurements and constraints on the standard model", arXiv:hep-ex/0612034.

[12] K. G. Wilson, "Confinement of Quarks", *Phys. Rev.* **D10** (1974) 2445–2459.

[13] M. Creutz, "Gauge Fixing, the Transfer Matrix, and Confinement on a Lattice", *Phys. Rev.* **D15** (1977) 1128.

[14] S. Aoki *et al.*, "Review of lattice results concerning low-energy particle physics", arXiv:1607.00299 [hep-lat].

[15] M. E. Peskin and D. V. Schroeder, *An Introduction to quantum field theory*. 1995.

[16] A. Zee, *Quantum Field Theory in a Nutshell*. Nutshell handbook. Princeton Univ. Press, Princeton, NJ, 2003.

[17] P. A. M. Dirac, "The quantum theory of the electron", *Proc. Roy. Soc. Lond.* **A117** (1928) 610–624.

[18] R. P. Feynman, "Mathematical formulation of the quantum theory of electromagnetic interaction", *Phys. Rev.* **80** (1950) 440–457.

[19] E. Rutherford, "The scattering of alpha and beta particles by matter and the structure of the atom", *Phil. Mag.* **21** (1911) 669–688.

[20] H. Yukawa, "On the Interaction of Elementary Particles I", *Proc. Phys. Math. Soc. Jap.* **17** (1935) 48–57. [Prog. Theor. Phys. Suppl.1,1(1935)].

[21] L. D. Faddeev and V. N. Popov, "Feynman Diagrams for the Yang-Mills Field", *Phys. Lett.* **B25** (1967) 29–30.

[22] P. Weisz, "Renormalization and lattice artifacts", in *Modern perspectives in lattice QCD: Quantum field theory and high performance computing. Proceedings, International School, 93rd Session, Les Houches, France, August 3-28, 2009*, pp. 93–160. 2010. arXiv:1004.3462 [hep-lat].

[23] **Particle Data Group** Collaboration, K. Olive *et al.*, "Review of Particle Physics", *Chin. Phys.* **C38** (2014) 090001.

[24] S. Aoki *et al.*, "Review of lattice results concerning low-energy particle physics", *Eur. Phys. J.* **C74** (2014) 2890, arXiv:1310.8555 [hep-lat].

[25] J. Gasser and G. R. S. Zarnauskas, "On the pion decay constant", *Phys. Lett.* **B693** (2010) 122–128, arXiv:1008.3479 [hep-ph].

[26] J. D. Richman and P. R. Burchat, "Leptonic and semileptonic decays of charm and bottom hadrons", *Rev. Mod. Phys.* **67** (1995) 893–976, arXiv:hep-ph/9508250.

[27] M. Kobayashi and T. Maskawa, "CP Violation in the Renormalizable Theory of Weak Interaction", *Prog. Theor. Phys.* **49** (1973) 652–657.

[28] F. Bloch and A. Nordsieck, "Note on the Radiation Field of the electron", *Phys. Rev.* **52** (1937) 54–59.

[29] R. Evans, G. Bali, and S. Collins, "Improved Semileptonic Form Factor Calculations in Lattice QCD", *Phys. Rev.* **D82** (2010) 094501, arXiv:1008.3293 [hep-lat].

[30] H. Georgi, *Weak Interactions and Modern Particle Theory, revised and updated*. Dover Publications, Inc., Mineola, NY, 2009.

[31] J. S. Bell and R. Jackiw, "A PCAC Puzzle: $\pi^0 \to \gamma\gamma$ in the σ-Model", *Nuovo Cim.* **A60** (1969) 47–61.

[32] S. L. Adler, "Axial vector vertex in spinor electrodynamics", *Phys. Rev.* **177** (1969) 2426–2438.

[33] M. L. Goldberger and S. B. Treiman, "Decay of the Pi Meson", *Phys. Rev.* **110** (1958) 1178–1184.

[34] R. Miskimen, "Neutral pion decay", *Ann. Rev. Nucl. Part. Sci.* **61** (2011) 1–21.

[35] **PrimEx** Collaboration, I. Larin *et al.*, "A New Measurement of the π^0 Radiative Decay Width", *Phys. Rev. Lett.* **106** (2011) 162303, arXiv:1009.1681 [nucl-ex].

[36] D. Babusci, H. Czyz, F. Gonnella, S. Ivashyn, M. Mascolo, R. Messi, D. Moricciani, A. Nyffeler, and G. Venanzoni, "On the possibility to measure the $\pi^0 \to \gamma\gamma$ decay width and the $\gamma^*\gamma \to \pi^0$ transition form factor with the KLOE-2 experiment", *Eur. Phys. J.* **C72** (2012) 1917, arXiv:1109.2461 [hep-ph].

[37] A. Nyffeler, "Hadronic light-by-light scattering in the muon g-2: impact of proposed measurements of the $\pi^0 \to \gamma\gamma$ decay width and the $\gamma^*\gamma \to \pi^0$ transition form factor with the KLOE-2 experiment", *PoS* **CD12** (2013) 045, arXiv:1306.5987 [hep-ph].

[38] A. E. Dorokhov, A. E. Radzhabov, and A. S. Zhevlakov, "The pseudoscalar hadronic channel contribution of the light-by-light process to the muon $(g-2)_\mu$ within the nonlocal chiral quark model", *Eur. Phys. J.* **C71** (2011) 1702, arXiv:1103.2042 [hep-ph].

[39] T. Blum, N. Christ, M. Hayakawa, T. Izubuchi, L. Jin, and C. Lehner, "Lattice Calculation of Hadronic Light-by-Light Contribution to the Muon Anomalous Magnetic Moment", *Phys. Rev.* **D93** no. 1, (2016) 014503, arXiv:1510.07100 [hep-lat].

[40] H. W. Kendall, "Deep inelastic scattering: Experiments on the proton and the observation of scaling", *Rev. Mod. Phys.* **63** (1991) 597–614.

[41] G. J. Feldman, "REVIEW OF tau LEPTON PROPERTIES", in *International Meeting on Frontier of Physics Singapore, Singapore, August 14-18, 1978*, p. 421. 1978.

[42] M. L. Perl, "Reflections on the discovery of the tau lepton", in *In *Ekspong, G. (ed.): Nobel lectures in physics 1991-1995* 168-195.* 1996.

[43] **UA1** Collaboration, G. Arnison *et al.*, "Experimental Observation of Isolated Large Transverse Energy Electrons with Associated Missing Energy at $\sqrt{s} =$ 540 GeV", *Phys. Lett.* **B122** (1983) 103–116.

[44] **UA2** Collaboration, P. Bagnaia *et al.*, "Evidence for Z0 → e+ e- at the CERN anti-p p Collider", *Phys. Lett.* **B129** (1983) 130–140.

[45] **BaBar** Collaboration, B. Aubert *et al.*, "The BaBar detector", *Nucl. Instrum. Meth.* **A479** (2002) 1–116, arXiv:hep-ex/0105044.

[46] **Belle** Collaboration, K. Abe *et al.*, "Observation of large CP violation in the neutral B meson system", *Phys. Rev. Lett.* **87** (2001) 091802, arXiv:hep-ex/0107061 [hep-ex].

[47] E. I. Rosenberg, "Review of CKM results from BaBar", in *Particle physics at the year of 250th anniversary of Moscow University. Proceedings, 12th Lomonosov Conference on elementary particle physics, Moscow, Russia, August 25-31*, pp. 290–297. 2005.

[48] E. V. Shuryak, "What RHIC experiments and theory tell us about properties of quark-gluon plasma?", *Nucl. Phys.* **A750** (2005) 64–83, arXiv:hep-ph/0405066.

[49] T. D. Lee and C.-N. Yang, "Question of Parity Conservation in Weak Interactions", *Phys. Rev.* **104** (1956) 254–258.

[50] C. S. Wu, E. Ambler, R. W. Hayward, D. D. Hoppes, and R. P. Hudson, "Experimental Test of Parity Conservation in Beta Decay", *Phys. Rev.* **105** (1957) 1413–1414.

[51] R. L. Garwin, L. M. Lederman, and M. Weinrich, "Observations of the Failure of Conservation of Parity and Charge Conjugation in Meson Decays: The Magnetic Moment of the Free Muon", *Phys. Rev.* **105** (1957) 1415–1417.

[52] **STAR** Collaboration, B. I. Abelev *et al.*, "Azimuthal Charged-Particle Correlations and Possible Local Strong Parity Violation", *Phys. Rev. Lett.* **103** (2009) 251601, arXiv:0909.1739 [nucl-ex].

[53] F. Wang, "Effects of Cluster Particle Correlations on Local Parity Violation Observables", *Phys. Rev.* **C81** (2010) 064902, arXiv:0911.1482 [nucl-ex].

[54] B. Müller and A. Schäfer, "Charge Fluctuations from the Chiral Magnetic Effect in Nuclear Collisions", *Phys. Rev.* **C82** (2010) 057902, arXiv:1009.1053 [hep-ph].

[55] V. Voronyuk, V. D. Toneev, W. Cassing, E. L. Bratkovskaya, V. P. Konchakovski, and S. A. Voloshin, "(Electro-)Magnetic field evolution in relativistic heavy-ion collisions", *Phys. Rev.* **C83** (2011) 054911, arXiv:1103.4239 [nucl-th].

[56] M. Gell-Mann, "Symmetries of baryons and mesons", *Phys. Rev.* **125** (1962) 1067–1084.

[57] M. Gell-Mann, R. J. Oakes, and B. Renner, "Behavior of current divergences under SU(3) x SU(3)", *Phys. Rev.* **175** (1968) 2195–2199.

[58] S. Weinberg, "Phenomenological Lagrangians", *Physica* **A96** (1979) 327–340.

[59] H. Leutwyler, "On the foundations of chiral perturbation theory", *Annals Phys.* **235** (1994) 165–203, arXiv:hep-ph/9311274.

[60] S. Sharpe, "Applications of Chiral Perturbation theory to lattice QCD", in *Workshop on Perspectives in Lattice QCD Nara, Japan, October 31-November 11, 2005*. 2006. arXiv:hep-lat/0607016.

[61] G. Ecker, "Chiral perturbation theory", *Prog. Part. Nucl. Phys.* **35** (1995) 1–80, arXiv:hep-ph/9501357.

[62] S. Scherer, "Introduction to chiral perturbation theory", *Adv. Nucl. Phys.* **27** (2003) 277, arXiv:hep-ph/0210398.

[63] A. Walker-Loud, "Nuclear Physics Review", *PoS* **LATTICE2013** (2014) 013, arXiv:1401.8259 [hep-lat].

[64] E. Witten, "Global Aspects of Current Algebra", *Nucl. Phys.* **B223** (1983) 422–432.

[65] M. Creutz, *Quarks, gluons and lattices*. Cambridge Monographs on Mathematical Physics. Cambridge Univ. Press, Cambridge, UK, 1985.

[66] H. Rothe, *Lattice gauge theories: An Introduction*, vol. 43. 1992.

[67] T. DeGrand and C. E. Detar, *Lattice methods for quantum chromodynamics*. 2006.

[68] C. Gattringer and C. B. Lang, *Quantum chromodynamics on the lattice*, vol. 788. 2010.

[69] R. Gupta, "Introduction to lattice QCD: Course", in *Probing the standard model of particle interactions. Proceedings, Summer School in Theoretical Physics, NATO Advanced Study Institute, 68th session, Les Houches, France, July 28-September 5, 1997. Pt. 1, 2*, pp. 83–219. 1997. arXiv:hep-lat/9807028.

[70] M. Luscher, "Advanced lattice QCD", in *Probing the standard model of particle interactions. Proceedings, Summer School in Theoretical Physics, NATO Advanced Study Institute, 68th session, Les Houches, France, July 28-September 5, 1997. Pt. 1, 2*, pp. 229–280. 1998. arXiv:hep-lat/9802029.

[71] H. B. Nielsen and M. Ninomiya, "No Go Theorem for Regularizing Chiral Fermions", *Phys. Lett.* **B105** (1981) 219.

[72] P. H. Ginsparg and K. G. Wilson, "A Remnant of Chiral Symmetry on the Lattice", *Phys. Rev.* **D25** (1982) 2649.

[73] H. Neuberger, "More about exactly massless quarks on the lattice", *Phys. Lett.* **B427** (1998) 353–355, arXiv:hep-lat/9801031.

[74] P. Hasenfratz, "Prospects for perfect actions", *Nucl. Phys. Proc. Suppl.* **63** (1998) 53–58, arXiv:hep-lat/9709110.

[75] K. Symanzik, "Continuum Limit and Improved Action in Lattice Theories. 1. Principles and ϕ^4 Theory", *Nucl. Phys.* **B226** (1983) 187.

[76] B. Sheikholeslami and R. Wohlert, "Improved Continuum Limit Lattice Action for QCD with Wilson Fermions", *Nucl. Phys.* **B259** (1985) 572.

[77] M. Lüscher and P. Weisz, "On-Shell Improved Lattice Gauge Theories", *Commun. Math. Phys.* **97** (1985) 59.

[78] Y. Iwasaki, "Renormalization Group Analysis of Lattice Theories and Improved Lattice Action. II. Four-dimensional non-Abelian SU(N) gauge model", arXiv:1111.7054 [hep-lat].

[79] S. Capitani, S. Durr, and C. Hoelbling, "Rationale for UV-filtered clover fermions", *JHEP* **11** (2006) 028, arXiv:hep-lat/0607006.

[80] T. A. DeGrand, A. Hasenfratz, and T. G. Kovacs, "Instantons and exceptional configurations with the clover action", *Nucl. Phys.* **B547** (1999) 259–280, arXiv:hep-lat/9810061.

[81] D. H. Weingarten and D. N. Petcher, "Monte Carlo Integration for Lattice Gauge Theories with Fermions", *Phys. Lett.* **B99** (1981) 333–338.

[82] J. B. Kogut, "A Review of the Lattice Gauge Theory Approach to Quantum Chromodynamics", *Rev. Mod. Phys.* **55** (1983) 775.

[83] S. Duane, A. D. Kennedy, B. J. Pendleton, and D. Roweth, "Hybrid Monte Carlo", *Phys. Lett.* **B195** (1987) 216–222.

[84] **ALPHA** Collaboration, U. Wolff, "Monte Carlo errors with less errors", *Comput. Phys. Commun.* **156** (2004) 143–153, arXiv:hep-lat/0306017. [Erratum: Comput. Phys. Commun.176,383(2007)].

[85] M. R. Hestenes and E. Stiefel, "Methods of Conjugate Gradients for Solving Linear Systems", *Journal of Research of the National Bureau of Standards* **49** no. 6, (Dec., 1952) 409–436.

[86] H. A. Van der Vorst, "Bi-CGSTAB: A fast and smoothly converging variant of Bi-CG for the solution of nonsymmetric linear systems", *SIAM Journal on scientific and Statistical Computing* **13** no. 2, (1992) 631–644.

[87] Y. Saad and M. H. Schultz, "GMRES: A generalized minimal residual algorithm for solving nonsymmetric linear systems", *SIAM Journal on scientific and statistical computing* **7** no. 3, (1986) 856–869.

[88] M. Lüscher, "Local coherence and deflation of the low quark modes in lattice QCD", *JHEP* **0707** (2007) 081, arXiv:0706.2298 [hep-lat].

[89] A. Frommer, K. Kahl, S. Krieg, B. Leder, and M. Rottmann, "Adaptive Aggregation Based Domain Decomposition Multigrid for the Lattice Wilson Dirac Operator", *SIAM J. Sci. Comput.* **36** (2014) A1581–A1608, arXiv:1303.1377 [hep-lat].

[90] **UKQCD** Collaboration, M. Foster and C. Michael, "Quark mass dependence of hadron masses from lattice QCD", *Phys. Rev.* **D59** (1999) 074503, arXiv:hep-lat/9810021.

[91] P. A. Boyle, A. Juttner, C. Kelly, and R. D. Kenway, "Use of stochastic sources for the lattice determination of light quark physics", *JHEP* **08** (2008) 086, arXiv:0804.1501 [hep-lat].

[92] S. Güsken, "A study of smearing techniques for hadron correlation functions", *Nuclear Physics B - Proceedings Supplements* **17** no. 0, (1990) 361–364.

[93] J. S. S. Najjar, *Nucleon structure from stochastic estimators*. PhD thesis, September, 2014. http://epub.uni-regensburg.de/30694/.

[94] G. S. Bali, B. Lang, B. U. Musch, and A. Schäfer, "A novel quark smearing for hadrons with high momenta in lattice QCD", arXiv:1602.05525 [hep-lat].

[95] **Hadron Spectrum** Collaboration, M. Peardon, J. Bulava, J. Foley, C. Morningstar, J. Dudek, R. G. Edwards, B. Joo, H.-W. Lin, D. G. Richards, and K. J. Juge, "A Novel quark-field creation operator construction for hadronic physics in lattice QCD", *Phys. Rev.* **D80** (2009) 054506, arXiv:0905.2160 [hep-lat].

[96] **UKQCD** Collaboration, C. R. Allton *et al.*, "Gauge invariant smearing and matrix correlators using Wilson fermions at Beta = 6.2", *Phys. Rev.* **D47** (1993) 5128–5137, arXiv:hep-lat/9303009.

[97] G. M. von Hippel, B. Jäger, T. D. Rae, and H. Wittig, "The Shape of Covariantly Smeared Sources in Lattice QCD", *JHEP* **09** (2013) 014, arXiv:1306.1440 [hep-lat].

[98] **APE** Collaboration, M. Albanese *et al.*, "Glueball Masses and String Tension in Lattice QCD", *Phys. Lett.* **B192** (1987) 163–169.

[99] A. Hasenfratz and F. Knechtli, "Flavor symmetry and the static potential with hypercubic blocking", *Phys. Rev.* **D64** (2001) 034504, arXiv:hep-lat/0103029.

[100] C. Morningstar and M. Peardon *Phys. Rev.* **D69** 054501, arXiv:hep-lat/0311018v1.

[101] D. Weingarten, "Masses and Decay Constants in Lattice QCD", *Nucl. Phys.* **B215** (1983) 1–22.

[102] G. S. Bali *et al.*, "Light-cone distribution amplitudes of the baryon octet", *JHEP* **02** (2016) 070, arXiv:1512.02050 [hep-lat].

[103] G. S. Bali, S. Collins, B. Gläßle, M. Göckeler, J. Najjar, *et al.*, "Nucleon isovector couplings from $N_f = 2$ lattice QCD", *Phys. Rev.* **D91** no. 5, (2015) 054501, arXiv:1412.7336 [hep-lat].

[104] G. Bali, L. Castagnini, M. Diehl, J. Gaunt, B. Gläßle, A. Schäfer, and C. Zimmermann. in preparation.

[105] M. Göckeler, "Scaling of non-perturbatively O(a) improved Wilson fermions: Hadron spectrum, quark masses and decay constants", *Phys. Rev.* **D57** (1998) 5562–5580, arXiv:hep-lat/9707021.

[106] S. Sint and P. Weisz, "Further results on O(a) improved lattice QCD to one-loop order of perturbation theory", *Nucl. Phys.* **B502** (Apr., 1997) 251–268, arXiv:hep-lat/9704001v1.

[107] S. Aoki, R. Frezzotti, and P. Weisz, "Computation of the improvement coefficient $c_{\rm SW}$ to one loop with improved gluon actions", *Nucl. Phys.* **B540** (1999) 501–519, arXiv:hep-lat/9808007.

[108] J. Bulava, M. D. Morte, J. Heitger, and C. Wittemeier, "Non-perturbative improvement of the axial current in $N_{\rm f} = 3$ lattice QCD with Wilson fermions and tree-level improved gauge action", arXiv:1502.04999 [hep-lat].

[109] S. Durr, Z. Fodor, J. Frison, C. Hoelbling, R. Hoffmann, *et al.*, "Ab-Initio Determination of Light Hadron Masses", *Science* **322** (2008) 1224–1227, arXiv:0906.3599 [hep-lat].

[110] R. Sommer, "A New way to set the energy scale in lattice gauge theories and its applications to the static force and alpha-s in SU(2) Yang-Mills theory", *Nucl. Phys.* **B411** (1994) 839–854, arXiv:hep-lat/9310022.

[111] C. W. Bernard, T. Burch, K. Orginos, D. Toussaint, T. A. DeGrand, C. E. DeTar, S. A. Gottlieb, U. M. Heller, J. E. Hetrick, and B. Sugar, "The Static quark potential in three flavor QCD", *Phys. Rev.* **D62** (2000) 034503, arXiv:hep-lat/0002028.

[112] M. Lüscher, "Properties and uses of the Wilson flow in lattice QCD", *JHEP* **08** (2010) 071, arXiv:1006.4518 [hep-lat]. [Erratum: JHEP03,092(2014)].

[113] S. Borsanyi *et al.*, "High-precision scale setting in lattice QCD", *JHEP* **09** (2012) 010, arXiv:1203.4469 [hep-lat].

[114] M. Luscher, "Volume Dependence of the Energy Spectrum in Massive Quantum Field Theories. 1. Stable Particle States", *Commun. Math. Phys.* **104** (1986) 177.

[115] K. Sasaki and S. Sasaki, "Excited baryon spectroscopy from lattice QCD: Finite size effect and hyperfine mass splitting", *Phys. Rev.* **D72** (2005) 034502, arXiv:hep-lat/0503026 [hep-lat].

[116] Y. Taniguchi and A. Ukawa, "Perturbative calculation of improvement coefficients to $\mathcal{O}(g^2a)$ for bilinear quark operators in lattice QCD", *Phys. Rev.* **D58** (1998) 114503, arXiv:hep-lat/9806015.

[117] A. Vladikas, "Three Topics in Renormalization and Improvement", June, 2011. arXiv:1103.1323v2 [hep-lat].

[118] G. Martinelli, C. Pittori, C. T. Sachrajda, M. Testa, and A. Vladikas, "A General method for nonperturbative renormalization of lattice operators", *Nucl. Phys.* **B445** (1995) 81–108, arXiv:hep-lat/9411010.

[119] W. Bietenholz, V. Bornyakov, M. Göckeler, R. Horsley, W. Lockhart, *et al.*, "Flavour blindness and patterns of flavour symmetry breaking in lattice simulations of up, down and strange quarks", *Phys. Rev.* **D84** (2011) 054509, arXiv:1102.5300 [hep-lat].

[120] S. Borsanyi, S. Durr, Z. Fodor, C. Hoelbling, S. Katz, *et al.*, "Ab initio calculation of the neutron-proton mass difference", *Science* **347** (2015) 1452–1455, arXiv:1406.4088 [hep-lat].

[121] M. Creutz, L. Jacobs, and C. Rebbi, "Monte Carlo Study of Abelian Lattice Gauge Theories", *Phys. Rev.* **D20** (1979) 1915.

[122] K. J. M. Moriarty, "Monte Carlo Study of Compact U(1) Four-dimensional Lattice Gauge Theory", *Phys. Rev.* **D25** (1982) 2185.

[123] K. J. M. Moriarty, "MONTE CARLO STUDY OF THE STRING TENSION OF COMPACT U(1) GAUGE THEORY IN FOUR-DIMENSIONS", *J. Phys.* **G9** (1983) L33.

[124] G. Arnold, B. Bunk, T. Lippert, and K. Schilling, "Compact QED under scrutiny: It's first order", *Nucl. Phys. Proc. Suppl.* **119** (2003) 864–866, arXiv:hep-lat/0210010.

[125] M. Göckeler, R. Horsley, V. Linke, P. E. L. Rakow, G. Schierholz, and H. Stuben, "Is there a Landau pole problem in QED?", *Phys. Rev. Lett.* **80** (1998) 4119–4122, arXiv:hep-th/9712244.

[126] J. B. Kogut and C. G. Strouthos, "The Logarithmic triviality of compact QED coupled to a four Fermi interaction", *Phys. Rev.* **D71** (2005) 094012, arXiv:hep-lat/0501003.

[127] A. Duncan, E. Eichten, and H. Thacker, "Electromagnetic splittings and light quark masses in lattice QCD", *Phys. Rev. Lett.* **76** (1996) 3894–3897, arXiv:hep-lat/9602005.

[128] A. Duncan, E. Eichten, and H. Thacker, "Electromagnetic structure of light baryons in lattice QCD", *Phys. Lett.* **B409** (1997) 387–392, arXiv:hep-lat/9607032.

[129] T. Blum, T. Doi, M. Hayakawa, T. Izubuchi, and N. Yamada, "Determination of light quark masses from the electromagnetic splitting of pseudoscalar meson masses computed with two flavors of domain wall fermions", *Phys. Rev.* **D76** (2007) 114508, arXiv:0708.0484 [hep-lat].

[130] T. Blum, R. Zhou, T. Doi, M. Hayakawa, T. Izubuchi, *et al.*, "Electromagnetic mass splittings of the low lying hadrons and quark masses from 2+1 flavor lattice QCD+QED", *Phys. Rev.* **D82** (2010) 094508, arXiv:1006.1311 [hep-lat].

[131] S. Aoki, K. Ishikawa, N. Ishizuka, K. Kanaya, Y. Kuramashi, *et al.*, "1+1+1 flavor QCD + QED simulation at the physical point", *Phys. Rev.* **D86** (2012) 034507, arXiv:1205.2961 [hep-lat].

[132] A. Portelli, S. Durr, Z. Fodor, J. Frison, C. Hoelbling, *et al.*, "Systematic errors in partially-quenched QCD plus QED lattice simulations", *PoS* **LATTICE2011** (2011) 136, arXiv:1201.2787 [hep-lat].

[133] G. Bali, B. B. Brandt, G. Endrődi, and B. Gläßle, "QCD spectroscopy and quark mass renormalisation in external magnetic fields with Wilson fermions", *PoS* **LATTICE2015** (2015) , arXiv:1510.03899 [hep-lat].

[134] N. Carrasco, V. Lubicz, G. Martinelli, C. T. Sachrajda, N. Tantalo, C. Tarantino, and M. Testa, "QED Corrections to Hadronic Processes in Lattice QCD", *Phys. Rev.* **D91** no. 7, (2015) 074506, arXiv:1502.00257 [hep-lat].

[135] **RM123** Collaboration, G. de Divitiis *et al.*, "Leading isospin breaking effects on the lattice", *Phys. Rev.* **D87** no. 11, (2013) 114505, arXiv:1303.4896 [hep-lat].

[136] A. Portelli, "Review on the inclusion of isospin breaking effects in lattice calculations", *PoS* **KAON13** (2013) 023, arXiv:1307.6056 [hep-lat].

[137] B. Lucini, A. Patella, A. Ramos, and N. Tantalo, "Charged hadrons in local finite-volume QED+QCD with C boundary conditions", *JHEP* **02** (2016) 076, arXiv:1509.01636 [hep-th].

[138] Z. Davoudi and M. J. Savage, "Finite-Volume Electromagnetic Corrections to the Masses of Mesons, Baryons and Nuclei", *Phys. Rev.* **D90** no. 5, (2014) 054503, arXiv:1402.6741 [hep-lat].

[139] Z. Fodor, C. Hoelbling, S. Katz, L. Lellouch, A. Portelli, *et al.*, "Quantum electrodynamics in finite volume and nonrelativistic effective field theories", arXiv:1502.06921 [hep-lat].

[140] S. Drury, T. Blum, M. Hayakawa, T. Izubuchi, C. Sachrajda, *et al.*, "Non-degenerate light quark masses from 2+1f lattice QCD+QED", *PoS* **LATTICE2013** (2014) 268, arXiv:1312.0477 [hep-lat].

[141] Z. Fodor, C. Hoelbling, S. Krieg, L. Lellouch, T. Lippert, A. Portelli, A. Sastre, K. K. Szabo, and L. Varnhorst, "Up and down quark masses and corrections to Dashen's theorem from lattice QCD and quenched QED", arXiv:1604.07112 [hep-lat].

[142] J. Bijnens and N. Danielsson, "Electromagnetic Corrections in Partially Quenched Chiral Perturbation Theory", *Phys. Rev.* **D75** (2007) 014505, arXiv:hep-lat/0610127.

[143] **QCDSF** Collaboration, R. Horsley *et al.*, "Electromagnetic splitting of quark and pseudoscalar meson masses from dynamical QCD + QED", *PoS* **LATTICE2013** (2014) 499, arXiv:1311.4554 [hep-lat].

[144] T. Ishikawa, T. Blum, M. Hayakawa, T. Izubuchi, C. Jung, *et al.*, "Full QED+QCD low-energy constants through reweighting", *Phys. Rev. Lett.* **109** (2012) 072002, arXiv:1202.6018 [hep-lat].

[145] F. Figueirido, G. S. Del Buono, and R. M. Levy, "On finitesize effects in computer simulations using the Ewald potential", *The Journal of Chemical Physics* **103** no. 14, (1995) 6133–6142.

[146] M. Hayakawa and S. Uno, "QED in finite volume and finite size scaling effect on electromagnetic properties of hadrons", *Prog. Theor. Phys.* **120** (2008) 413–441, arXiv:0804.2044 [hep-ph].

[147] A. S. Kronfeld and U. J. Wiese, "SU(N) gauge theories with C periodic boundary conditions. 1. Topological structure", *Nucl. Phys.* **B357** (1991) 521–533.

[148] L. Polley, "Boundaries for $SU(3)_c \times U(1)_{el}$ lattice gauge theory with a chemical potential", *Z. Phys.* **C59** (1993) 105–108.

[149] C. Lehner and T. Izubuchi, "Towards the large volume limit - A method for lattice QCD + QED simulations", *PoS* **LATTICE2014** (2015) 164, arXiv:1503.04395 [hep-lat].

[150] M. G. Endres, A. Shindler, B. C. Tiburzi, and A. Walker-Loud, "Massive photons: an infrared regularization scheme for lattice QCD+QED", arXiv:1507.08916 [hep-lat].

[151] M. Bochicchio, L. Maiani, G. Martinelli, G. C. Rossi, and M. Testa, "Chiral Symmetry on the Lattice with Wilson Fermions", *Nucl. Phys.* **B262** (1985) 331.

[152] G. Bali, B. B. Brandt, G. Endrődi, and B. Gläßle. in preparation.

[153] N. Cundy, M. Göckeler, R. Horsley, T. Kaltenbrunner, A. D. Kennedy, Y. Nakamura, H. Perlt, D. Pleiter, P. E. L. Rakow, A. Schäfer, G. Schierholz, A. Schiller, H. Stüben, and J. M. Zanotti, "Non-perturbative improvement of stout-smeared three flavour clover fermions", *Phys. Rev.* **D79** (June, 2009) 094507, arXiv:0901.3302v2 [hep-lat].

[154] W. Bietenholz *et al.*, "Tuning the strange quark mass in lattice simulations", *Phys. Lett.* **B690** (2010) 436–441, arXiv:1003.1114 [hep-lat].

[155] **CSSM, QCDSF/UKQCD** Collaboration, P. Shanahan *et al.*, "Magnetic form factors of the octet baryons from lattice QCD and chiral extrapolation", *Phys. Rev.* **D89** (2014) 074511, arXiv:1401.5862 [hep-lat].

[156] G. Bali, "Static quark potential in lattice QED". private communication.

[157] I. L. Bogolubsky, V. K. Mitrjushkin, M. Muller-Preussker, and P. Peter, "Lorentz gauge and Gribov ambiguity in the compact lattice U(1) theory", *Phys. Lett.* **B458** (1999) 102–108, arXiv:hep-lat/9904001.

[158] **QCDSF** Collaboration, B. Gläßle and G. S. Bali, "Electromagnetic corrections to pseudoscalar decay constants", *PoS* **LATTICE2011** (2011) 282, arXiv:1111.3958 [hep-lat].

[159] **QCDSF-UKQCD** Collaboration, S. Booth *et al.*, "Determination of $\Lambda_{\overline{\rm MS}}$ from quenched and $N_f = 2$ dynamical QCD", *Phys. Lett.* **B519** (2001) 229–237, arXiv:hep-lat/0103023.

[160] P. Pérez-Rubio, S. Collins, and G. S. Bali, "Charmed baryon spectroscopy and light flavor symmetry from lattice QCD", *Phys. Rev.* **D92** (2015) 034504, arXiv:1503.08440 [hep-lat].

[161] M. Constantinou, R. Horsley, H. Panagopoulos, H. Perlt, P. E. L. Rakow, G. Schierholz, A. Schiller, and J. M. Zanotti, "Renormalization of local quark-bilinear operators for $N_{\rm f} = 3$ flavors of SLiNC fermions", *Phys. Rev.* **D91** (Aug., 2015) 014502, arXiv:1408.6047v1 [hep-lat].

[162] T. Bhattacharya, R. Gupta, W. Lee, S. R. Sharpe, and J. M. S. Wu, "Improved bilinears in lattice QCD with non-degenerate quarks", *Phys. Rev.* **D73** (2006) 034504, arXiv:hep-lat/0511014 [hep-lat].

[163] **QCDSF-UKQCD** Collaboration, R. Horsley, J. Najjar, Y. Nakamura, H. Perlt, D. Pleiter, P. E. L. Rakow, G. Schierholz, A. Schiller, H. Stben, and J. M. Zanotti, "SU(3) flavour symmetry breaking and charmed states", *PoS* **LATTICE2013** (2014) 249, arXiv:1311.5010 [hep-lat].

[164] **European Twisted Mass** Collaboration, N. Carrasco *et al.*, "Up, down, strange and charm quark masses with $\mathrm{N}_f = 2{+}1{+}1$ twisted mass lattice QCD", *Nucl. Phys.* **B887** (2014) 19–68, arXiv:1403.4504 [hep-lat].

[165] R. F. Dashen, "Chiral SU(3) x SU(3) as a symmetry of the strong interactions", *Phys. Rev.* **183** (1969) 1245–1260.

[166] P. Korcyl and G. S. Bali, "Non-perturbative determination of improvement coefficients using coordinate space correlators in $N_f = 2 + 1$ lattice QCD", arXiv:1607.07090 [hep-lat].

[167] M. Lüscher, S. Sint, R. Sommer, and P. Weisz, "Chiral symmetry and O(a) improvement in lattice QCD", *Nucl. Phys.* **B478** (1996) 365–400, arXiv:hep-lat/9605038.

[168] M. Luscher and P. Weisz, "O(a) improvement of the axial current in lattice QCD to one loop order of perturbation theory", *Nucl. Phys.* **B479** (1996) 429–458, arXiv:hep-lat/9606016.

[169] C. Quigg and J. L. Rosner, "Quantum Mechanics with Applications to Quarkonium", *Phys. Rept.* **56** (1979) 167–235.

[170] J. J. Sakurai and J. Napolitano, *Modern quantum mechanics*. Addison-Wesley, 2011.

[171] M. Lüscher and P. Weisz, "Locality and exponential error reduction in numerical lattice gauge theory", *JHEP* **09** (2001) 010, arXiv:hep-lat/0108014.

[172] M. Cè, L. Giusti, and S. Schaefer, "Domain decomposition, multi-level integration and exponential noise reduction in lattice QCD", arXiv:1601.04587 [hep-lat].

[173] N. Tantalo, "Isospin Breaking Effects on the Lattice", *PoS* **LATTICE2013** (2014) 007, arXiv:1311.2797 [hep-lat].

[174] V. Lubicz, N. Carrasco, G. Martinelli, C. Sachrajda, N. Tantalo, C. Tarantino, and M. Testa, "QED corrections to hadronic processes: a strategy for lattice QCD", *PoS* **CD15** (2016) 023.

[175] J. L. Goity, A. M. Bernstein, and B. R. Holstein, "The decay $\pi^0 \to \gamma\gamma$ to next to leading order in chiral perturbation theory", *Phys. Rev.* **D66** (2002) 076014, arXiv:hep-ph/0206007.

[176] B. L. Ioffe and A. G. Oganesian, "Axial anomaly and the precise value of the $\pi^0 \to 2\gamma$ decay width", *Phys. Lett.* **B647** (2007) 389–393, arXiv:hep-ph/0701077.

[177] K. Kampf and B. Moussallam, "Chiral expansions of the π^0 lifetime", *Phys. Rev.* **D79** (2009) 076005, arXiv:0901.4688 [hep-ph].

[178] A. H. Gasparian, "Preliminary Results from the PrimEx-II experiment at Jefferson Lab", *PoS* **CD15** (2016) 048.

[179] **KLOE-2** Collaboration, D. Moricciani, "Review on $\gamma\gamma$ physics at KLOE-2", *EPJ Web Conf.* **118** (2016) 01023.

[180] K. Kampf, "Anomalous processes and leading logarithms", *PoS* **CD12** (2013) 039, arXiv:1302.7311 [hep-ph].

[181] N. Meyer, M. Ries, S. Solbrig, and T. Wettig, "iDataCool: HPC with Hot-Water Cooling and Energy Reuse", *CoRR* **abs/1309.4887** (2013) , arXiv:1309.4887 [cs.DC].

[182] P. Arts *et al.*, "QPACE 2 and Domain Decomposition on the Intel Xeon Phi", *PoS* **LATTICE2014** (2015) 021, arXiv:1502.04025 [cs.DC].

[183] 2017. www.uni-regensburg.de/rechenzentrum/it-services/scientific-computing/index.html.

[184] **SciDAC, LHPC, UKQCD** Collaboration, R. G. Edwards and B. Joo, "The Chroma software system for lattice QCD", *Nucl. Phys. Proc. Suppl.* **140** (2005) 832, arXiv:hep-lat/0409003.

[185] The HDF Group, "Hierarchical Data Format, version 5", 1997-NNNN. http://www.hdfgroup.org/HDF5/.

[186] T. Kurth, A. Pochinsky, A. Sarje, S. Syritsyn, and A. Walker-Loud, "High-Performance I/O: HDF5 for Lattice QCD", *PoS* **LATTICE2014** (2015) 045, arXiv:1501.06992 [hep-lat].

[187] S. Heybrock, M. Rottmann, P. Georg, and T. Wettig, "Adaptive algebraic multigrid on SIMD architectures", *PoS* **LATTICE2015** (2015) , arXiv:1512.04506 [physics.comp-ph].

[188] https://rqcd.ur.de:8443/bglaessle/woiperdinger.git.

[189] C. Sanderson, "Armadillo: An Open Source C++ Linear Algebra Library for Fast Prototyping and Computationally Intensive Experiments", tech. rep., NICTA, Sept., 2010.

[190] F. James and M. Roos, "Minuit - a system for function minimization and analysis of the parameter errors and correlations", *Computer Physics Communications* **10** no. 6, (Dec., 1975) 343–367.

[191] J. D. Hunter, "Matplotlib: A 2D graphics environment", *Computing In Science & Engineering* **9** no. 3, (2007) 90–95.

[192] T. Ohl, "Drawing Feynman diagrams with Latex and Metafont", *Comput. Phys. Commun.* **90** (1995) 340–354, arXiv:hep-ph/9505351.

[193] R. G. Miller, "The jackknife-a review", *Biometrika* **61** no. 1, (1974) 1–15.

[194] M. Luscher, "Computational Strategies in Lattice QCD", in *Modern perspectives in lattice QCD: Quantum field theory and high performance computing. Proceedings, International School, 93rd Session, Les Houches, France, August 3-28, 2009*, pp. 331–399. 2010. arXiv:1002.4232 [hep-lat].

[195] B. Efron, *Bootstrap methods: another look at the jackknife*. Springer, 1992.

[196] C. Michael, "Fitting correlated data", *Phys. Rev.* **D49** (1994) 2616–2619, arXiv:hep-lat/9310026.

[197] **MILC** Collaboration, C. Bernard, S. Datta, T. A. DeGrand, C. E. DeTar, S. A. Gottlieb, U. M. Heller, C. McNeile, K. Orginos, R. Sugar, and D. Toussaint, "Lattice calculation of heavy light decay constants with two flavors of dynamical quarks", *Phys. Rev.* **D66** (2002) 094501, arXiv:hep-lat/0206016.

[198] D. Peña and F. J. Prieto, "Multivariate Outlier Detection and Robust Covariance Matrix Estimation", *Technometrics* **43** no. 3, (2001) 286–310.

[199] G. S. Bali, K. Schilling, J. Fingberg, U. M. Heller, and F. Karsch, "Computation of the spatial string tension in high temperature SU(2) gauge theory", *Int. J. Mod. Phys.* **C4** (1993) 1179–1193, arXiv:hep-lat/9308003.

[200] H. R. Schwarz and N. Köckler, *Numerische Mathematik*. Lehrbuch: Mathematik. Teubner, Wiesbaden, 6., überarb. aufl ed., 2006.

[201] E. Dagotto, A. Kocic, and J. B. Kogut, "Finite Size, Fermion Mass and N_f Systematics in Computer Simulations of Quantum Electrodynamics", *Nucl. Phys.* **B331** (1990) 500–514.

[202] G. Endrődi, "Projection to real QED fields". private communication.

[203] **Budapest-Marseille-Wuppertal** Collaboration, A. Portelli *et al.*, "Electromagnetic corrections to light hadron masses", *PoS* **LATTICE2010** (2010) 121, arXiv:1011.4189 [hep-lat].

[204] T. Hattori and H. Nakajima, "Improvement of efficiency in generating random U(1) variables with Boltzmann distribution", *Nucl. Phys. Proc. Suppl.* **B26** (1992) 635–637, arXiv:hep-lat/9210016.

[205] S. L. Adler, "An Overrelaxation Method for the Monte Carlo Evaluation of the Partition Function for Multiquadratic Actions", *Phys. Rev.* **D23** (1981) 2901.

E. Acknowledgments

During the work on this thesis I have received support from multiple people and institutions. First of all I am indebted to my advisor Gunnar for offering me this thesis and guiding me.

Many of my colleagues have influenced this work, either directly through discussion of the work or related subjects or indirectly in breaks and off-work activities. I want to especially mention Bastian B. and Gergely E. for offering me to collaborate on PCAC masses. Johannes N., Jakob S., Rudolf R., Daniel R. and the above proofread my thesis and deserve PRAISE. Daniel furthermore provided illustrations of LQCD elements used in chapter 3. Monika and Heidi are the foundation of our group and helped to successfully master any bureaucracy encountered during this thesis.

I acknowledge support by the GSI Hochschulprogramm (RSCHAE), the European Union under Grant Agreement number 238353 (ITN STRONGnet) and by the Deutsche Forschungsgemeinschaft SFB/Transregio 55.

My parents and my family where always helpful and supportive. I also want thank my parents-in-law and grandparents. I will fondly remember Alessio B., 3 of my grandparents and Monika who passed during the time I worked on my dissertation.

And lastly I want to thank my former girlfriend and now wife Raphaela for her great support and overall endurance.